

**A THERMO-MECHANICAL FINITE ELEMENT ANALYSIS OF ACOUSTIC
SOFTENING DURING ULTRASONIC CONSOLIDATION OF ALUMINUM
FOILS**

by

Gregory S. Kelly

A thesis submitted to the Faculty of the University of Delaware in partial fulfillment of the requirements for the degree of Master of Science in Mechanical Engineering

Summer 2012

© 2012 Gregory S. Kelly
All Rights Reserved

**A THERMO-MECHANICAL FINITE ELEMENT ANALYSIS OF ACOUSTIC
SOFTENING DURING ULTRASONIC CONSOLIDATION OF ALUMINUM
FOILS**

by

Gregory S. Kelly

Approved: _____
Suresh G. Advani, Ph.D.
Co- advisor in charge of thesis on behalf of the Advisory Committee

Approved: _____
John W. Gillespie Jr., Ph.D.
Co- advisor in charge of thesis on behalf of the Advisory Committee

Approved: _____
Anette M. Karlsson, Ph.D.
Chair of the Department of Mechanical Engineering

Approved: _____
Babatunde A. Ogunnaike, Ph.D.
Interim Dean of the College of Engineering

Approved: _____
Charles G. Riordan, Ph.D.
Vice Provost for Graduate and Professional Education

ACKNOWLEDGMENTS

I would like to express my sincere gratitude and love for my family for always encouraging and supporting me throughout my time at UD.

I would like to thank my advisors, Dr. Suresh Advani and Dr. Jack Gillespie, for their support and guidance during my time at CCM. I have learned a great deal from them during our discussions. They were both essential to the success of this work.

I would like to thank Dr. Travis Bogetti and Dr. John Tierney. Our discussions and their insight throughout my time at CCM were most helpful.

I would also like to thank Jenny Mueller and Steve Koellhoffer, as well as all of the other CCM associates that supported me during my studies at UD.

Finally, I would like to thank the Army Research Laboratory for funding this research through the Composite Materials Research Program.

TABLE OF CONTENTS

LIST OF TABLES	vii
LIST OF FIGURES	viii
ABSTRACT	xiii
 Chapter	
1 INTRODUCTION	1
1.1 Research Motivation.....	1
1.2 Ultrasonic Consolidation (UC).....	1
1.2.1 Role of Plastic Deformation in UC Bonding.....	3
1.2.2 Material Softening Mechanisms.....	4
1.2.2.1 Thermal Softening.....	4
1.2.2.1.1 Frictional Heating (q_{fr})	5
1.2.2.1.2 Volumetric Heating	8
1.2.2.2 Acoustic Softening	9
1.3 Relevant Literature	12
1.4 Thesis Objective	15
1.5 Summary.....	15
1.6 Thesis Outline.....	16
2 THERMO-MECHANICAL MODELING OF ULTRASONIC CONSOLIDATION	18
2.1 Thermal Finite Element Model	19
2.1.1 Boundary Conditions.....	19
2.1.2 Thermal Material Properties.....	20
2.1.3 Frictional Heat (q_{fr}) Calculation	21
2.1.4 Coefficient of Friction (μ) Calculation	23
2.2 Mechanical Finite Element Model	23

2.2.1	Boundary Conditions	23
2.2.2	Mechanical Material Model	26
2.2.3	Acoustic Softening Calculation	28
2.2.4	Volumetric Heat Generation (q_{vol}) Calculation	30
2.2.5	Mesh Refinement Study	31
2.3	Summary.....	33
3	EQUIPMENT, MATERIALS AND EXPERIMENTS	34
3.1	Equipment.....	34
3.1.1	Ultrasonic Welder.....	34
3.1.1.1	UC Weld Parameter Ranges	36
3.1.1.2	Sonotrode.....	36
3.1.1.3	Vise.....	38
3.1.2	Infrared (IR) Camera	39
3.1.2.1	Emissivity Calibration	40
3.2	Weld Materials	43
3.3	Experimental Procedure	45
3.3.1	Temperature Measurement	46
3.3.2	Measurement of Foil Width Increase	50
3.4	Experimental Test Array Results.....	51
3.4.1	Temperature Results	52
3.4.2	Width Increase ($\Delta W/W_0$) Results	56
3.5	Summary.....	57
4	RESULTS AND DISCUSSION.....	58
4.1	Frictional Heat Generation	59
4.1.1	Coefficient of Friction	60
4.2	Acoustic Softening	61
4.3	Thermal Softening	67
4.3.1	Volumetric Heat Generation.....	69

4.4	Contact Length (l_c)	71
4.5	Model Validation.....	75
4.6	Summary.....	78
5	SUMMARY AND FUTURE WORK.....	79
5.1	Overview of the Methodology.....	80
5.2	Future Work.....	81
	REFERENCES	83
Appendix		
A	PRELIMINARY BOND STRENGTH DATA	87
A.1	Experimental Methods.....	87
A.1.1	Peel Testing	87
A.1.2	Optical Microscopy	90
A.2	Relationship Between Bond Area and Peel Strength	90
A.3	Summary.....	94
B	FIGURE REPRINT PERMISSIONS	95

LIST OF TABLES

Table 2.1.	Thermal material properties.	21
Table 2.2.	Temperature dependence of the Al 1100-0 power law constants used in Equation (2.2) and Equation (2.3).	27
Table 3.1.	Range of available UC process parameters on the AmTech seam welder. Peak-to-peak amplitude (λ), clamping force (F_c) and speed (S) are shown.	36
Table 3.2.	Material and geometry of the foils and substrates.	44
Table 4.1.	Acoustic softening constants used in equation (4.3).	64
Table 4.2.	Influence of thermal and acoustic softening during UC on the K term in Equation (2.3).	69
Table 4.3.	Influence of l_c on ξ calculation from Equation (4.3).	74
Table A.1.	Acoustic softening calculated using Equation (4.3) for the process parameters shown in Figure A.6.	94

LIST OF FIGURES

Figure 1.1.	Schematic of the UC process.	2
Figure 1.2.	Friction coefficient trends reported by Koellhoffer et al. (2011) for UC of Al 6061-T6 foils (reproduced with permission).	7
Figure 1.3.	The acoustic softening effect reported by Blaha and Langenecker (1955) of zinc monocrystals in compression. Solid lines are without applied ultrasonic energy and dashed lines are with applied ultrasonic energy (reproduced with permission).	10
Figure 2.1.	Thermal boundary conditions and temperature distribution at time = 1.5 s for a weld with $\lambda = 32 \mu\text{m}$ and $F_c = 1451\text{N}$. The resulting $q_{fr} = 249 \text{ W}$. Units are in degrees Celsius.	20
Figure 2.2.	Experimental temperature measurements for a UC bond with $T_{ss} = 135\text{C}$ from 30 to 60 mm along the length of the weld in the y-direction compared to thermal finite element model temperatures for $q_{fr} = 249 \text{ W}$ from Figure 2.1.	22
Figure 2.3.	Schematic of the mechanical finite element model showing (a) boundary conditions on the sonotrode, (b) F_c and zero y-displacement boundary condition on the foil (c) all boundary conditions on the foil. ...	24
Figure 2.4.	Plastic dissipation (W_p) in the foil as a function of time.	26
Figure 2.5.	Contour plot of model displacements in the foil's width direction (x-direction). The initial foil geometry (left) and processed foil geometry (right) are shown. Units are in meters.	29
Figure 2.6.	Flow chart summarizing the thermo-mechanical modeling process used to quantify acoustic softening.	30
Figure 2.7.	Comparison of $\Delta W/W_0$ for one, two and three elements through the foil's thickness in the mechanical model.	32
Figure 2.8.	Simulation time required to run the mechanical model with one, two and three elements through the foil's thickens.	32

Figure 3.1. (a) schematic and (b) photo of the ultrasonic seam welder built by AmTech.	35
Figure 3.2. Image of the EDM textured sonotrode.....	37
Figure 3.3. SWLI image of the sonotrode’s EDM texture.	38
Figure 3.4. Image of the vise used during UC holding a substrate.	39
Figure 3.5. Schematic of the ultrasonic welder and the IR camera position.	40
Figure 3.6. Image of (a) smooth foil without insulation, (b) textured foil without insulation and (c) textured foil with insulation during emissivity calibration.	41
Figure 3.7. IR image of emissivity calibration of Al 1100-0 foil (a) without insulation and (b) with insulation covering the hot plate. IR reflection is significantly reduced with insulation.	42
Figure 3.8. Plot of emissivity v. temperature for smooth foil without insulation (green), foil with knurl pattern without insulation (red), and foil with knurl pattern and insulation (blue). All plots are for Al 1100-0.....	43
Figure 3.9. Image of the three Al 1100-0 foil geometries used during UC. The dimensions are 9.5mm x 0.52mm (top), 13mm x 0.52mm (middle), and 9.5mm x 1.04mm (bottom).....	45
Figure 3.10. Image of the Al 3003-H14 substrates used during UC (26.5mm x 4.76mm).....	45
Figure 3.11. Initial foil geometry (left) and foil geometry after UC (right). Processed foil has increased in width and knurl pattern has been imprinted on the top of the foil.....	46
Figure 3.12. IR image taken during UC. Temperature measurements are taken across the foil width at the nip point between the sonotrode and the top of the foil.	47
Figure 3.13. Temperature profiles measured across the foil width by the IR camera during UC. Temperature profiles are measured every 10mm along the length of the weld in the y-direction.....	48

Figure 3.14. Maximum measured IR camera temperature at each position along the length of the weld in the y-direction. Error bars indicate the standard deviation in IR camera measurements between the three specimens.	49
Figure 3.15. Image of welded specimen used to calculate average width increase (ΔW) in Image J.	50
Figure 3.16. Maximum IR camera temperature measurements for various amplitudes at each position along the weld length for welds produced at $P_c = 17.0$ MPa.	52
Figure 3.17. Maximum IR camera temperature measurements for various amplitudes at each position along the weld length for welds produced at $P_c = 28.3$ MPa.	53
Figure 3.18. Maximum IR camera temperature measurements for various amplitudes at each position along the weld length for welds produced at $P_c = 45.2$ MPa.	53
Figure 3.19. Maximum IR camera temperature measurements for various amplitudes at each position along the weld length for welds produced at $P_c = 62.0$ MPa.	54
Figure 3.20. Maximum IR camera temperature measurements for various amplitudes at each position along the weld length for welds produced at $P_c = 78.9$ MPa.	54
Figure 3.21. Experimentally measured steady-state temperatures (T_{ss}) for each combination of UC process parameters. Error bars indicate the standard deviation of all maximum temperature measurements in the steady-state region of the weld.	55
Figure 3.22. Experimentally measured Al 1100-0 foil width increases ($\Delta W/W_0$) for each combination of UC process parameters. Error bars indicate the standard deviation in ($\Delta W/W_0$) measurements of the three specimens made at each set of process parameters for each foil geometry.	56
Figure 4.1. q_{fr} as a function of UC process parameters determined using the 9.5 x 0.52mm foil IR camera temperature measurements from Figure 3.21 and the thermal finite element model.	59

Figure 4.2. UC parameter dependent friction coefficients determined using q_{fr} calculations from the 9.5 x 0.52mm foil in Figure 4.1 and equation (2.1).	61
Figure 4.3. Experimentally measured $\Delta W/W_0$ and modeled $\Delta W/W_0$ using three different values of acoustic softening ($\zeta = 0$, $\zeta = 0.17$ and $\zeta = 0.22$) from Equation (2.3). The results shown are from the 9.5 x 0.52mm foil array.	62
Figure 4.4. Acoustic softening of Al 1100-0 as a function of dimensionless amplitude (A) for five values of dimensionless pressure (P) during UC. Data points are calculated using the experimental data from the 9.5 x 0.52mm foil array.	63
Figure 4.5. Plot of acoustic softening values from Figure 4.4 and Equation (4.3) for varying A and P	65
Figure 4.6. Experimentally measured and modeled decrease in the foil's thickness for the 9.5 x 0.52 mm foil array. Error bars indicate the precision of the experimental thickness measurement.	66
Figure 4.7. Comparison of the stress-strain curves of Al 1100-0 with thermal softening (20 C and 198C) and acoustic softening ($\zeta = 1$ and 0.177) calculated using Equation (2.3).	67
Figure 4.8. Volumetric heat generation as a function of amplitude (A) and pressure (P) using $\beta=0.9$ from Equation (1.6).	70
Figure 4.9. Schematic showing the contact length (l_c) during UC.	71
Figure 4.10. A typical contour plot of model displacements in the foil's thickness direction (z -direction). Areas in contact with the sonotrode have displacements in the negative z -direction. l_c is measured in the y -direction. Units are in meters.	72
Figure 4.11. Contact length (l_c) as a function of UC process parameters calculated using the mechanical finite element model.	73
Figure 4.12. Flow chart summarizing the validation model.	75
Figure 4.13. Validation test array for the 13.0 x 0.52mm foils. Experimentally measured $\Delta W/W_0$ is compared to model predictions using ζ values from equation (4.3) as an input to the model.	76

Figure 4.14. Validation test array for the 9.5 x 1.04mm foils. Experimentally measured $\Delta W/W_0$ is compared to model predictions using ζ values from equation (4.3) as an input to the model.	77
Figure 5.1. Flow chart summarizing the steps required to quantify acoustic softening.....	81
Figure A.1. Image of the floating roller peel test fixture.....	88
Figure A.2. Plot of peel strength and temperature vs. weld position for UC bonds created with two different sets of process parameters. The Al 1100-0 foils are 9.5 x 0.52mm.	89
Figure A.3. Optical microscopy image of the surface of the substrate after the peel test. Dark regions in the image were bonded during UC.	90
Figure A.4. Comparison of peel strength and bonded area overlaid onto optical microscopy images of the bonded surface. The entire weld length is shown in (a). The two peaks in peel strength in (a) are focused on in more detail in (b) and (c). The Al 1100-0 foils are 9.5 x 0.52mm.	91
Figure A.5. Plot of peel strength and bonded area vs. weld position for UC bonds created with two different sets of process parameters. The Al 1100-0 foils are 9.5 x 0.52mm.	92
Figure A.6. Plot of peel strength and bonded area for 9.5 x 1.04 mm Al 1100-0 foils.	93

ABSTRACT

Ultrasonic consolidation (UC) is a solid state bonding process in which thin metal foils are bonded under the influence of ultrasonic vibration and pressure. Large parts can be made by placing foils side by side or built up in layers to create thicker parts. Thermal and acoustic softening of metals during UC leads to increased plastic deformation and plays an important role in bond formation. In this work, a thermo-mechanical finite element model is developed to quantify the degree of thermal and acoustic softening occurring in Al 1100-0 foils during UC. The model uses experimentally measured temperatures and changes in the foil's geometry during UC to quantify the amount of thermal and acoustic softening. Acoustic softening is shown to reduce the yield stress of Al 1100-0 by up to 82%. In addition, thermal softening is found to be relatively minor, typically less than 5% of the total material softening. This method to quantify acoustic softening during UC allows for a better overall understanding of the bonding process and will allow for several aspects of the UC bonding process to be improved and optimized.

Chapter 1

INTRODUCTION

1.1 Research Motivation

The purpose of this work is to underline the importance of thermal and acoustic softening during the ultrasonic consolidation (UC) bonding process and to present a method to quantify these softening mechanisms. This work focuses on experimental and thermo-mechanical finite element modeling techniques that are used to quantify acoustic and thermal softening of Al 1100-0 foils during UC. The approach that will be outlined in this work can be generalized to quantify acoustic softening for a wide range of metals that are used in UC. After introducing UC, the factors that influence thermal and acoustic softening and their role in bond formation will be discussed.

1.2 Ultrasonic Consolidation (UC)

UC is a bonding process in which two materials are joined under the influence of ultrasonic vibrations and pressure. A foil and a substrate or multiple foils are bonded together by a sonotrode that applies the ultrasonic vibration and pressure. Three adjustable process parameters influence UC weld properties as shown in Figure 1.1; they are (i) the sonotrode's clamping force (F_c) in the negative z -direction, (ii) the sonotrode's oscillation amplitude (λ) in the x -direction, and (iii) the sonotrode's speed (S) in the y -direction. Typically one would expect stronger UC bonds when λ is high, F_c is high and S is low. A rough knurl pattern on the sonotrode prevents relative

displacement at the sonotrode-foil interface and causes bonding to occur only at the foil-foil or foil-substrate interface. The UC process is illustrated in Figure 1.1.

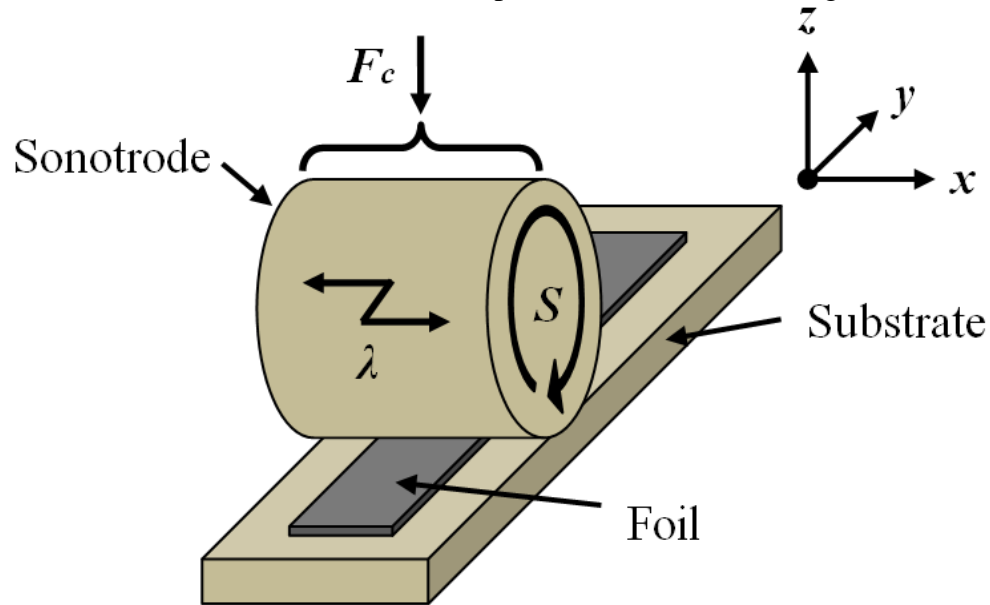


Figure 1.1. Schematic of the UC process.

UC is similar to the automated tape placement (ATP) process used for thermoplastic materials described in detail by Pitchumani et al (1997). Tierney and Gillespie (2006) investigated how the choice of process parameters in ATP will ultimately determine the bond properties and the strength of the final part. Similarly in UC, the choice of process parameters also influences the bond strength. Bonds produced at low λ and F_c are generally weak. On the other hand, bonds produced at high λ and F_c can cause excessive deformations and misalignment in the part, resulting in a poor quality bond. In order to create high strength UC bonds, it is essential to identify the proper weld parameters for a given material and geometry. This was shown by Kong et al. (2003) for Al 6061 and Kong et al. (2004) for Al 3003 where

windows of process parameters were identified for each material which resulted in good bond formation.

UC is a low temperature solid-state bonding process in which thick parts can be fabricated by building up the thickness one layer at a time as discussed by Obielodan et al. (2010). There are many advantages in using UC over other welding techniques. Koellhoffer et al. (2011) measured the temperature of UC using an infrared camera and reported that temperatures during UC are typically less than 50% of the material's melting temperature. Yang et al. (2009) examined the microstructure of UC bonds and found no evidence of melting, indicating that bonding is solid-state and that the materials would retain much of their original microstructure. The low temperature bonding process has the advantage of significantly reducing residual stresses in parts made with UC. The low temperatures of UC also allow thermally sensitive materials to be embedded into structures. A unique benefit to using UC over other welding techniques is that two different materials can be bonded during the process. This was shown by Obielodan et al. (2011) where titanium and aluminum were bonded together.

1.2.1 Role of Plastic Deformation in UC Bonding

The fundamental bonding mechanisms of UC are currently not fully understood; however, plastic deformation is accepted by many, including de Vries (2004), Kong et al. (2005) and Yang et al. (2009), to be an important factor in bond formation during UC. Janaki Ram et al. (2006) found that UC process parameters that resulted in the largest amounts of plastic deformation also had the greatest linear weld density. In their work, linear weld density was determined by investigating a cross

sectional cut of a UC bond and calculating the percent of the material that is bonded together.

Plastic deformation is an important part of the bonding process since it allows the two surfaces to come into intimate contact and aids in breaking apart oxide layers and contaminants. Only once the two materials are in intimate contact can bonding take place and plastic deformation during UC brings more material into intimate contact. Thermal and acoustic material softening are an important part of the UC bonding process since they lead to increased plastic deformations in the foil and consequently could result in higher bond strengths.

1.2.2 Material Softening Mechanisms

As discussed by Siddiq and Ghassemieh (2009), thermal and acoustic softening are important during the UC bonding process. While thermal softening has been well characterized for a wide range of materials, a straightforward method to quantify acoustic softening has not been identified. In this section, thermal softening will first be discussed, followed by acoustic softening. Previous investigations of acoustic softening will be presented and the lack of reliable data on acoustic softening will be highlighted.

1.2.2.1 Thermal Softening

Thermal softening during UC is caused by heat generated due to the friction at the foil-foil or foil-substrate interface and volumetric heat generation due to hysteresis energy loss during cyclic plastic deformation in the foil. These two heating mechanisms are discussed in detail in the following sections.

1.2.2.1.1 Frictional Heating (q_{fr})

Friction heating (q_{fr}) during UC occurs at the interface between the foil and the substrate as the motion of the sonotrode causes the two surfaces to move relative to each other. Many investigations have focused on friction heat generation during UC. Koellhoffer et al. (2011) studied in detail how material selection and UC process parameters influence the coefficient of friction. Similar works by Elangovan et al. (2009), Zhang and Li (2008) and Huang and Ghassemieh (2007) used finite element modeling to investigate temperature fields due to frictional heating during UC and the effect of the resulting thermal softening on UC stress fields.

In the study by Koellhoffer et al. (2011) and in this work, it is assumed that all work done by friction is uniformly dissipated as heat over the area of contact between the metal foil and the substrate. Friction heat generation (q_{fr}) during the UC process is given as the product of the coefficient of friction between the two surfaces (μ), the horn's clamping force (F_c), and the average oscillation speed of the metal foil relative to the substrate (S_{avg}) as follows:

$$q_{fr} = S_{avg}\mu F_c \quad (1.1)$$

S_{avg} is a function of the oscillation frequency (f) and the peak-to-peak oscillation amplitude (λ) and is expressed as:

$$S_{avg} = 2\lambda f \quad (1.2)$$

Equation (1.1) and Equation (1.2) can be combined to show the final expression for q_{fr} as follows:

$$q_{fr} = 2\lambda f\mu F_c \quad (1.3)$$

The coefficient of friction during UC is a function of the process parameters. Previous work on the ultrasonic fretting behavior of aluminum gives some insight into the expected friction coefficient trends that are seen in UC. Naidu and Raman (2005) investigated the friction coefficient trends during ultrasonic fretting of aluminum and the results were confirmed by Koellhoffer et al. (2011) for UC. The coefficient of friction during UC is primarily influenced by λ and F_c . The coefficient of friction will decrease with increasing F_c and increase with increasing λ . Sonotrode speed (S) has little effect on the coefficient of friction. Figure 1.2 shows the described UC coefficient of friction trends that were reported by Koellhoffer et al (2011).

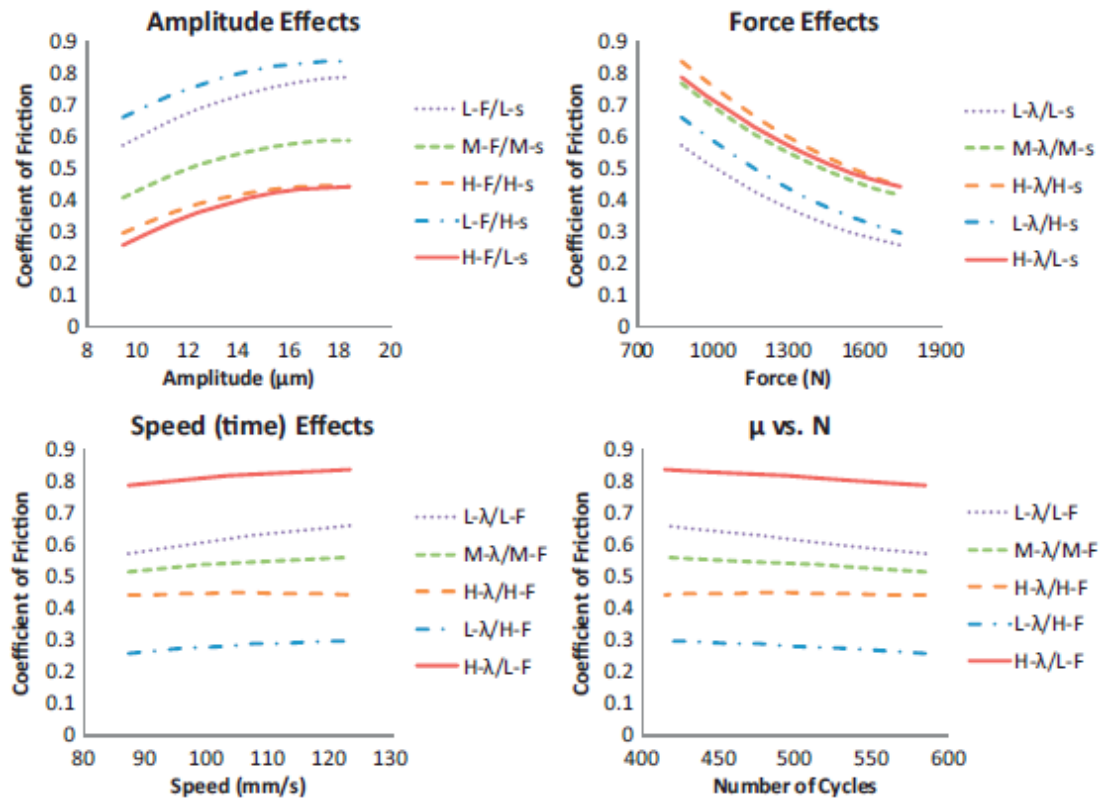


Figure 1.2. Friction coefficient trends reported by Koellhoffer et al. (2011) for UC of Al 6061-T6 foils (reproduced with permission).

In order to study and compare UC of foils with different initial widths (W_0), it is useful to convert clamping force (F_c) to a contact pressure (P_c). P_c is related to the clamping force (F_c), initial foil width (W_0) and contact length (l_c) by Equation (1.4). l_c is defined as the distance in the y -direction that the sonotrode and the foil are in contact during UC. For the purpose of this work, it is assumed that $l_c = 5.4$ mm during all UC process parameters. In reality, l_c will be a function of the UC process parameters and vary slightly. This assumption is examined in more detail in Section 4.4.

$$P_c = \frac{F_c}{W_0 l_c} \quad (1.4)$$

1.2.2.1.2 Volumetric Heating

Volumetric heat generation is typically considered to be small in comparison to friction heat generation for typical process parameters in UC as discussed by Koellhoffer et al. (2011). Volumetric heat generation during UC has been studied by Zhang and Li (2009), but this work did not account for the influence of acoustic softening on the yield stress of the material. In order to calculate volumetric heat generation, plastic work (W_p) must first be calculated. W_p is related to the yield stress (σ_y), the plastic strain rate ($\dot{\epsilon}_p$) and the material volume (V) as follows (Dassault Systems (2009)):

$$W_p = V \int_0^t \sigma_y : \dot{\epsilon}_p dt \quad (1.5)$$

Volumetric heat generation (q_{vol}) is given in equation (1.6) and is related to the plastic work (W_p), a material dependent heat conversion factor (β) and time (t).

$$q_{vol} = \frac{\beta W_p}{t} \quad (1.6)$$

Hodowany et al. (1999) investigated the value of β in equation (1.6) specifically for aluminum. It was found that β is a function of the amount of plastic strain and ranged from approximately $\beta = 0.3$ at low plastic strains up to $\beta = 0.9$ at

higher plastic strains. Once acoustic softening during UC is calculated using the method described in this work, the contribution of volumetric heat generation to thermal softening can be investigated using Equation (1.5) and Equation (1.6).

1.2.2.2 Acoustic Softening

Acoustic softening is the second source of material softening during UC. Pušćár (1982) describes acoustic softening as the reduction in the apparent static stress necessary for plastic deformation in a material under the influence of ultrasonic energy. Acoustic softening was first observed by Blaha and Langenecker (1955) when ultrasonic energy at a frequency of 800 KHz was imposed on zinc monocrystals in compression. The results of this test are shown in Figure 1.3. In Figure 1.3, a compression test with intermittent ultrasonic energy (curve A) and a compression test with constant ultrasonic energy (curve B) are shown. It was found that acoustic softening of the material occurs immediately upon application of the ultrasonic energy and ends immediately upon removal of the ultrasonic energy. In their work, a reduction in yield stress of up to 40% was found.

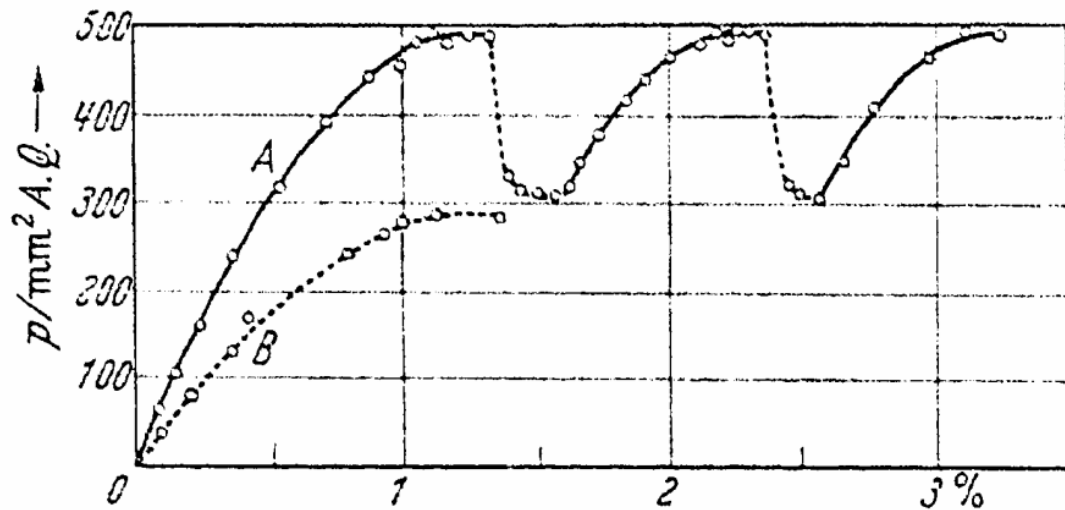


Figure 1.3. The acoustic softening effect reported by Blaha and Langenecker (1955) of zinc monocrystals in compression. Solid lines are without applied ultrasonic energy and dashed lines are with applied ultrasonic energy (reproduced with permission).

Langenecker (1966) performed tension tests on several materials under the presence of ultrasonic irradiation including tungsten, iron, zinc, aluminum and beryllium. All of the materials experienced acoustic softening in the presence of ultrasonic energy. In that work, it was shown that at a sufficient level of ultrasonic energy, the yield stress of a material can effectively be reduced to zero. Kirchner et al. (1984) performed quasi-static compression tests on several aluminum alloys and also reported a similar reduction in yield stress under the presence of ultrasonic energy for a wide range of frequencies. Izumi et al. (1966a) and Izumi et al. (1966b) investigated acoustic softening during ultrasonic irradiation of aluminum, copper, silver, steel, lead and magnesium in compression. Acoustic softening in each material was related to the acoustic impedance, Young's modulus, melting point and the material's work hardenability. It was reported that acoustic softening is more effective in materials

with a high acoustic impedance, a high Young's modulus, a low melting temperature and a low work hardening coefficient.

The fundamental mechanisms of acoustic softening have been investigated by many researchers, but due to the complexity of the process, a clear consensus has not been reached. As discussed by Cai (2006) and Siddiq and Ghassemieh (2008), the two process parameters that control the amount of ultrasonic energy in UC - and therefore the amount of acoustic softening - are the oscillation amplitude (λ) and frequency (f). Langenecker (1966) found that significantly less ultrasonic energy is needed to soften a material than thermal energy, suggesting that the ultrasonic energy must be absorbed primarily by the dislocations of metal grains, rather than uniformly throughout the material like thermal energy. Malygin (2000) investigated stress superimposition as an explanation of the experimentally observed acoustic softening. This stress superimposition theory stated that oscillatory stresses induced by ultrasonic vibrations are added onto the static loading, making the material's yield stress appear lower during experimental measurements. The stress superimposition method is not easy to verify experimentally since detailed dynamic stress profiles within acoustically softened specimens would be required. Cai (2006) investigated stress superimposition through numerical methods by modeling the dynamic stress profiles of metals under the influence of ultrasonic vibrations; however, this work did not consider the influence of dislocations on acoustic softening. Daud et al. (2007) compared a finite element model of acoustic softening effects during tension and compression tests of aluminum with experimental measurements and found that superimposing ultrasonic vibrations on a static load alone does not explain the observed acoustic softening. It was suggested that ultrasonic energy is absorbed by the material and changing the way

it deforms. The acoustic softening study by Daud et al. (2007) was limited to only one amplitude and one frequency.

Izumi et al. (1966) performed compression tests under the influence of ultrasonic irradiation and found a linear relationship between acoustic softening and the amplitude of vibrations for several materials. Equation (1.7) shows the relationship between the measured static yield stress (σ_y), the original yield stress (σ_{y0}), the amplitude (λ) and a material dependant constant (Q). For aluminum, $Q= 0.40 \text{ kg/mm}^3$.

$$\sigma_y = \sigma_{y0} - Q\lambda \quad (1.7)$$

The relationship found by Izumi et al. (1966) does not apply to acoustic softening during UC for two reasons: (i) the ultrasonic vibrations are parallel to the static loading direction, whereas in UC ultrasonic vibrations are perpendicular to static loading and (ii) the sliding surfaces during UC complicate the acoustic softening process, a portion of the input amplitude is absorbed by the material and the rest dissipates at the sliding surface. In addition, amplitudes only up to 20 μm were studied by Izumi et al. (1966), whereas during UC, amplitudes over 40 μm may be needed to create strong bonds.

1.3 Relevant Literature

This section will outline previous works that have focused on thermo-mechanical finite element modeling of UC and UC softening mechanisms. Previous areas of research will briefly be covered and the lack of available of useful information to quantify acoustic softening during UC will be highlighted.

Finite element investigations of UC are useful since experimental studies of the UC bonding process are difficult due to the high frequency of vibrations and short time-scales. Thermo-mechanical modeling of UC has generally focused on the investigation of friction heat generation and its role in thermal softening during UC, the study of stresses at the weld interface and plastic deformation during UC. The vast majority of previous thermo-mechanical finite element studies on the mechanics of UC have not taken into account acoustic softening. Without knowledge of the amount of acoustic softening during UC, stress fields and plastic deformation cannot be accurately modeled.

Doumanidis and Gao (2004) developed a mechanical finite element model to study plastic deformation and stress fields during ultrasonic welding and used it to determine optimum process conditions. It was concluded that plastic deformation was an important part of the bonding process. In their work it was assumed that temperature did not rise significantly and that thermal softening did not take place. Acoustic softening was not included in the model.

The work by Elangovan et al. (2009) is similar to that done by Doumanidis and Gao (2004), but included thermal softening in the analysis. Thermo-mechanical modeling was used to study friction heat generation, volumetric heat generation, temperature distribution, plastic deformation and stresses at the bonding interface during ultrasonic welding. Volumetric and frictional heating were considered to both be important in the bonding process. While material softening due to temperature rise was included in the analysis, acoustic softening was not included.

Zhang and Li (2009) used thermo-mechanical modeling to study the mechanics at the bonding interface during UC. In their work, it was concluded that severe plastic

deformation in the bonding region was responsible for bond formation during UC. A correlation was found between plastic strain from the thermo-mechanical model and experimentally measured bonded area. Weld parameters that produced higher plastic strains also resulted in bonds with higher bonded areas. Acoustic softening was not accounted for in the model and it was concluded that thermal softening at the interface was responsible for the material softening and that thermal softening is an important part of UC bonding.

Bakavos and Prangnell (2010) experimentally studied the mechanisms of bond formation in ultrasonic spot welding and concluded that material softening plays an important role in bond formation. Lap-shear specimens were produced with an ultrasonic welder and processing temperatures were monitored using thermocouples. Specimens that were produced at higher energies experienced the greatest temperature rises, the most plastic deformation and had the highest tensile shear strength. Optical microscopy was used to investigate cross-sections of the bonded interface, and it was seen that welds produced with higher energies had a higher percentage of bonded areas. While it was concluded that material softening was important to the bonding process, only thermal material softening was considered.

The thermo-mechanical model of UC by Siddiq and Ghassemieh (2008) included many important bonding factors including thermal softening, acoustic softening, friction and plasticity. While acoustic softening is included in the analysis, the work investigated a small range of process parameters and was only compared to a small set of experimental acoustic softening data by Langenecker (1966) that was not specific to UC. This work is not sufficient to establish an understanding of the

relationship between UC process parameters (λ , F_c), material selection, material geometry and the amount of acoustic softening.

1.4 Thesis Objective

The vast majority of previous works on acoustic softening have investigated the mechanisms behind the experimentally observed softening in tension and compression specimens. There is limited data on methods to quantify acoustic softening under any type of ultrasonic vibration and even less that is specifically related to UC. In addition, previous attempts to quantify acoustic softening have been limited to a small range of process conditions. A method to quantify acoustic softening over a wide range of process parameters is especially important for UC, since many different process parameters are used to create bonds with varying properties. The goal of this work is to evaluate in detail how varying UC process parameters influence acoustic softening. A method to quantify acoustic softening under UC conditions will allow for a better overall understanding of the UC bonding process.

1.5 Summary

Ultrasonic consolidation is a low temperature bonding process in which materials are bonded by ultrasonic vibrations and pressure. Plastic deformation and material softening are an important part of the bonding process since they bring material into intimate contact and facilitate bonding. Acoustic softening is known to play a significant role in materials under the influence of ultrasonic energy, but limited data exists to quantify the extent of acoustic softening during UC. The objective of this work is to develop a method to quantify acoustic softening during UC that can be used

to characterize acoustic softening under a wide range of process parameters, materials and geometries.

1.6 Thesis Outline

In Chapter 2, the thermo-mechanical finite element modeling process is presented that is used to quantify acoustic softening during UC. A thermal finite element model is used to determine frictional heating (q_{fr}) and the coefficient of friction (μ) during UC. Boundary conditions and the material properties used in the thermal model are presented. A mechanical model is presented that is used to calculate the percent acoustic softening (ξ) that occurs under a given set of UC process parameters. All boundary conditions used in the mechanical finite element model are presented. The material model used in the mechanical finite element model accounts for both thermal and acoustic softening during UC. A method to calculate volumetric heat generation (q_{vol}) during UC is also presented. Finally, a mesh refinement study is used to ensure that the mechanical model is accurately predicting deformations in the foils during UC.

In Chapter 3, the equipment, materials, experiments and experimental results are described. The UC equipment and its capabilities are described along with the infrared camera that is used to measure temperatures. The importance of IR camera emissivity calibration is shown. An experimental test array is identified and UC process parameters are chosen that result a wide range of bond qualities. The experimental data that is collected during UC are weld temperature measurements using an infrared camera and geometry change measurements of foils processed during UC. The temperature and foil geometry change data collected in this section

are used in the thermo-mechanical modeling of UC to quantify the amount of acoustic softening.

In Chapter 4, the results of the thermo-mechanical modeling and experimental measurements are presented. Frictional heat generation and coefficient of friction results from the thermal finite element model are shown. Acoustic softening and volumetric heat generation are quantified using experimental results and the mechanical finite element model. Acoustic softening is found to be a function of amplitude and contact pressure. Thermal softening is shown to be relatively minor compared to acoustic softening during UC. An overview of the methodology used to quantify acoustic softening is presented.

In Chapter 5, a summary of the work is presented and conclusions are made. An outline summarizing the procedure used in this work to quantify acoustic softening during UC is presented. Finally, several areas of future work are suggested.

Chapter 2

THERMO-MECHANICAL MODELING OF ULTRASONIC CONSOLIDATION

The amount of acoustic and thermal softening occurring during UC is quantified in this work using thermo-mechanical finite element modeling in Abaqus 6.9-2 by Dassault Systems (2009). The two material attributes that are needed in order to predict the temperature field and the deformation field as a function of the UC process parameters are the coefficient of friction between the foil and the substrate and a constitutive equation describing the yield stress behavior due to UC process parameters. The friction coefficient can be determined independently by choosing a value of frictional heat (q_{fr}) that when input into the thermal finite element model, predicts a steady state temperature that matches the experimentally measured steady state temperature. When q_{fr} is calculated, the friction coefficient between the foil and the substrate can be found using Equation (1.3). Once the friction coefficient is established for a given set of UC process parameters, an acoustic softening parameter (ζ) can be selected in the constitutive equation describing the yield stress in the mechanical finite element model to match the experimentally measured change in the width of the foil. The thermal and mechanical finite element models are described in detail in the following sections.

2.1 Thermal Finite Element Model

2.1.1 Boundary Conditions

A 2D thermal finite element model is used to solve the frictional heat (q_{fr}) that is produced during UC under a given set of process parameters. The thermal model, created in Abaqus 6.9-2, uses 4,479 six-node quadratic triangular elements. The entire cross section of the foil and the substrate are modeled, but only a portion of the sonotrode is modeled to improve computational efficiency since the sonotrode is very large in comparison to the foil and the substrate. In order to ensure that the size of the modeled sonotrode region does not affect the temperature distribution, a sufficiently large portion of the sonotrode is modeled such that there is no heat flux through the boundary. A fixed temperature boundary condition is applied to the edges of the sonotrode and the edges of the substrate in contact with the vise. All surfaces exposed to air have been modeled using a convection boundary condition with a convective heat transfer coefficient of $h = 5 \text{ W/m}^2\cdot\text{C}$ and a $T_{\infty} = 20\text{C}$. The value of h was varied from $2 - 15 \text{ W/m}^2\cdot\text{C}$ and it was seen that it did not influence the temperature distribution in the foil. Perfect thermal conductance is assumed at the sonotrode-foil and substrate-foil interfaces. The frictional heat (q_{fr}) is applied at the substrate-foil interface. The thermal finite element model's boundary conditions and a typical temperature distribution are shown in Figure 2.1.

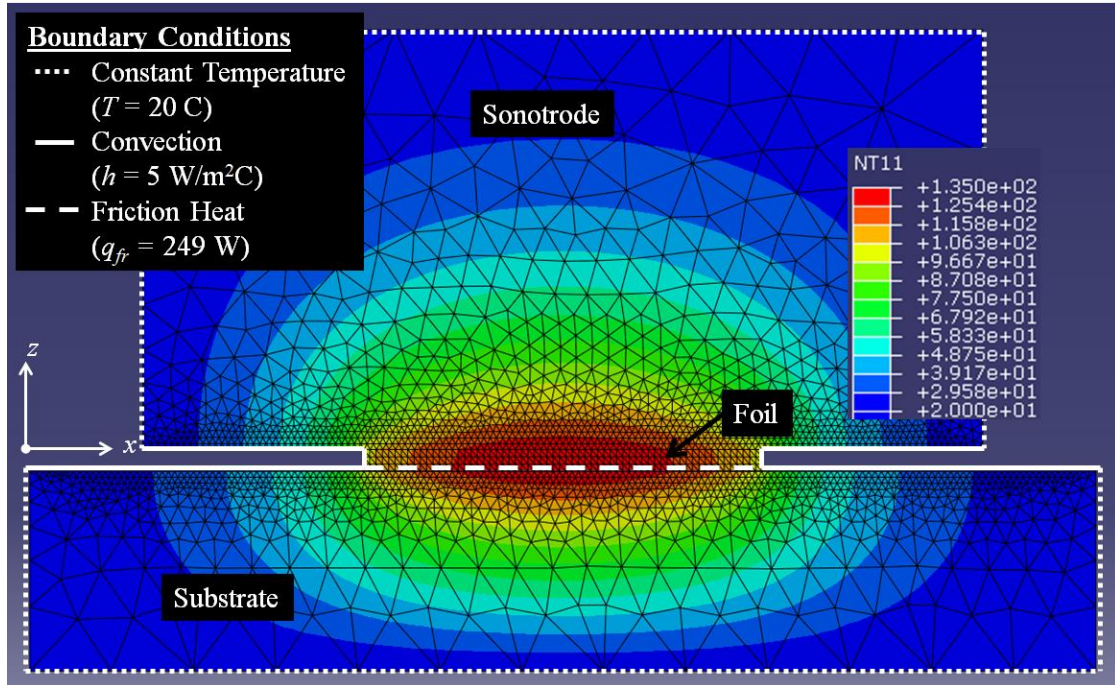


Figure 2.1. Thermal boundary conditions and temperature distribution at time = 1.5 s for a weld with $\lambda = 32\ \mu\text{m}$ and $F_c = 1451\text{N}$. The resulting $q_{fr} = 249\text{ W}$. Units are in degrees Celsius.

2.1.2 Thermal Material Properties

Table 2.1 summarizes the material properties used in the thermal finite element analysis. The three required material properties are the thermal conductance (k), density (ρ) and specific heat (c). The substrate is modeled using Al 3003-H14 properties, the sonotrode is modeled using Ti-6Al-4V properties and the foil is modeled using Al 1100-0 properties.

Table 2.1. Thermal material properties.

Material	k (W/m·C)	ρ (kg/m³)	c (J/kg·C)
Al 1100-0	237	2,700	898
Al 3003-H14	159	2,730	893
Ti-6Al-4V	17	4,500	528

2.1.3 Frictional Heat (q_{fr}) Calculation

The thermal finite element model is used to determine the frictional heat (q_{fr}) generated between the foil and the substrate during UC. In this work, it is assumed that q_{fr} is distributed evenly over the entire contact area between the foil and the substrate. q_{fr} is a function of the UC process parameters, so it must be calculated for each set of weld parameters. The measured steady-state temperature (T_{ss}) during a weld is used in combination with the 2D thermal model to determine the q_{fr} generated during the weld. The thermal model is executed for 1.5 seconds (equal to the time it takes the sonotrode to travel down the length of the 60 mm weld at 40 mm/s). For each set of process parameters, an increasing value of heat input of q_{fr} is imposed at the interface between the foil and the substrate until the error between the experimental steady state temperature and the predicted values from the thermal finite element model are

minimized. The q_{fr} value for minimized error between the steady state values can then be used to compare the entire temperature profile of the model and experimental measurements. Figure 2.2 shows experimentally measured temperatures for a weld with $T_{ss} = 135\text{C}$ and modeled temperatures with $q_{fr} = 249\text{ W}$. It can be seen that $q_{fr} = 249\text{ W}$ accurately predicts the value and location of T_{ss} .

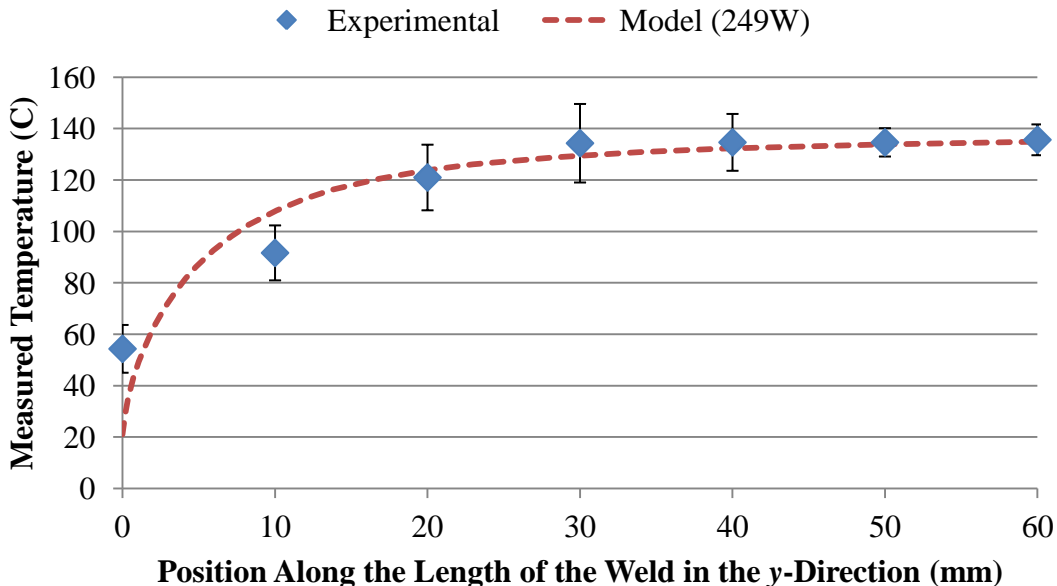


Figure 2.2. Experimental temperature measurements for a UC bond with $T_{ss} = 135\text{C}$ from 30 to 60 mm along the length of the weld in the y-direction compared to thermal finite element model temperatures for $q_{fr} = 249\text{ W}$ from Figure 2.1.

q_{fr} can be calculated for any given set of process parameters based on experimentally measured temperatures.

2.1.4 Coefficient of Friction (μ) Calculation

The q_{fr} that gives the minimum error between the temperature predicted from the thermal finite element model and the experimental temperature measurements for the selected UC parameters is used to find the UC parameter dependent friction coefficient (μ). Equation (1.3) is rearranged as follows to solve for μ :

$$\mu = \frac{q_{fr}}{2\lambda f F_c} \quad (2.1)$$

μ can be calculated for any given set of process parameters and is used as an input to the mechanical finite element model discussed in the next section. For example, the coefficient of friction for the weld shown in Figure 2.1 and Figure 2.2 is $\mu = 0.134$, since $q_{fr} = 249\text{W}$, $\lambda = 32 \mu\text{m}$, $f = 20 \text{ kHz}$ and $F_c = 1451\text{N}$.

2.2 Mechanical Finite Element Model

2.2.1 Boundary Conditions

The 3D mechanical finite element model of UC used in this work was created in Abaqus 6.9-2 (Dassault Systems (2009)) and uses the explicit solver. Figure 2.3 summarizes the boundary conditions of the mechanical finite element model.

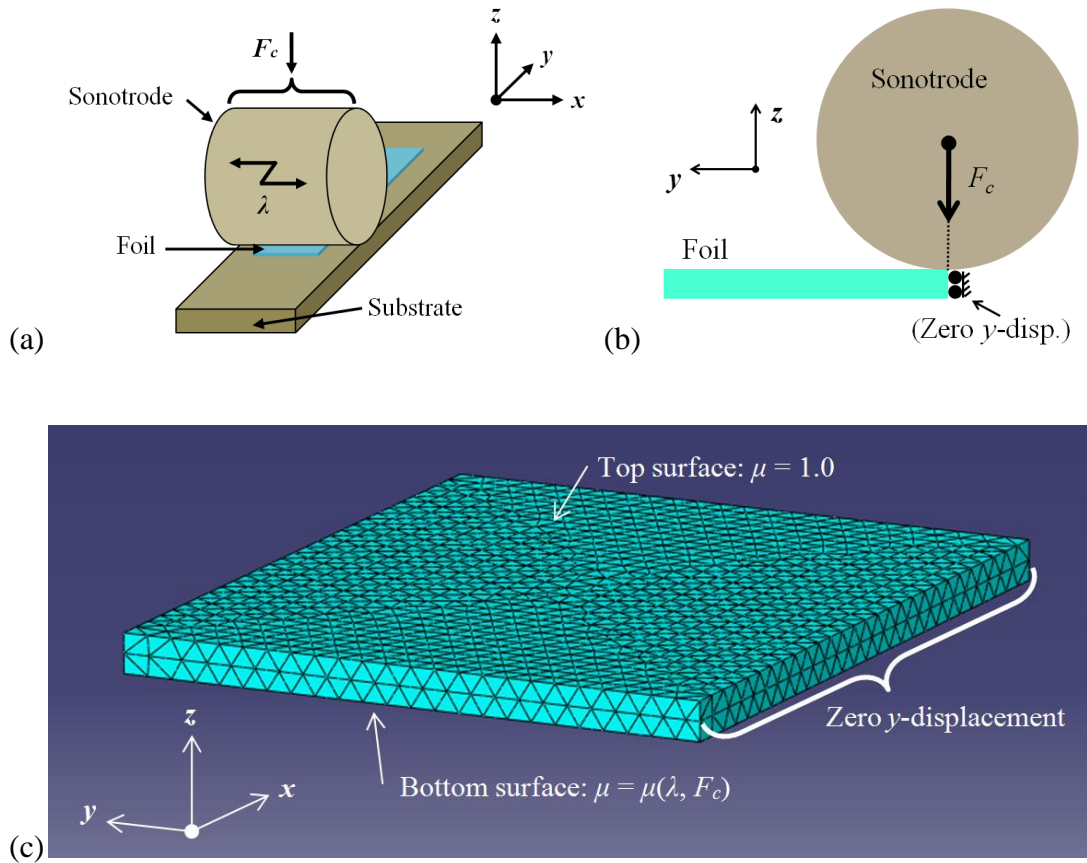


Figure 2.3. Schematic of the mechanical finite element model showing (a) boundary conditions on the sonotrode, (b) F_c and zero y -displacement boundary condition on the foil (c) all boundary conditions on the foil.

In Figure 2.3 (a), the sonotrode and substrate are modeled as rigid bodies since both materials have a much higher yield stress than the Al 1100-0 foil. The following boundary conditions apply to the sonotrode: λ in the x -direction and F_c in the negative z -direction. The sonotrode is allowed zero displacement in the y -direction and is free to displace in the z -direction. Zero rotation is assigned to the sonotrode in the x -, y -

and z -directions. The substrate is assigned an encastre boundary condition (zero displacements and rotations in all directions).

In Figure 2.3 (c), the Al 1100-0 foil is modeled with 10-node quadratic tetrahedron elements (C3D10M). In order to improve computational efficiency, only an 8 mm length of the foil is modeled rather than the full 60 mm weld length. Surface-to-surface boundary conditions are defined on the top and the bottom of the foil using the penalty contact method. Tangential contact between the sonotrode and the top of the foil is defined using a penalty friction formulation with a friction coefficient of 1.0, preventing relative motion between the sonotrode and top of the foil. This coefficient of friction was ranged from 0.5 to 1.5 and no influence on the results was seen. Tangential contact between the substrate and the bottom of the foil is also defined using a penalty friction formulation. The friction coefficient used in the mechanical model at the foil-substrate interface is calculated using the thermal model and the experimental temperature measurements. This procedure was described in detail in Section 2.1. A zero y -displacement boundary condition is assigned to one edge of the foil to match what occurs physically during the UC process: regions of the foil that sonotrode has previously bonded will no longer be able to displace in the y -direction.

To increase computational efficiency, the model is executed for a time period of only 0.001 seconds. This time period was chosen after running the model and observing the time required for the amount of plastic deformation in the foil to plateau. The time required for the plastic deformation to plateau varies with oscillation amplitude, clamping force and the material properties of the tape. W_p in the foil reaches a plateau when the applied normal and shear stresses imposed on the foil become equal to the strain-hardened yield stress of the material. Figure 2.4 shows a

typical plateau in plastic work (W_p) from Equation (1.5) calculated in the mechanical finite element model.

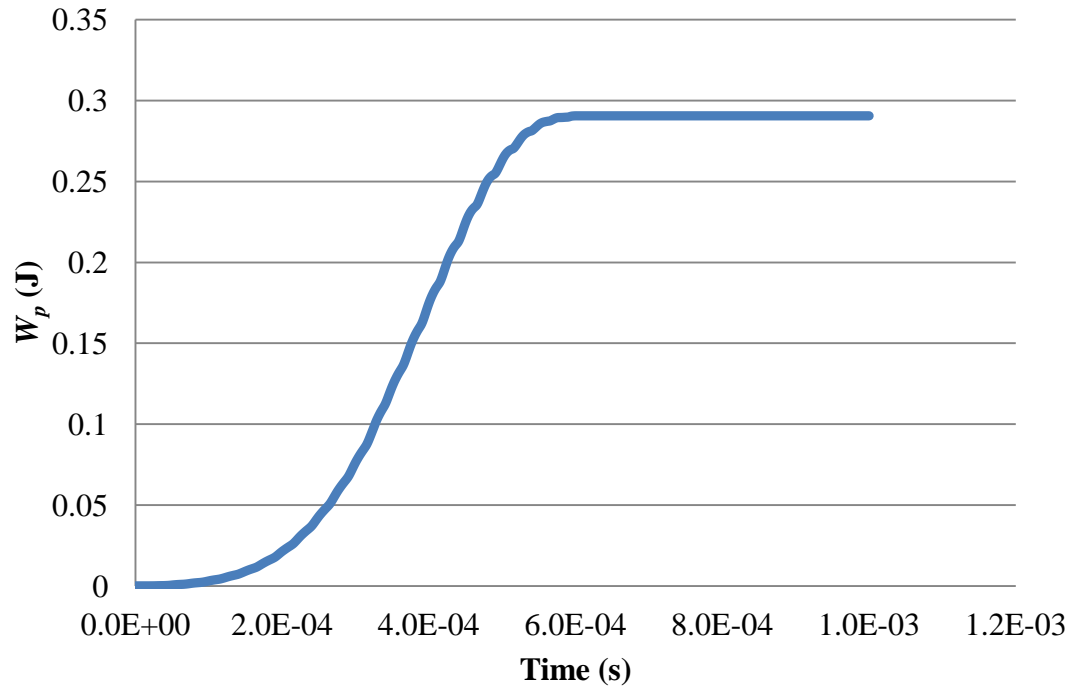


Figure 2.4. Plastic dissipation (W_p) in the foil as a function of time.

The time period of 0.001 seconds is enough to capture all plastic deformation in the three foil geometries for each combination of UC process parameters investigated in this work. The sonotrode speed (S) in the y -direction is ignored in the simulation since it has no effect on the amount of deformation in the x -direction in the foil.

2.2.2 Mechanical Material Model

In order to model the width increase of Al 1100-0 foils during UC, a material model is required that accounts for thermal softening, acoustic softening, and strain

hardening. The relationship between yield stress, strain and temperature has been studied for Al 1100-0 in compression. Strain hardening behavior of Al 1100-0 is observed along with thermal softening. As reported by Hockett (1967), the stress-strain curve of Al 1100-0 at a given temperature can best be represented in the plastic region by the law power equation shown in Equation (2.2).

$$\sigma_y = K \varepsilon_p^n \quad (2.2)$$

In order to capture the effect of temperature on the yield stress of Al 1100-0, Hockett (1967) identified a series of constants for the power law model at different temperatures. These constants are shown in Table 2.2.

Table 2.2. Temperature dependence of the Al 1100-0 power law constants used in Equation (2.2) and Equation (2.3).

Temperature (C)	K (MPa)	n
20	157.8	0.213
180	123.4	0.201
380	60.4	0.136

Linear interpolation is used to calculate the values of K and n at temperatures between those listed in Table 2.2. The power law model presented by Hockett (1967) is modified in this work to account for acoustic softening during UC. A percent acoustic softening term (ζ) is added to Equation (2.2) to account for acoustic softening. This term ranges from zero to one, depending on the amount of acoustic softening. At a value of $\zeta = 1$, there is no acoustic softening in the material and it will deform normally. At a value of $\zeta = 0$, there is sufficient ultrasonic energy to reduce the yield stress of the material to zero. Equation (2.3) shows the power law equation including the percent acoustic softening term (ζ).

$$\sigma_y = \zeta K \varepsilon_p^n \quad (2.3)$$

For the purpose of this work, it is assumed that acoustic softening linearly affects the K term in the power law equation and that the n term remains unchanged by acoustic softening since the K term is primarily responsible for significant changes in σ_y .

2.2.3 Acoustic Softening Calculation

In order to quantify the amount of acoustic softening during a UC weld, the value of ζ in Equation (2.3) is incrementally decreased until the error between the foil's width increase in the mechanical model and the experimental measurements for a given set of UC process parameters is minimized. Figure 2.5 shows a typical contour plot of modeled foil deformations before and after UC processing.

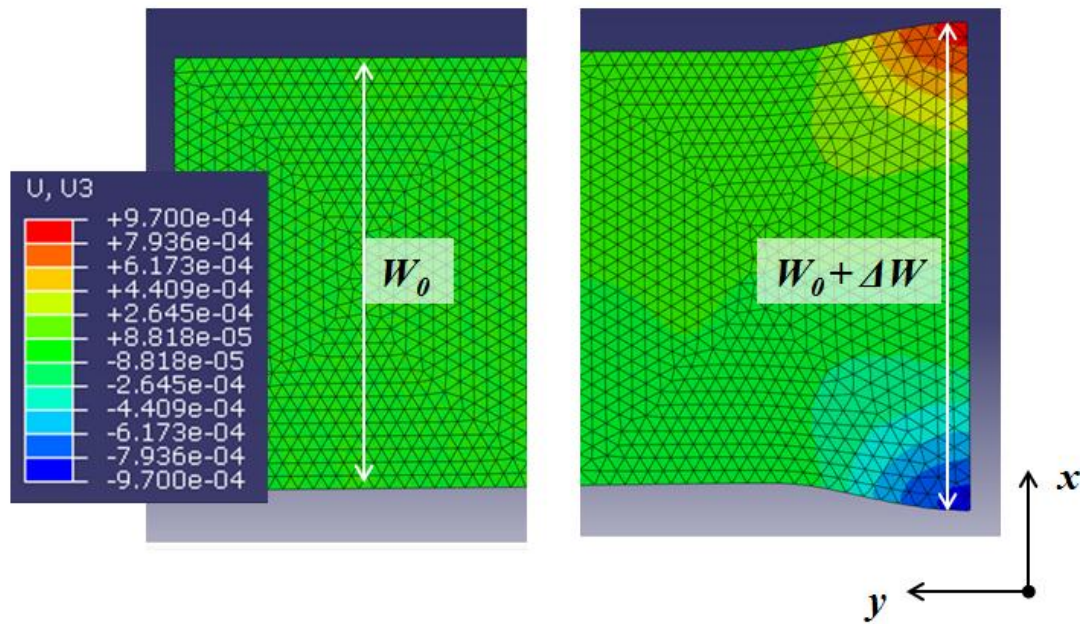


Figure 2.5. Contour plot of model displacements in the foil's width direction (x -direction). The initial foil geometry (left) and processed foil geometry (right) are shown. Units are in meters.

A flow chart summarizing the all of the steps involved in the thermo-mechanical modeling process can be seen in Figure 2.6.

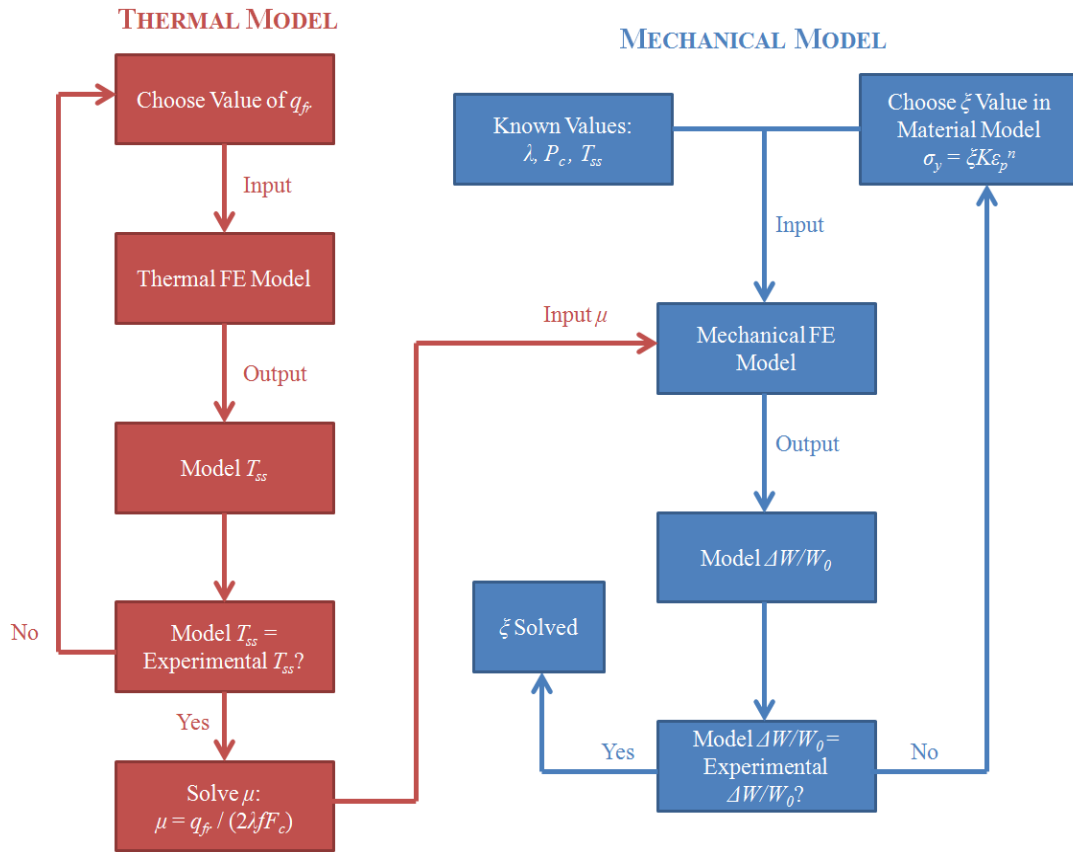


Figure 2.6. Flow chart summarizing the thermo-mechanical modeling process used to quantify acoustic softening.

2.2.4 Volumetric Heat Generation (q_{vol}) Calculation

Plastic work (W_p) calculated by the mechanical finite element model and shown in Figure 2.4 can be used to calculate volumetric heat generation (q_{vol}) according to equation (1.6). The time (t) used in this calculation is equal to the contact length (l_c) divided by the sonotrode speed (S). The material dependent heat conversion factor (β) used in this work for Al 1100-0 is 0.9 as reported by Hodowany et al. (1999). The final expression for q_{vol} is as follows:

$$q_{vol} = \frac{\beta W_{pl} S}{l_c} \quad (2.4)$$

2.2.5 Mesh Refinement Study

A mesh refinement study of the mechanical finite element model shows that two elements through the foil thickness are sufficient to capture accurate foil deformations. The study was conducted under process parameters that result in a relatively large amount of plastic deformation ($\lambda = 36 \mu\text{m}$, $P_c = 45.2 \text{ MPa}$). Since the Abaqus Explicit solver is used in this work, the number of elements through the foil's thickness has a significant influence on the time required to run the model because with decreased element size there are more nodes and a smaller stable time increment. This combination results in a simulation with both an increased number of iterations and a longer simulation time per iteration. Figure 2.7 shows that the mesh is sufficiently refined when there are two elements through the foil's thickness. Figure 2.8 shows that increasing from one to two elements through the thickness does not significantly increase simulation time. Three elements through the foil thickness is not more accurate and adds significant time to the simulation.

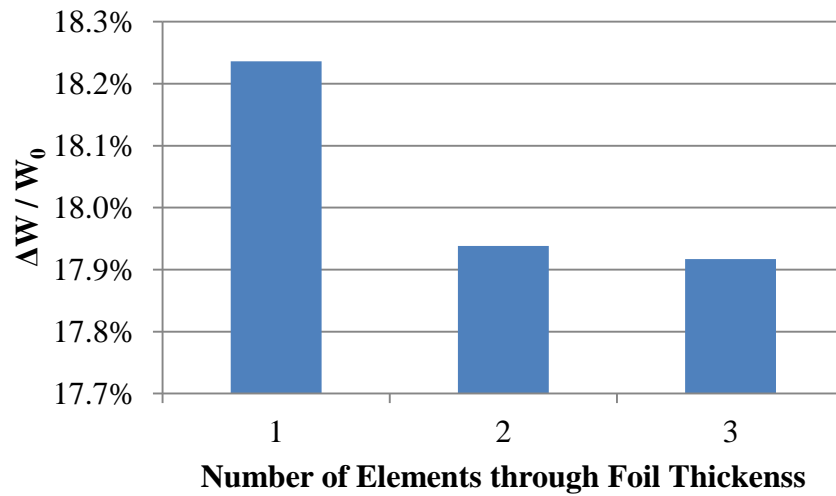


Figure 2.7. Comparison of $\Delta W / W_0$ for one, two and three elements through the foil's thickness in the mechanical model.

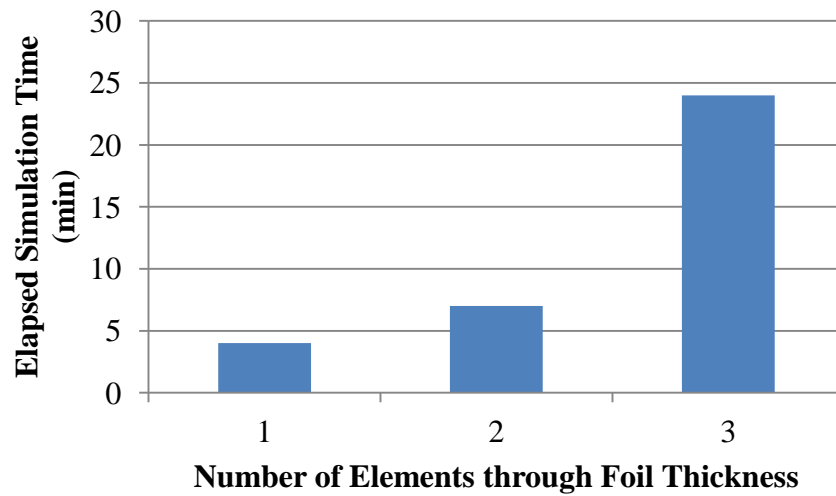


Figure 2.8. Simulation time required to run the mechanical model with one, two and three elements through the foil's thickness.

2.3 Summary

In this chapter, finite element models are described that allow thermal and acoustic softening to be quantified. The finite element models utilize the experimental data collected according to the procedure described in the next chapter. The thermal model is used to calculate the coefficient of friction during UC based on experimentally measured temperatures. The mechanical model is used to quantify acoustic softening based on experimentally measured geometry change measurements ($\Delta W/W_0$).

Chapter 3

EQUIPMENT, MATERIALS AND EXPERIMENTS

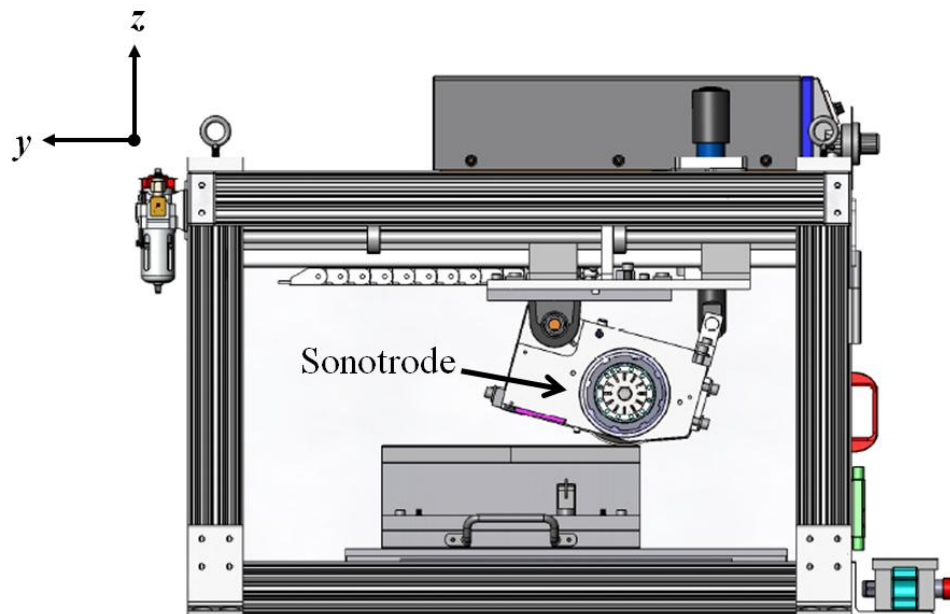
In this chapter, the equipment, materials, and experimental procedure are presented that are used to create the UC bonds that are investigated in this work. After discussing the equipment, materials and the experimental procedure used, experimental results for a selected array of UC bonds are presented. This experimental procedure covers all of the required experimental data required to quantify the amount of acoustic softening, frictional heating and volumetric heating that occurs during the UC process.

3.1 Equipment

3.1.1 Ultrasonic Welder

The UC equipment used in this work is a seam welder custom built by AmTech. A schematic of the welder can be seen in Figure 3.1. The welder's amplitude (λ) is in the x -direction, the clamping force (F_c) is in the negative z -direction, and the sonotrode travels at a speed (S) down the length of the weld in the y -direction. The welder is capable of producing both seam welds and spot welds by reducing S to zero.

(a)



(b)

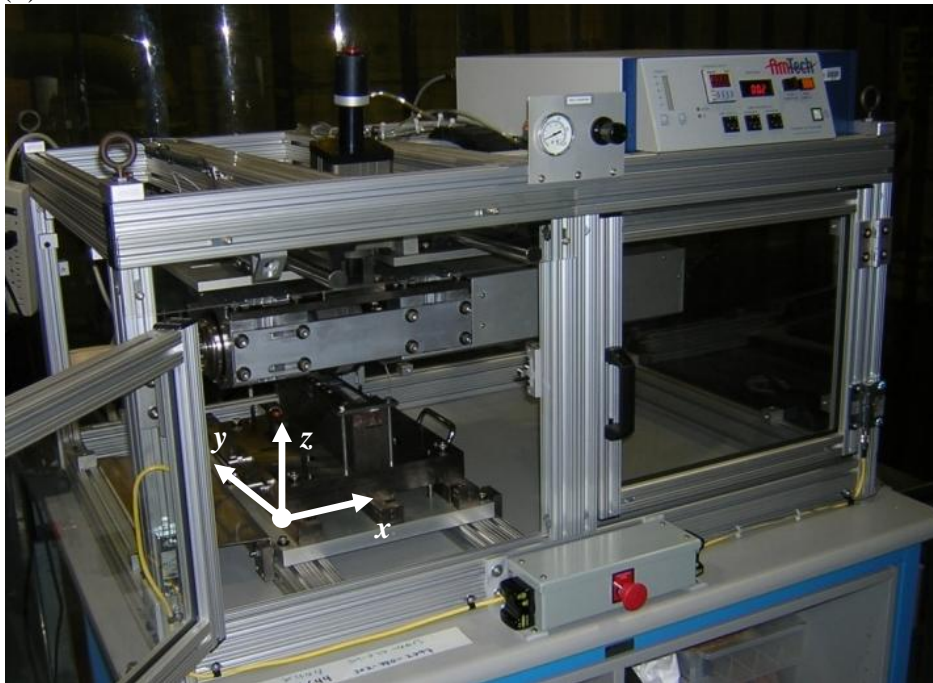


Figure 3.1. (a) schematic and (b) photo of the ultrasonic seam welder built by AmTech.

3.1.1.1 UC Weld Parameter Ranges

Weld quality is controlled by adjusting the three process parameters shown in Figure 1.1: the sonotrode's clamping force (F_c), peak-peak oscillation amplitude (λ) and speed (S). The minimum and maximum values of these three parameters are shown in Table 3.1. The available weld parameters allow a wide range of weld qualities to be produced. The frequency (f) of the welder is a constant 20 kHz, which is typical for many UC systems. The welder keeps the amplitude constant throughout the weld by automatically adjusting the power based on loading conditions. In general, stronger bonds are produced when λ is high, F_c is high, and S is low; however, the geometry and type of material being welded play an important role in choosing weld parameters.

Table 3.1. Range of available UC process parameters on the AmTech seam welder. Peak-to-peak amplitude (λ), clamping force (F_c) and speed (S) are shown.

	λ (μm)	F_c (N)	S (mm/s)
Parameter Range	7 – 44	300 - 6,000	0 - 300

3.1.1.2 Sonotrode

The knurl pattern on the welder's Ti-6Al-4V sonotrode is made using an electric discharge machining (EDM) technique and has a diameter of 147 mm. An image of the EDM sonotrode can be seen in Figure 3.2. An image of the EDM texture on the sonotrode was taken using a scanning white light interferometer (SWLI) and

can be seen in Figure 3.3. It can be seen that the EDM texture is non-uniform. The peak-valley surface roughness of the portion of the sonotrode seen in Figure 3.3 is $69\ \mu\text{m}$ and the root mean square surface roughness is $7\ \mu\text{m}$.



Figure 3.2. Image of the EDM textured sonotrode.

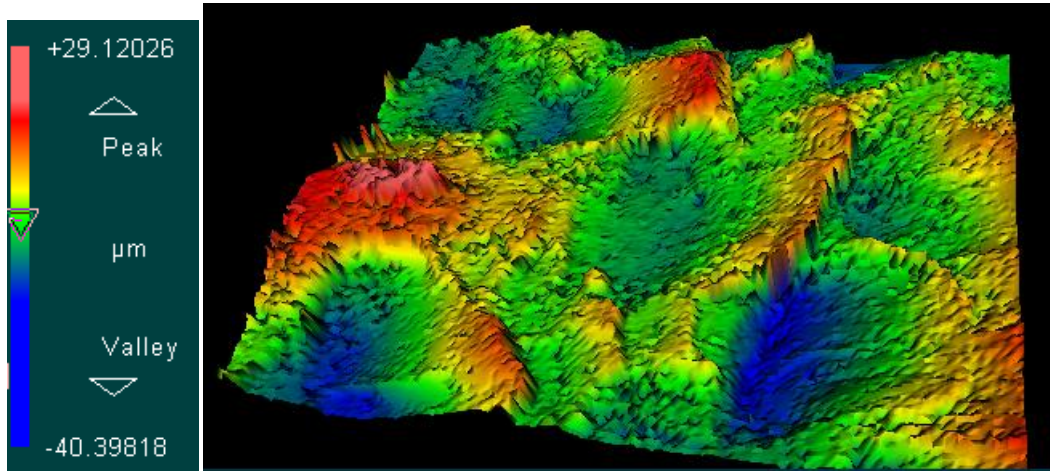


Figure 3.3. SWLI image of the sonotrode's EDM texture.

3.1.1.3 Vise

The substrate, seen in Figure 1.1, is held in place using a Wilton DPV/80 super precision sine vise. The vise is used to reduce resonance effects in the substrate, which can occur with bolted substrates and leads to inconsistent weld quality and properties as discussed by Koellhoffer (2011). Zhang and Li (2010) have also shown that resonance in the substrate influences bond quality. The vise supports the substrate along the entire weld length, reducing any resonance effects. The maximum weld length that can be created with the vise is 3-3/16", equal to the width of the vise's jaws. The vise can be mounted in different positions within the ultrasonic welder to accommodate materials of different geometries. The vise used in this work to secure the substrate during UC can be seen in Figure 3.4.



Figure 3.4. Image of the vise used during UC holding a substrate.

3.1.2 Infrared (IR) Camera

An infrared (IR) camera is used to monitor the temperature at which UC bonds are produced. There are several advantages in monitoring UC temperatures with an IR camera over other methods. The IR camera allows great flexibility in location and special resolution of measurements. Another method to measure UC temperatures, discussed by Sriraman et al. (2011), uses thermocouples. This method has three distinct disadvantages when compared to using an IR camera: (i) one thermocouple is required for each data point, (ii) placing a thermocouple between weld materials will alter the weld properties at that location and (iii) the thermocouple cannot be reused afterwards.

The IR camera used in this work is a FLIR ThermoVision Alert 194 and records images at 4 Hz. During each weld, the camera is placed 22" from the weld in the y-direction and 2" above the weld in the z-direction. Weld temperatures are

recorded throughout the entire weld process and the data is used to identify thermally transient and steady-state regions along the length of the weld. This work focuses entirely on weld areas at steady-state temperatures. The position of the IR camera relative to the ultrasonic welder is shown in Figure 3.5.

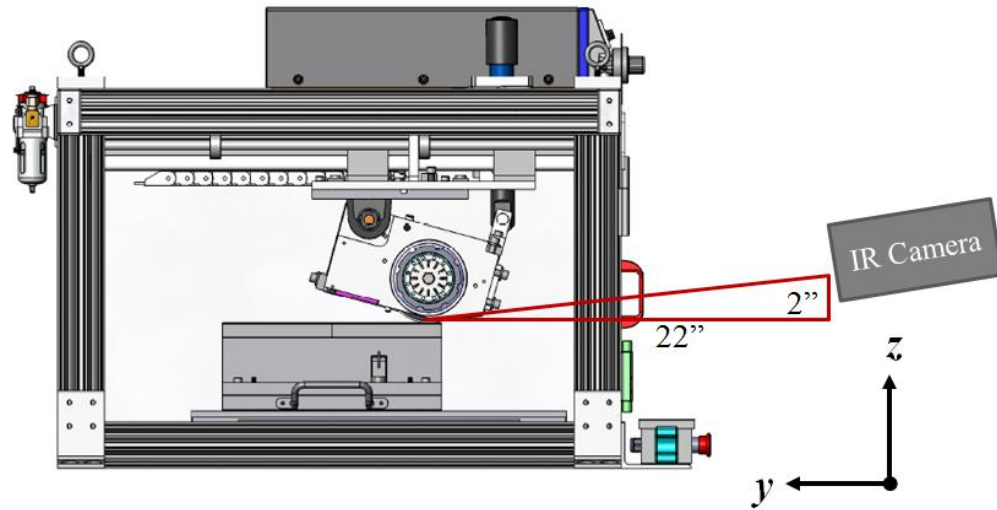


Figure 3.5. Schematic of the ultrasonic welder and the IR camera position.

3.1.2.1 Emissivity Calibration

In order to gather accurate temperature data from the IR camera during UC, the emissivity of the weld materials must be determined. Emissivity is calibrated over a wide temperature range. Temperatures up to approximately 300C are achieved during calibration using a hot plate while a thermocouple is used to monitor temperatures. During emissivity calibration, the camera is placed in the same position shown in Figure 3.5 to ensure accuracy while monitoring temperatures during UC.

During UC, the IR camera measures temperatures of the foil after it has been imprinted with the knurl pattern; therefore, it is important to determine how the

change in surface roughness during UC changes the emissivity of the foil. It is also important to know how IR reflections due to the hot plate during calibration affect the emissivity calibration of the foils. To investigate these two effects, the emissivity of the Al 1100-0 foils used in this work is calibrated on the hot plate in three different configurations: (i) smooth foil on a substrate, (ii) foil imprinted with the knurl pattern on a substrate and (iii) foil imprinted with the knurl pattern on a substrate with insulation covering the hot plate. The insulation reduces IR reflections from the hot plate and results in a more accurate emissivity calculation. These three configurations can be seen in Figure 3.6.

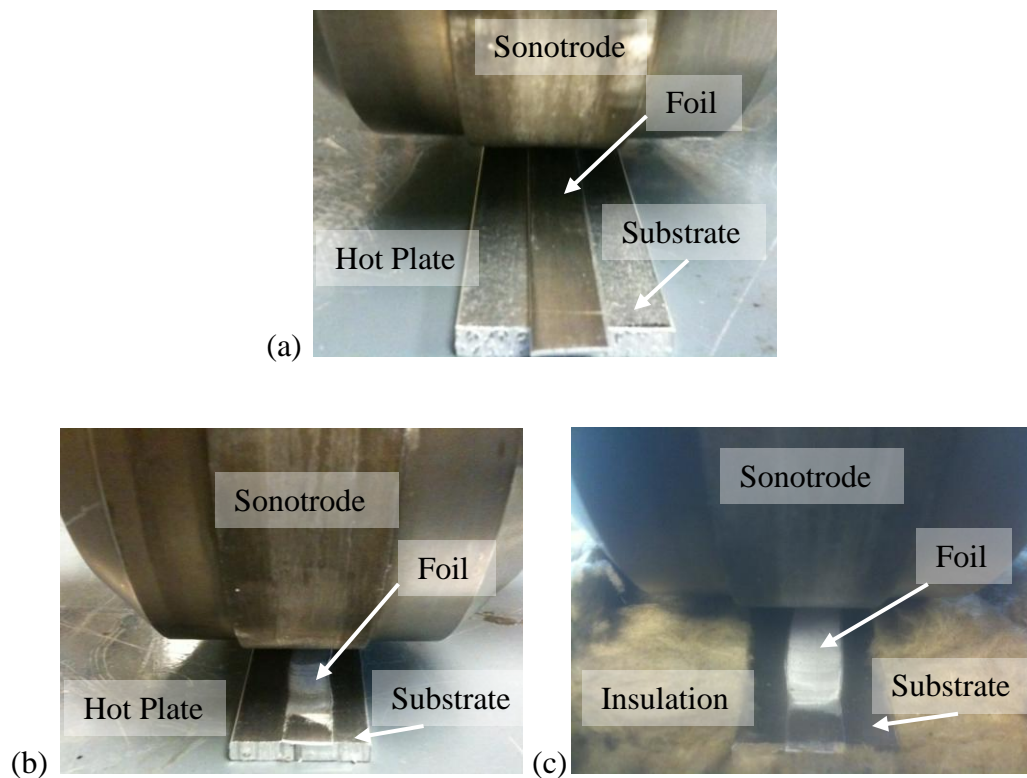


Figure 3.6. Image of (a) smooth foil without insulation, (b) textured foil without insulation and (c) textured foil with insulation during emissivity calibration.

Figure 3.7 shows IR images taken during calibration with and without insulation. It can clearly be seen that the added insulation reduces the amount of IR reflections from the hot plate. Figure 3.8 shows emissivity as a function of temperature for each of the three calibration set-ups shown in Figure 3.6. The foil textured with the knurl pattern and with insulation is most similar to UC, so this emissivity was used to determine temperatures during UC.

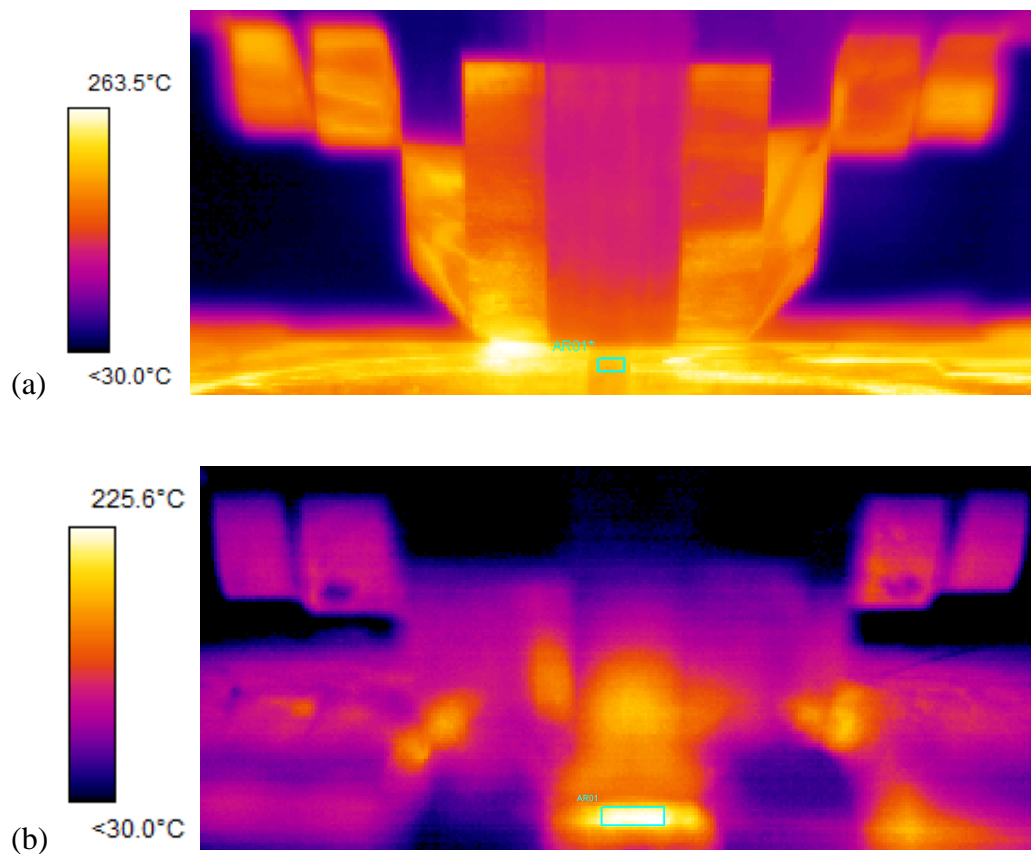


Figure 3.7. IR image of emissivity calibration of Al 1100-0 foil (a) without insulation and (b) with insulation covering the hot plate. IR reflection is significantly reduced with insulation.

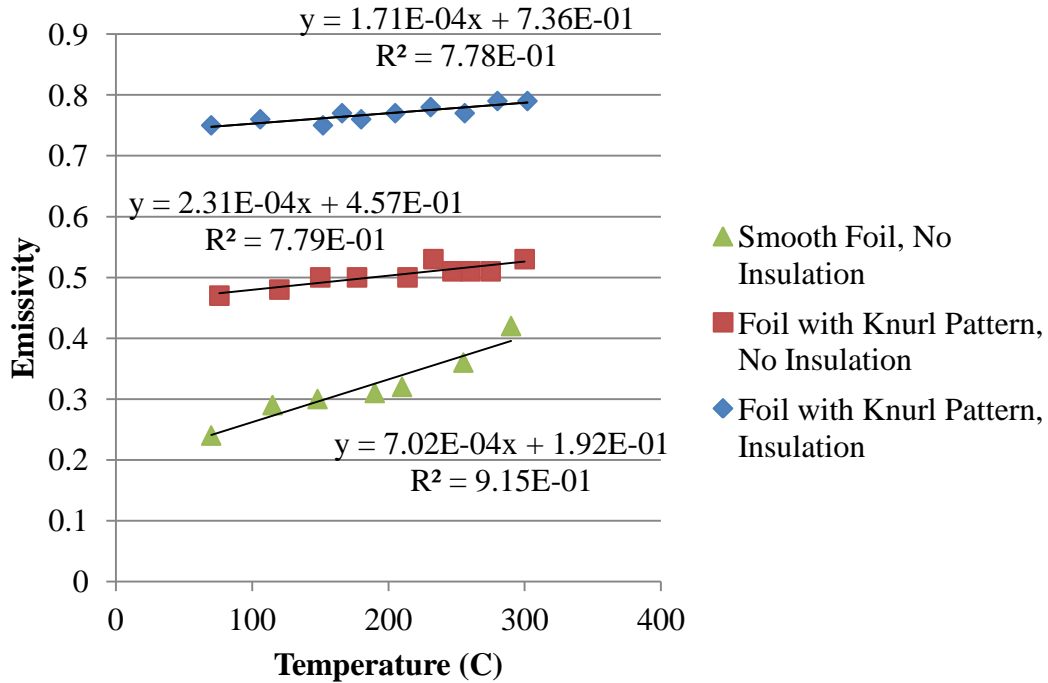


Figure 3.8. Plot of emissivity v. temperature for smooth foil without insulation (green), foil with knurl pattern without insulation (red), and foil with knurl pattern and insulation (blue). All plots are for Al 1100-0.

3.2 Weld Materials

The two materials used in this work are Al 1100-0 foils and Al 3003-H14 substrates. Since the yield stress of Al 1100-0 is much lower than the yield stress of Al 3003-H14, all plastic deformation occurs in the foil and allows finite element modeling of the process to be simplified. The materials were chosen over other aluminum alloys since both have a relatively thin oxide layer, which will reduce the possibility of inconsistent welds. Yang et al. (2009) have shown that the presence of significant oxide layers can weaken or prevent bonding via UC. Al 1100-0 was also chosen since its yield stress has been well characterized over a wide range of

temperatures by several authors including Hockett (1967), Pao and Gilat (1989) and Puchi et al. (1997). The material, width (W_0), and thickness (T) of the substrates and the three foil geometries are shown in Table 3.2

Table 3.2. Material and geometry of the foils and substrates.

Component	Material	W_0 (mm)	T (mm)
Foil 1	Al 1100-0	9.5	0.52
Foil 2	Al 1100-0	13.0	0.52
Foil 3	Al 1100-0	9.5	1.04
Substrate	Al 3003-H14	26.5	4.76

An image of the three foil geometries in Table 3.2 are shown in Figure 3.9 and an image of the substrate is shown in Figure 3.10.



Figure 3.9. Image of the three Al 1100-0 foil geometries used during UC. The dimensions are 9.5mm x 0.52mm (top), 13mm x 0.52mm (middle), and 9.5mm x 1.04mm (bottom).



Figure 3.10. Image of the Al 3003-H14 substrates used during UC (26.5mm x 4.76mm).

3.3 Experimental Procedure

The following experimental data is required to quantify the amount of thermal and acoustic softening that occurs during UC using a thermo-mechanical finite element model: (i) IR camera temperature measurements and (ii) the change in the foil's width during UC processing. Figure 3.11 shows a typical change in the foil's

width during UC processing. It can be seen that top of the foil is imprinted with the knurl pattern from the sonotrode during UC processing.

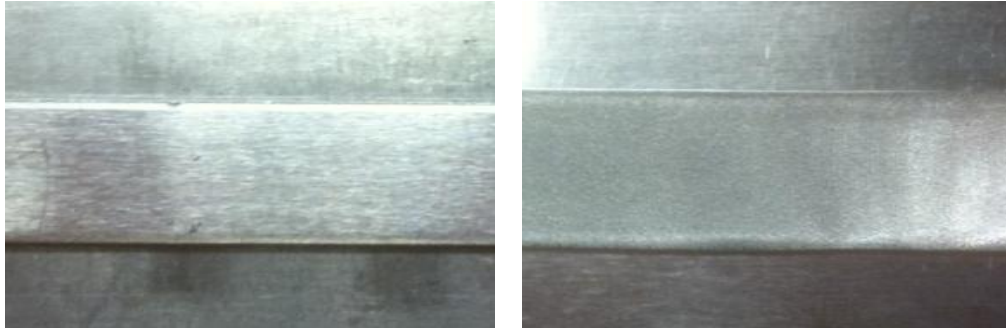


Figure 3.11. Initial foil geometry (left) and foil geometry after UC (right). Processed foil has increased in width and knurl pattern has been imprinted on the top of the foil.

3.3.1 Temperature Measurement

Temperature measurements are required to calculate thermal softening that occurs during UC and to calculate the coefficient of friction between the foil and the substrate. The procedure used to calculate the coefficient of friction was described in detail in section 2.1.3. Figure 3.12 shows a typical imaged taken by the IR camera during UC.

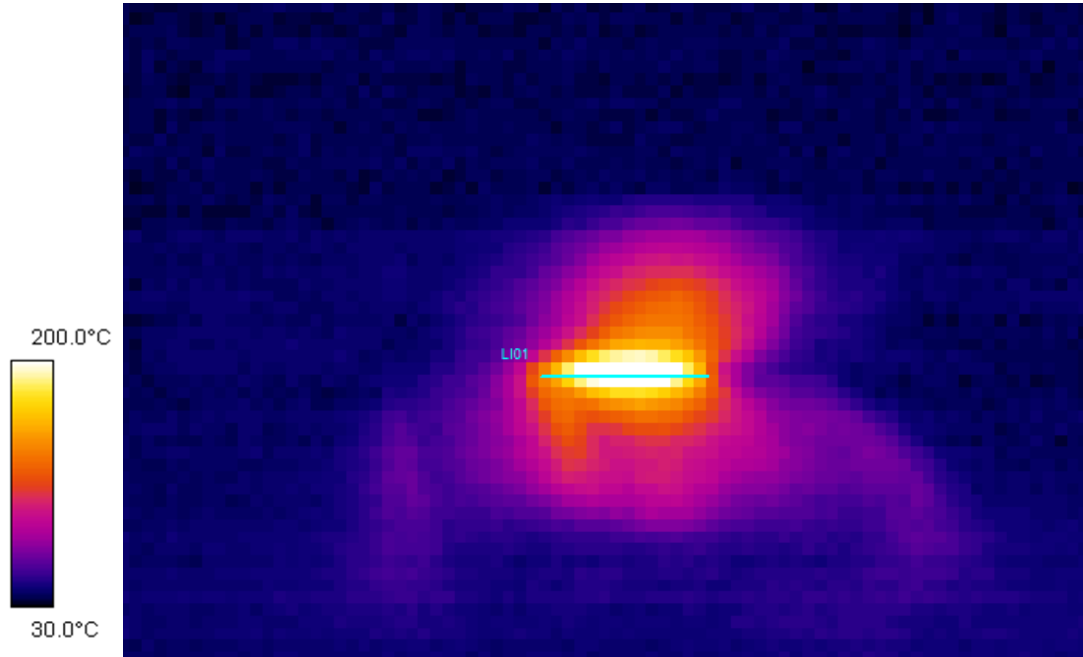


Figure 3.12. IR image taken during UC. Temperature measurements are taken across the foil width at the nip point between the sonotrode and the top of the foil.

The IR camera records images at 4 Hz and the sonotrode speed (S) is 40 mm/s, so the IR camera records an image every 10 mm along the length of the weld in the y -direction. From each image recorded by the IR camera temperatures can be monitored across the width of the foil (measurement locations are indicated in Figure 3.12 by the blue line). These temperature measurements across the foil width are plotted for each IR image taken during a typical weld in Figure 3.13.

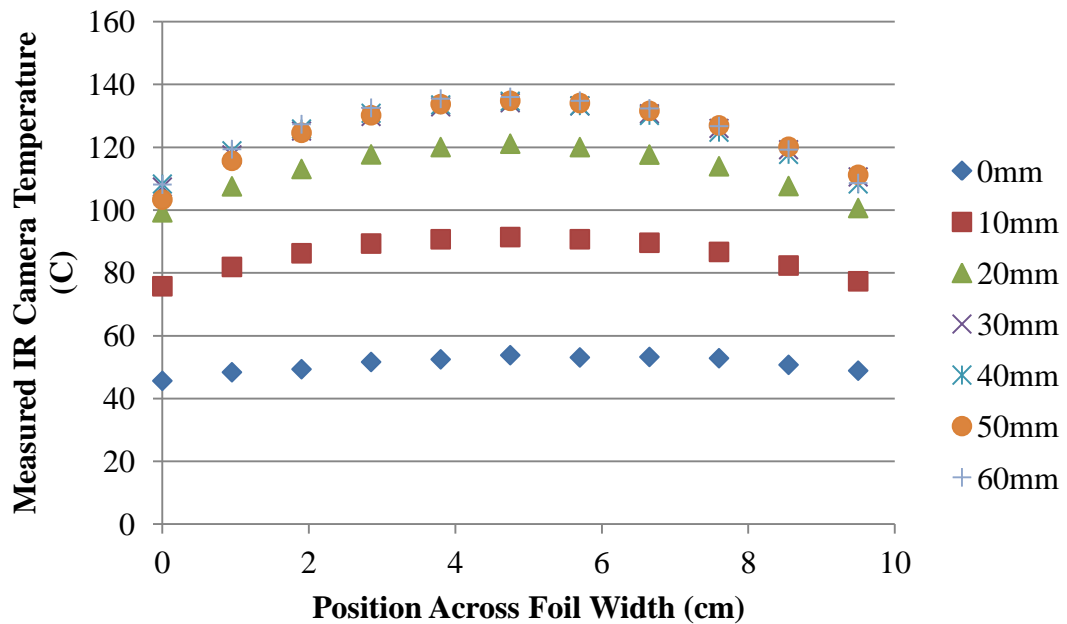


Figure 3.13. Temperature profiles measured across the foil width by the IR camera during UC. Temperature profiles are measured every 10mm along the length of the weld in the y-direction.

A plot of the thermal development of a typical UC bond along the length of the weld (y-direction) is shown in Figure 3.14. From this temperature data, a steady state weld temperature (T_{ss}) region can be identified. The maximum measured IR camera temperature for a typical weld is shown at each position along the weld length in Figure 3.14.

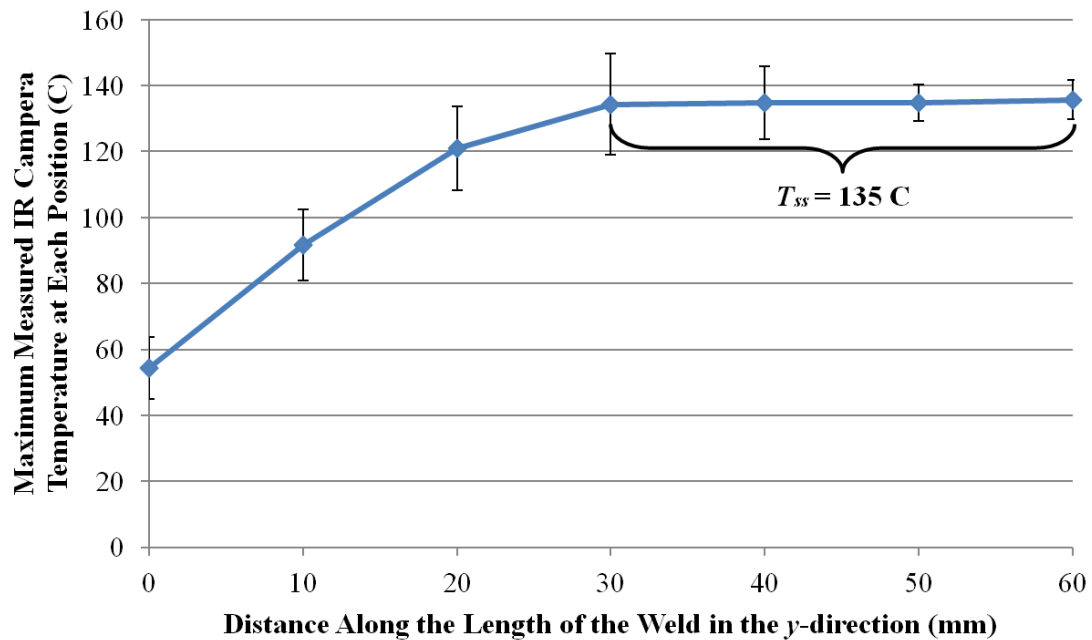


Figure 3.14. Maximum measured IR camera temperature at each position along the length of the weld in the y-direction. Error bars indicate the standard deviation in IR camera measurements between the three specimens.

Maximum temperature at each position along the length of the weld is used in this work rather than average temperature across the foil width for two reasons. Error is introduced when determining the temperature profile across the foil width in determining the location of the edges of the tape. This can be seen in Figure 3.12 where the location of the edges of the foil must be approximated. Use of maximum temperature eliminates this source of error. The second reason maximum temperature is used is that the difference in material softening between the maximum and average temperature across the width is 1.5% for the temperature profiles shown in Figure 3.13. This error is on par with the errors in estimating the edges of the foil in the IR camera image, so maximum temperature at each location is used for simplicity and consistency.

3.3.2 Measurement of Foil Width Increase

A digital image was taken of each welded specimen in order to measure the average width increase in the location of T_{ss} using Image J software (Ferreira and Rasband (2011)). The average UC processed foil width is calculated in Image J by dividing the area of the welded foil by the length of the T_{ss} region in the y -direction. The foil's processed width is the sum of the original tape width (W_0) and the increase in width after processing (ΔW). Figure 3.15 shows an image used to calculate the average width after UC processing.

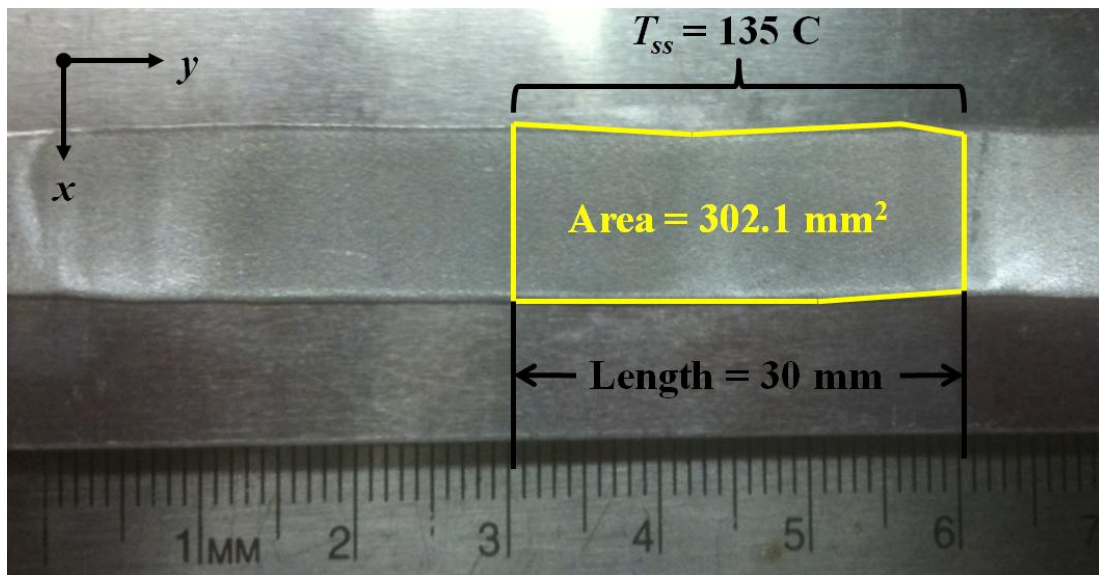


Figure 3.15. Image of welded specimen used to calculate average width increase (ΔW) in Image J.

The experimentally collected temperatures and foil geometry changes collected using the procedure described in this section allow thermal and acoustic softening to be calculated using thermo-mechanical finite element modeling described in Chapter 2.

3.4 Experimental Test Array Results

An array of UC process parameters was chosen that results in a wide range of bond qualities. Five amplitudes were chosen ($\lambda = 10, 18, 27, 32, 36 \mu\text{m}$) and five clamping pressures were chosen ($P_c = 17.0, 28.3, 45.2, 62.0, 78.9 \text{ MPa}$). The sonotrode speed (S) is a constant 40 mm/s for all sets of process parameters, since S will have no effect on acoustic softening. A total of 25 different combinations of UC process parameters were created using each combination of λ and P_c . 23 of the 25 sets of UC process parameters resulted in successful welding. Two sets of process parameters (36 μm , 62.0 MPa) and (36 μm , 78.9 MPa) did not successfully bond since the power required to produce these bonds exceeded the 3kW maximum power of the welder. Bonds made using the lowest λ can easily be separated by hand while bonds made at higher λ are sufficiently strong to have tensile failure in the base metal rather than failure at the bonded interface during peel testing. The array of 23 welds was produced using each of the three foil geometries shown in Table 3.2.

3.4.1 Temperature Results

IR temperatures profiles along the length of the weld (y-direction), such as that shown in Figure 3.14, are recorded for each combination of UC process parameters for each of the three foil geometries. Results for the 23 welds in the 9.5 x 0.52 foil array are shown in Figure 3.16 through Figure 3.20. Results are the average IR camera measurements of three weld specimens produced with each set of weld parameters. Error bars represent the standard deviation in IR camera measurements between the three specimens.

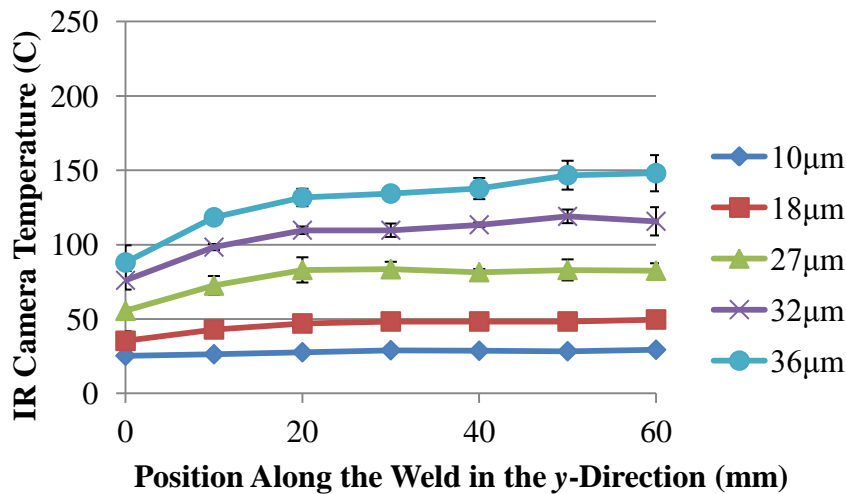


Figure 3.16. Maximum IR camera temperature measurements for various amplitudes at each position along the weld length for welds produced at $P_c = 17.0$ MPa.

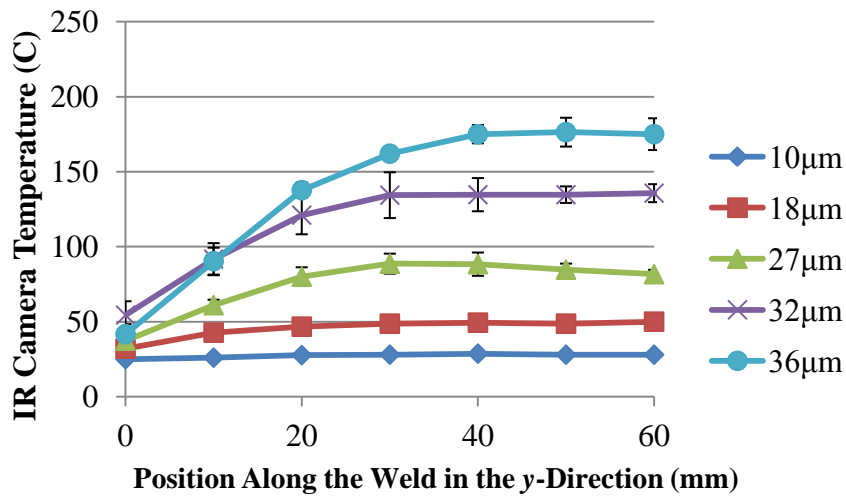


Figure 3.17. Maximum IR camera temperature measurements for various amplitudes at each position along the weld length for welds produced at $P_c = 28.3$ MPa.

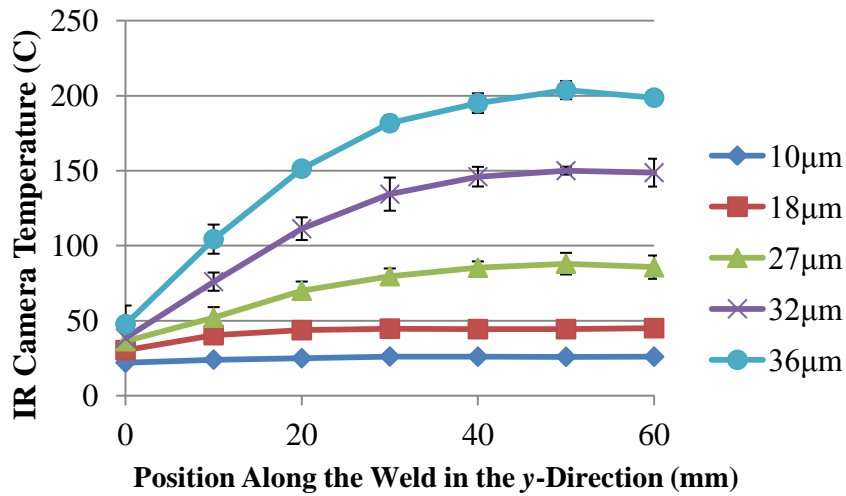


Figure 3.18. Maximum IR camera temperature measurements for various amplitudes at each position along the weld length for welds produced at $P_c = 45.2$ MPa.

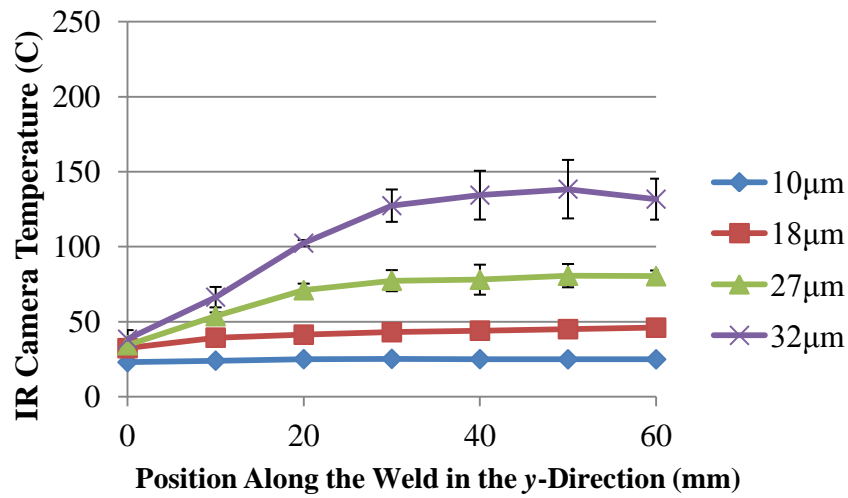


Figure 3.19. Maximum IR camera temperature measurements for various amplitudes at each position along the weld length for welds produced at $P_c = 62.0$ MPa.

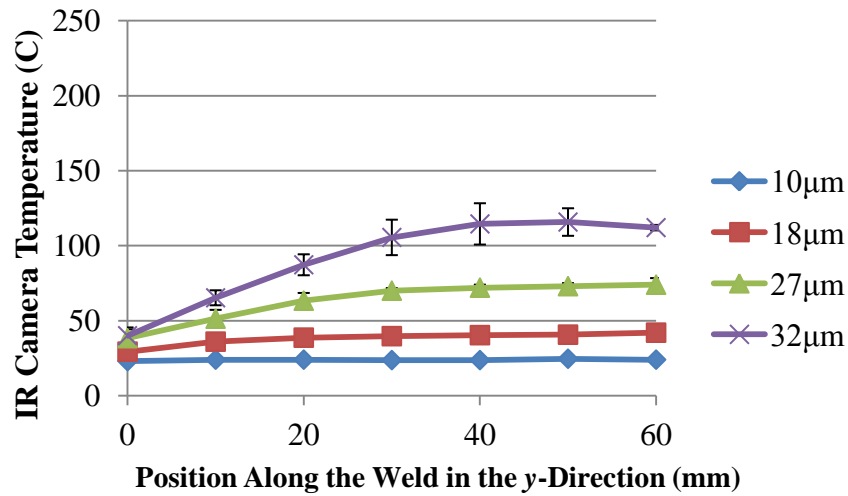


Figure 3.20. Maximum IR camera temperature measurements for various amplitudes at each position along the weld length for welds produced at $P_c = 78.9$ MPa.

A steady state temperature (T_{ss}) is calculated for each temperature profile shown in Figure 3.16 through Figure 3.20 for all three foil geometries. These T_{ss} measurements from the IR camera for the three experimental test arrays are shown in Figure 3.21. The value of T_{ss} ranges from 24C to 198C and is primarily a function of amplitude (λ).

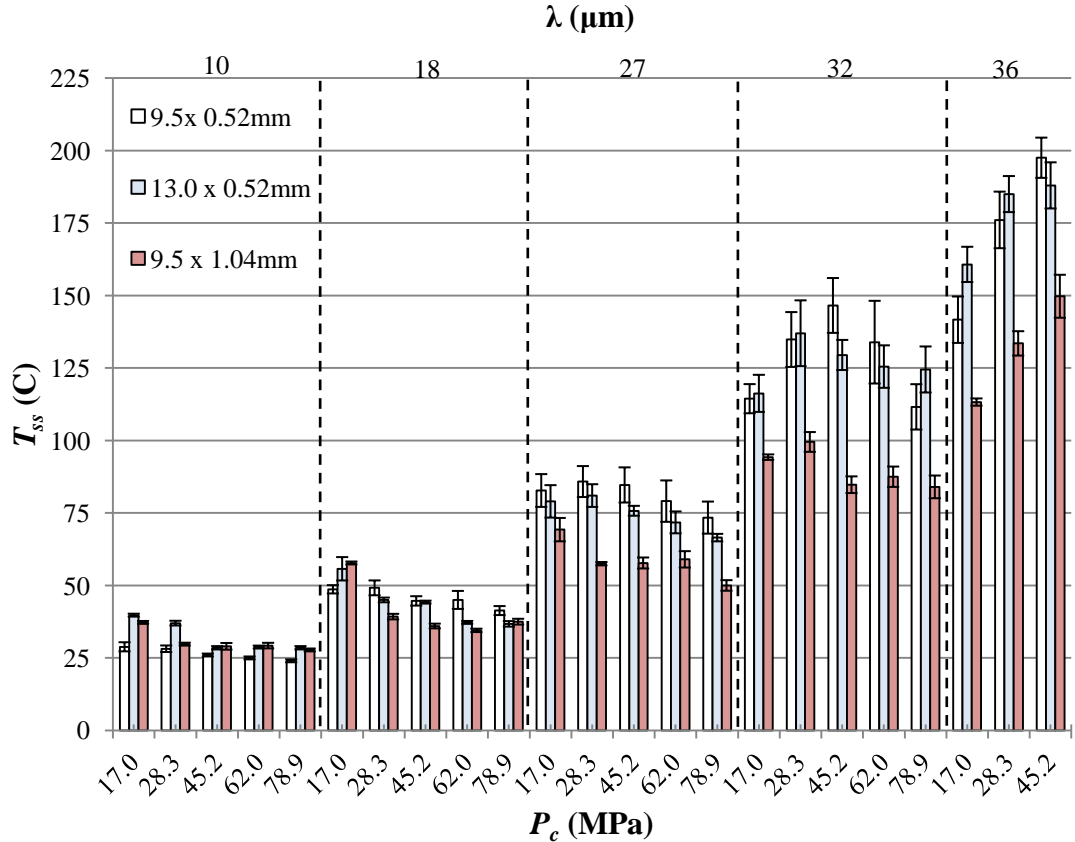


Figure 3.21. Experimentally measured steady-state temperatures (T_{ss}) for each combination of UC process parameters. Error bars indicate the standard deviation of all maximum temperature measurements in the steady-state region of the weld.

3.4.2 Width Increase ($\Delta W/W_0$) Results

Experimentally measured increases in the foil width ($\Delta W/W_0$) are calculated according to the procedure shown in Figure 3.15. Figure 3.22 shows the experimentally measured ($\Delta W/W_0$) for each combination of UC process parameters for the three foil geometries. All values of $\Delta W/W_0$ are taken in the region of T_{ss} for each weld. The value of $\Delta W/W_0$ ranges from 1.3% to 24.5% over the investigated test arrays.

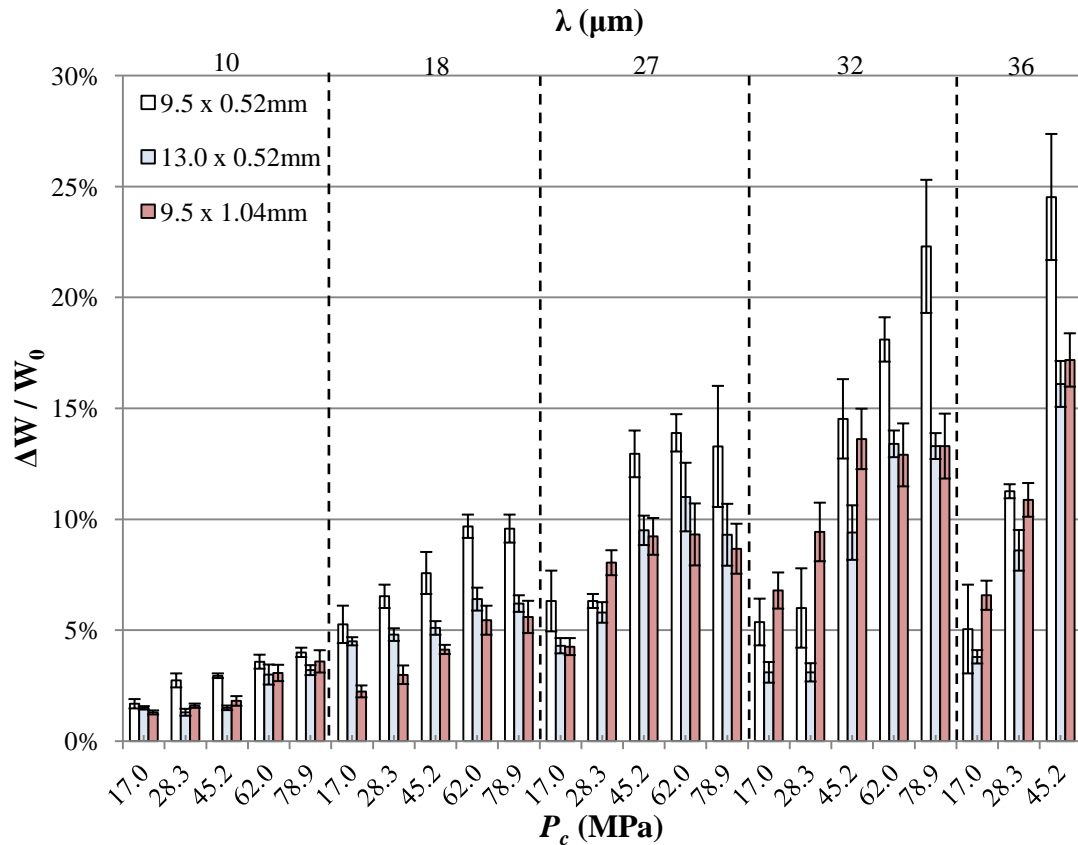


Figure 3.22. Experimentally measured Al 1100-0 foil width increases ($\Delta W/W_0$) for each combination of UC process parameters. Error bars indicate the standard deviation in ($\Delta W/W_0$) measurements of the three specimens made at each set of process parameters for each foil geometry.

3.5 Summary

In this chapter, the equipment, materials and experimental procedure used to create UC bonds was described. Steady-state temperatures (T_{ss}) and the foil's geometry change (ΔW) are measured and will be used as inputs to the thermo-mechanical finite element model described in Chapter 2 to characterize the acoustic softening during UC in the next chapter. An array of test parameters is also identified over which thermal and acoustic softening can be quantified.

Chapter 4

RESULTS AND DISCUSSION

In this section, T_{ss} and $\Delta W/W_0$ from Figure 3.21 and Figure 3.22 for the 9.5 x 0.52 mm foil array are used to calculate the acoustic softening factor (ζ) in Equation (2.3) using the thermo-mechanical modeling procedure described in Chapter 2. The T_{ss} and $\Delta W/W_0$ measurements from the 13.0 x 0.52 mm foil array and the 9.5 x 1.04 mm foil array are used to validate the acoustic softening model once the acoustic softening parameter is established. In order to investigate acoustic softening over the full range of process parameters and foil geometries, it is useful to present results in a dimensionless form. First a dimensionless amplitude (A) is defined according to equation (4.1) related to the peak-to-peak amplitude (λ) and the initial foil thickness (T).

$$A = \frac{\lambda}{T} \quad (4.1)$$

Dimensionless pressure (P) is shown in equation (4.2) and is related to the contact pressure (P_c) and the yield stress of Al 1100-0 at room temperature ($\sigma_{y0} = 34\text{MPa}$) before its exposure to ultrasonic energy.

$$P = \frac{P_c}{\sigma_{y0}} \quad (4.2)$$

4.1 Frictional Heat Generation

Friction heat generation is calculated for each set of UC process parameters according to the procedure described in section 2.1.3 and the T_{ss} values shown in Figure 3.21. q_{fr} results for the 9.5 x 0.52mm foil array are shown in Figure 4.1. q_{fr} was not calculated for ($\Lambda=0.069, P=1.82$) and ($\Lambda=0.069, P=2.32$) since it was not possible to produce these welds due to the maximum power limitations of the welder.

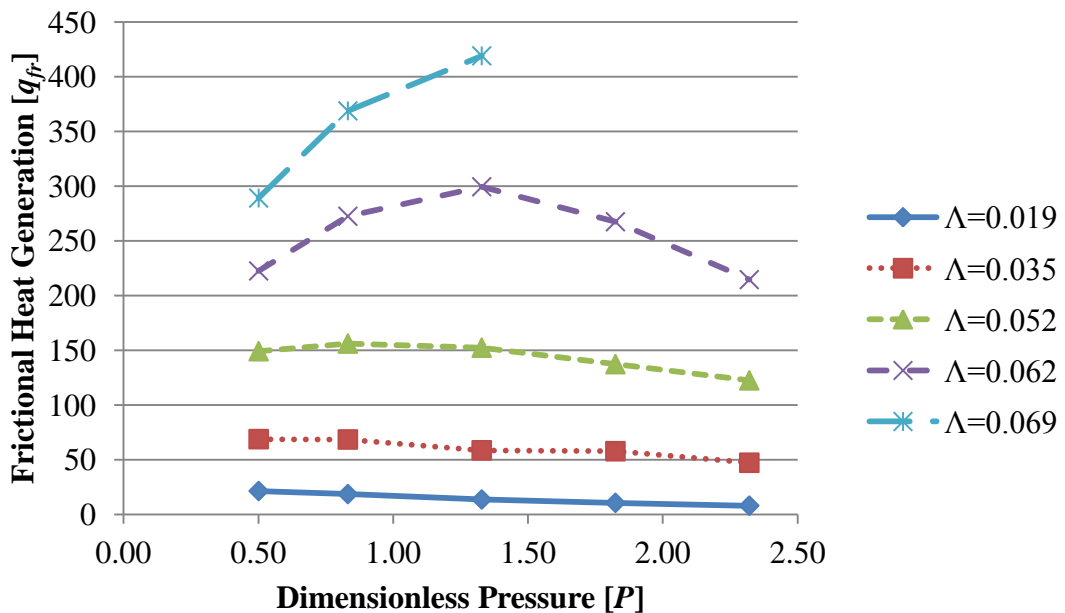


Figure 4.1. q_{fr} as a function of UC process parameters determined using the 9.5 x 0.52mm foil IR camera temperature measurements from Figure 3.21 and the thermal finite element model.

Frictional heat generation found to be primarily a function of amplitude. At low amplitudes, q_{fr} decreases linearly with increasing pressure. At higher amplitudes, pressure has a non-linear influence on q_{fr} . This non-linear influence can be explained by the dependence of μ on A and P , and is examined in the next section.

4.1.1 Coefficient of Friction

Friction coefficients are calculated using the values of q_{fr} shown in Figure 4.1 and equation (2.1). The trends found in this study – decreasing coefficient of friction with increasing clamping force and increasing coefficient of friction with increasing amplitude – agree with previous studies by Naidu and Raman (2005) and Koellhoffer et al. (2011). The results for the 9.5 x 0.52 mm foil array are shown in Figure 4.2. The increase in μ with increasing A and decrease in μ with increasing P are responsible for the q_{fr} trends shown in Figure 4.1.

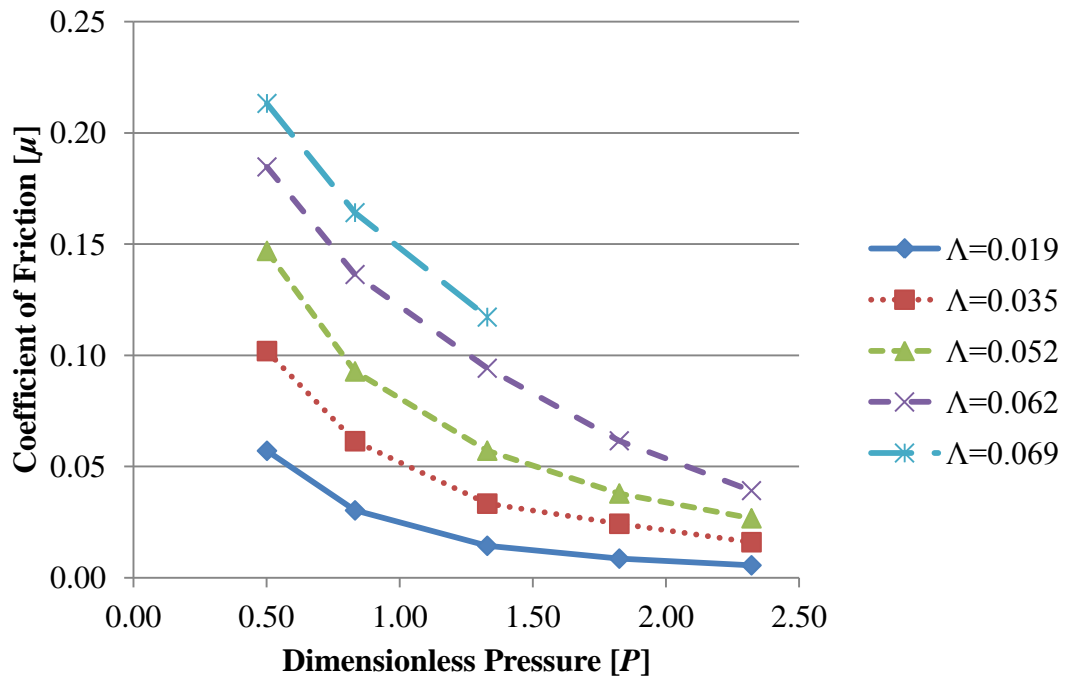


Figure 4.2. UC parameter dependent friction coefficients determined using q_{fr} calculations from the 9.5 x 0.52mm foil in Figure 4.1 and equation (2.1).

4.2 Acoustic Softening

The friction coefficients shown in Figure 4.2 are used in the mechanical finite element model described in section 2.2 and acoustic softening (ζ) is solved for by incrementally decreasing the value of ζ until the error between the experimental $\Delta W/W_0$ and the modeled $\Delta W/W_0$ is minimized. To highlight the importance of acoustic softening during UC, a few selected process parameters are shown in Figure 4.3. The figure shows experimentally measured $\Delta W/W_0$ in addition to modeled $\Delta W/W_0$ using three different amounts of acoustic softening (ζ).

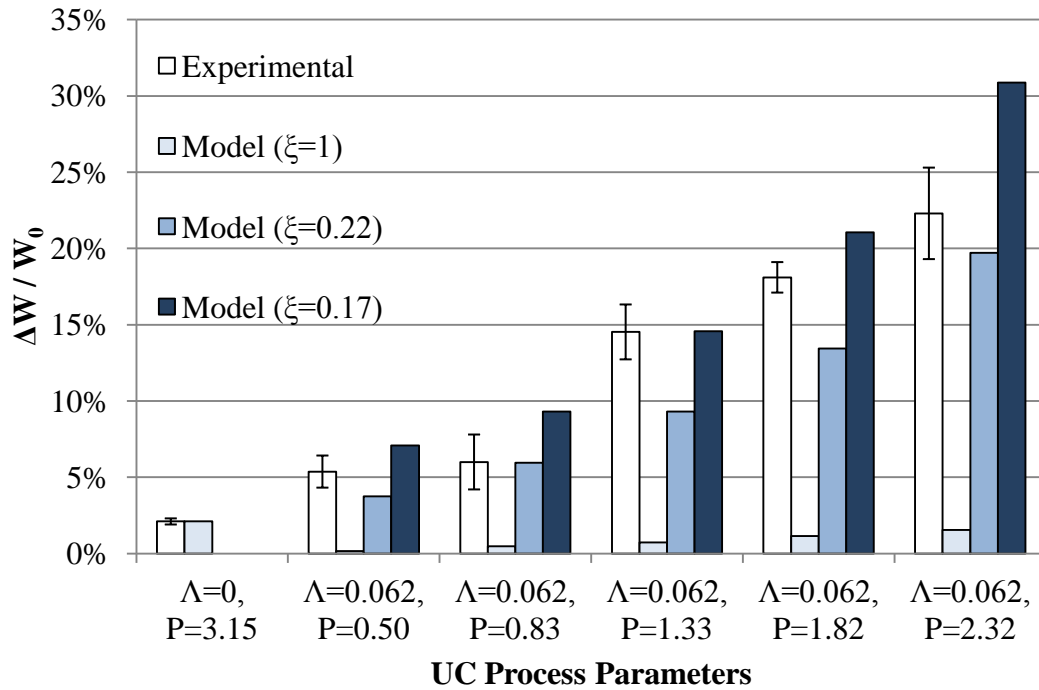


Figure 4.3. Experimentally measured $\Delta W / W_0$ and modeled $\Delta W / W_0$ using three different values of acoustic softening ($\xi = 0, \xi = 0.17$ and $\xi = 0.22$) from Equation (2.3). The results shown are from the 9.5 x 0.52mm foil array.

The mechanical finite element model accurately predicts the foil width increase without acoustic softening when $\Lambda=0$ and $P=3.15$. This comparison serves to validate the Al 1100-0 material model and the mechanical model's boundary conditions. It can clearly be seen that once ultrasonic energy is applied ($\Lambda > 0$), the material model with thermal softening and without acoustic softening ($\xi = 1$) severely under predicts the foil's width increase. Figure 4.3 clearly shows that the majority of material softening that occurs during UC is due to acoustic softening and that acoustic softening can be quantified using the method described in this work. At an amplitude of $\Lambda=0.062$, the average acoustic softening of the five weld parameters tested is

$\zeta=0.20$. All five combinations of UC process parameters fall into an acoustic softening range between $\zeta=0.17$ and $\zeta=0.22$.

Acoustic softening (ζ) is calculated for the full array of process parameters using the experimental results from the 9.5 x 0.52mm foil array in Figure 3.21 and Figure 3.22, in addition to the modeling procedure described in Chapter 2. Figure 4.4 shows the result of this acoustic softening (ζ) calculation. The values of acoustic softening shown in Figure 4.4 result in the minimum error between experimentally measured and modeled $\Delta W/W_0$ for the 9.5 x 0.52 mm foil array.

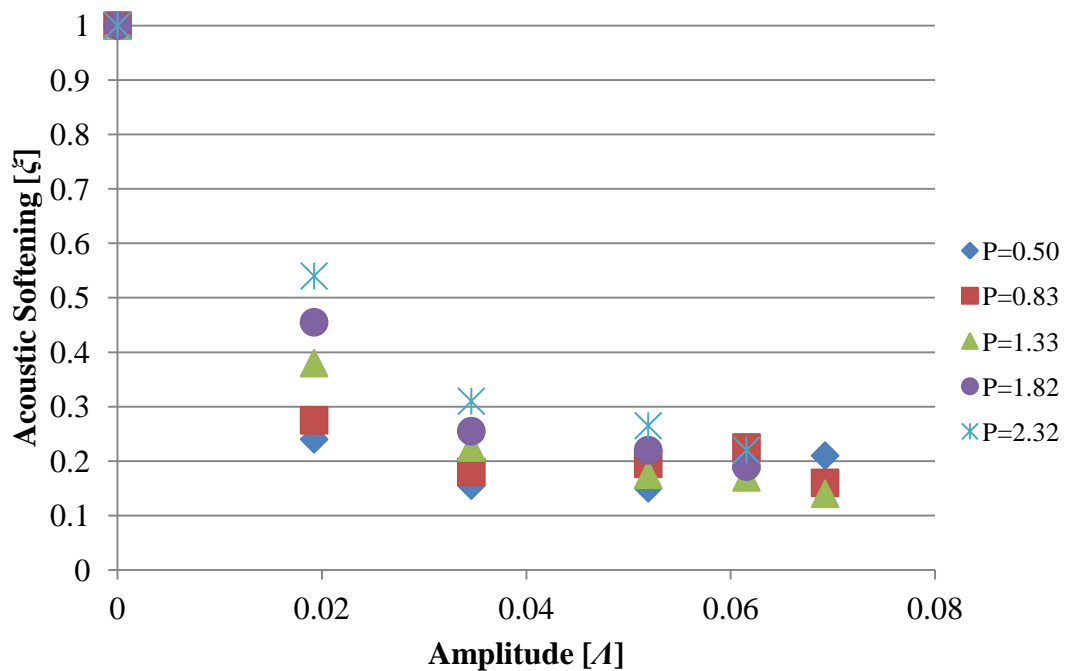


Figure 4.4. Acoustic softening of Al 1100-0 as a function of dimensionless amplitude (A) for five values of dimensionless pressure (P) during UC. Data points are calculated using the experimental data from the 9.5 x 0.52mm foil array.

Acoustic softening (ξ) is found to be a function of dimensionless amplitude (A) and dimensionless pressure (P) and can be expressed in a constitutive form according to equation (4.3). The values of the constants used in equation (4.3) are shown in Table 4.1.

$$\xi = \xi_0 + \frac{c_1}{1 + e^{(c_2 + c_3 A + c_4 AP)}} \quad (4.3)$$

Table 4.1. Acoustic softening constants used in equation (4.3).

ξ_0	c_1	c_2	c_3	c_4
0.177	1.74	0.109	171	-47.0

The calculated values of acoustic softening (ξ) from Figure 4.4 and Equation (4.3), which describes acoustic softening as a function of process parameters, are both plotted in Figure 4.5.

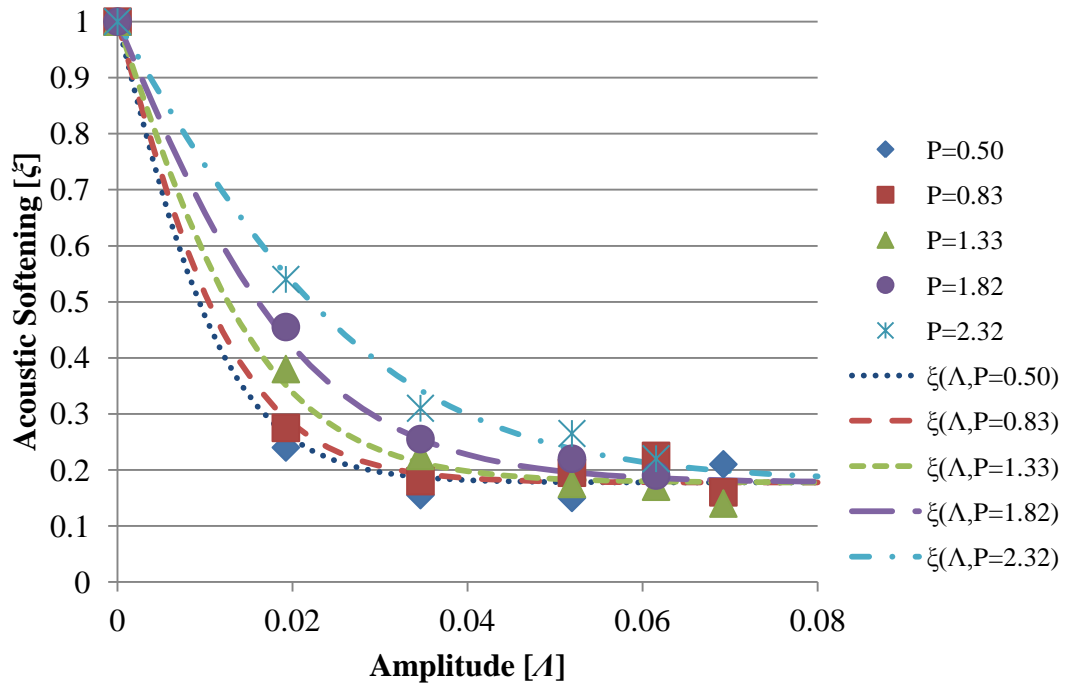


Figure 4.5. Plot of acoustic softening values from Figure 4.4 and Equation (4.3) for varying A and P .

Figure 4.5 shows that ξ decreases with amplitude (A) until it approaches its minimum value of $\xi_0 = 0.177$. The rate at which ξ approaches its minimum value is related to the dimensionless pressure (P): UC welds with a lower P approaches ξ_0 at a lower A than UC welds with higher values of P . It is also important to note that acoustic softening is a function of A rather than λ , so a material with a twice the initial thickness (T) will also require twice the initial amplitude (λ) to achieve the same amount of acoustic softening. The acoustic softening model shown in Figure 4.5 can be applied to any Al 1100-0 foil geometry during UC. The validation of this acoustic softening model is shown in Section 4.5 using the 13.0 x 0.52mm and 9.5 x 1.04mm foil arrays.

To ensure that the model is working properly, it is necessary check the modeled decrease in foil thickness against the experimentally measured decrease in foil thickness. This check is made once the value of ζ is solved for and error between the model and experimental $\Delta W/W_0$ is minimized. This comparison is shown in Figure 4.6 for the 9.5 x 0.52 mm foil array and a good agreement between the model and experimental measurements is seen.

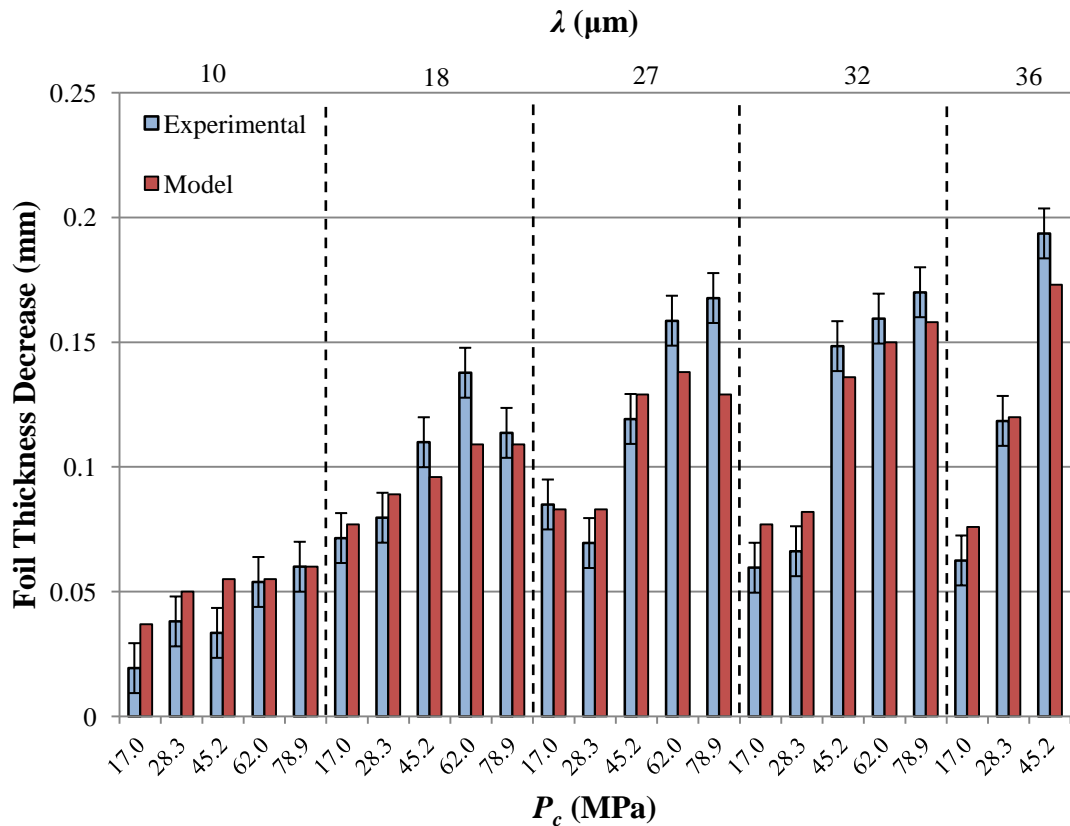


Figure 4.6. Experimentally measured and modeled decrease in the foil's thickness for the 9.5 x 0.52 mm foil array. Error bars indicate the precision of the experimental thickness measurement.

4.3 Thermal Softening

Figure 4.7 compares the relative contributions of thermal and acoustic softening during UC. The most significant acoustic softening is shown ($\xi_0 = 0.177$) in addition to the highest temperature ($T_{ss} = 198$ C) measured during the test arrays presented in this work. It can clearly be seen in Figure 4.7 that during UC, acoustic softening is far more significant than thermal softening.

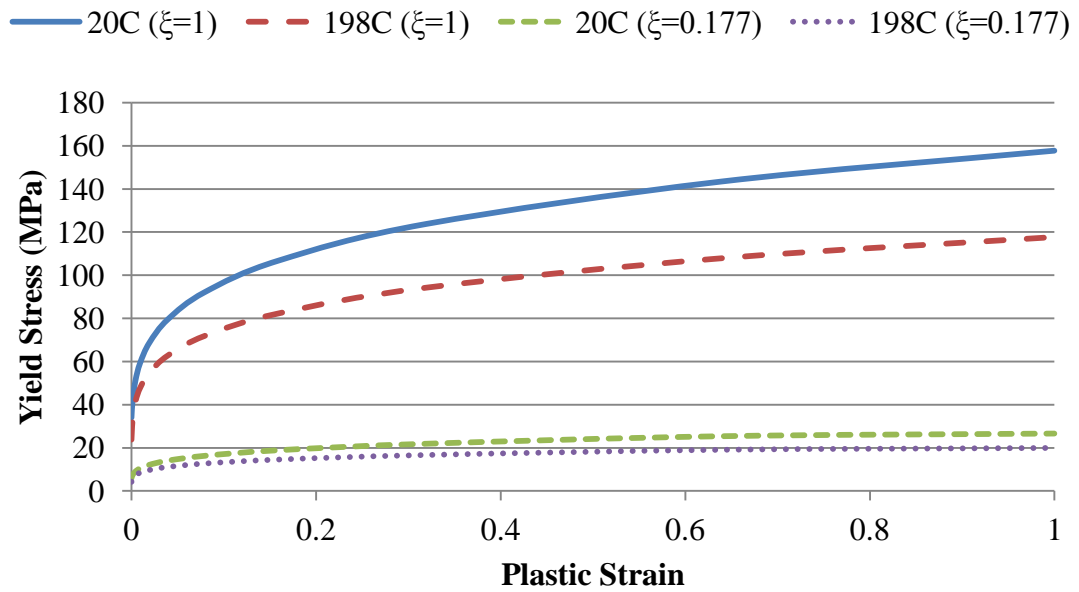


Figure 4.7. Comparison of the stress-strain curves of Al 1100-0 with thermal softening (20 C and 198C) and acoustic softening ($\xi = 1$ and 0.177) calculated using Equation (2.3).

Table 4.2 compares the influence of thermal and acoustic softening during UC on the K term in Equation (2.3). The minimum and maximum thermal and acoustic softening are again compared as in Figure 4.7. The influence of the n term in the equation is ignored since it plays a secondary role in the total material softening. It can

be seen that without the presence of acoustic softening, Al 1100-0 at 198 C experiences a significant amount of softening (25.4%) when compared to room temperature properties. When $\zeta = 0.177$, this same increase in temperature only increases material softening by 4.5%, compared to the 82.3% reduction due to acoustic softening. This shows that thermal softening plays a secondary role to acoustic softening during UC. Also, if thermal softening were ignored during the modeling process, a reasonable measurement of acoustic softening can still be made and the error should be no greater than 4.5% in the most extreme case.

Table 4.2. Influence of thermal and acoustic softening during UC on the K term in Equation (2.3).

Thermal / Acoustic Softening	K (MPa)	% Reduction in K Compared to ($T_{ss} = 20\text{ C} / \zeta = 1.0$)
$T_{ss} = 20\text{ C} / \zeta = 1.0$	157.8	0.0%
$T_{ss} = 198\text{ C} / \zeta = 1.0$	117.7	25.4%
$T_{ss} = 20\text{ C} / \zeta = 0.177$	27.9	82.3%
$T_{ss} = 198\text{ C} / \zeta = 0.177$	20.8	86.8%

4.3.1 Volumetric Heat Generation

With the acoustic softening model presented in section 4.2 it is possible to calculate volumetric heat generation (q_{vol}) and compare it to the heating contribution from friction (q_{fr}) shown in Figure 4.1. q_{vol} and q_{fr} are calculated over the full range of process parameters discussed in section 3.4. q_{vol} is calculated using Equation (2.4) and W_p is calculated for each combination of UC process parameters using the mechanical finite element model shown in Figure 2.4.

In the case of ultrasonic consolidation, the exact value of β from Equation (2.4) is not critical because even at a value of $\beta = 0.9$ (the upper limit for aluminum), the

volumetric contribution to total heat generation is less than 5% for typical UC process parameters ($A > 0.04$). At $A < 0.04$, little to no bonding of the materials takes place, so these processing conditions would not typically be used where strong bonding is required. Volumetric heat generation is small relative to friction heat generation under process conditions where strong bonds are produced. In the extreme case where A is low and P is high, the maximum contribution from volumetric heating is found and is equal to 18%. The ratio of volumetric heat generation to total heat generation for the full range of process parameters is shown in Figure 4.8.

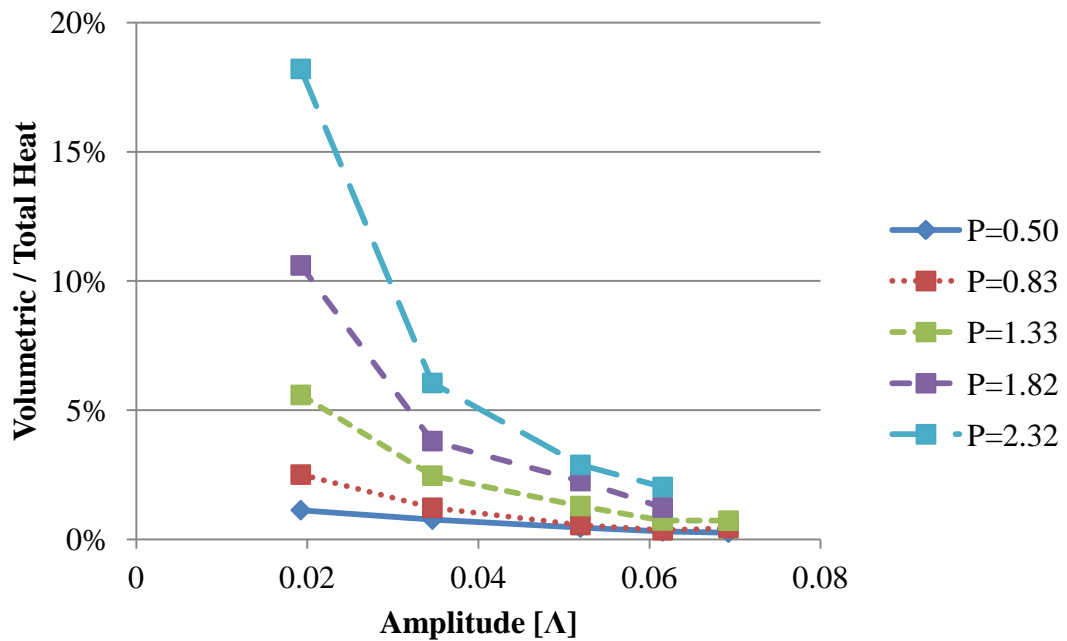


Figure 4.8. Volumetric heat generation as a function of amplitude (A) and pressure (P) using $\beta=0.9$ from Equation (1.6).

4.4 Contact Length (l_c)

In Chapter 1 it was assumed that $l_c = 5.4$ mm for all process parameters. That assumption is investigated in more detail in this section. Figure 4.9 shows a diagram of l_c during UC. As the sonotrode rolls down the length of the weld in the y -direction, the sonotrode is only in contact with the foil on the front half since the rear portion has already been processed and the height has been reduced.

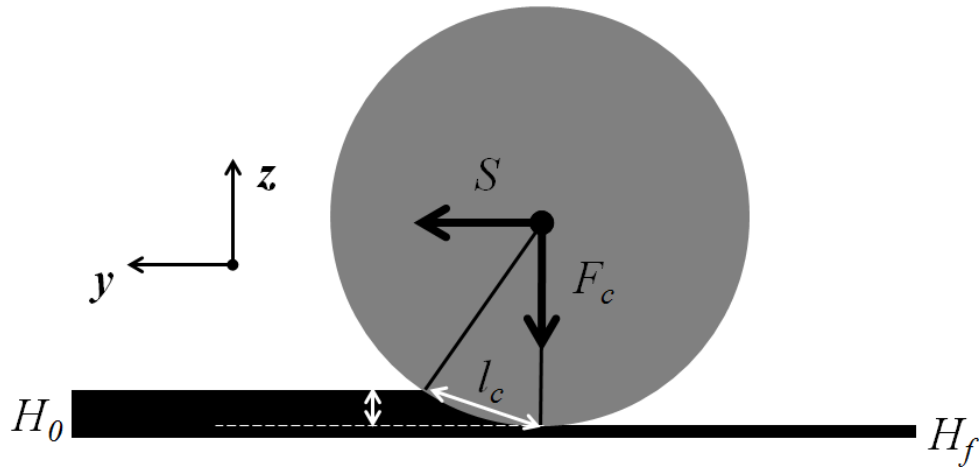


Figure 4.9. Schematic showing the contact length (l_c) during UC.

Since the contact length is difficult to measure experimentally for a rolling sonotrode, the contact length is investigated in the mechanical finite element model. l_c is determined by measuring the distance in the y -direction that the sonotrode has caused the foil to decrease in thickness. A contour plot of displacements in the foil's thickness direction and the measurement of l_c are shown in Figure 4.10.

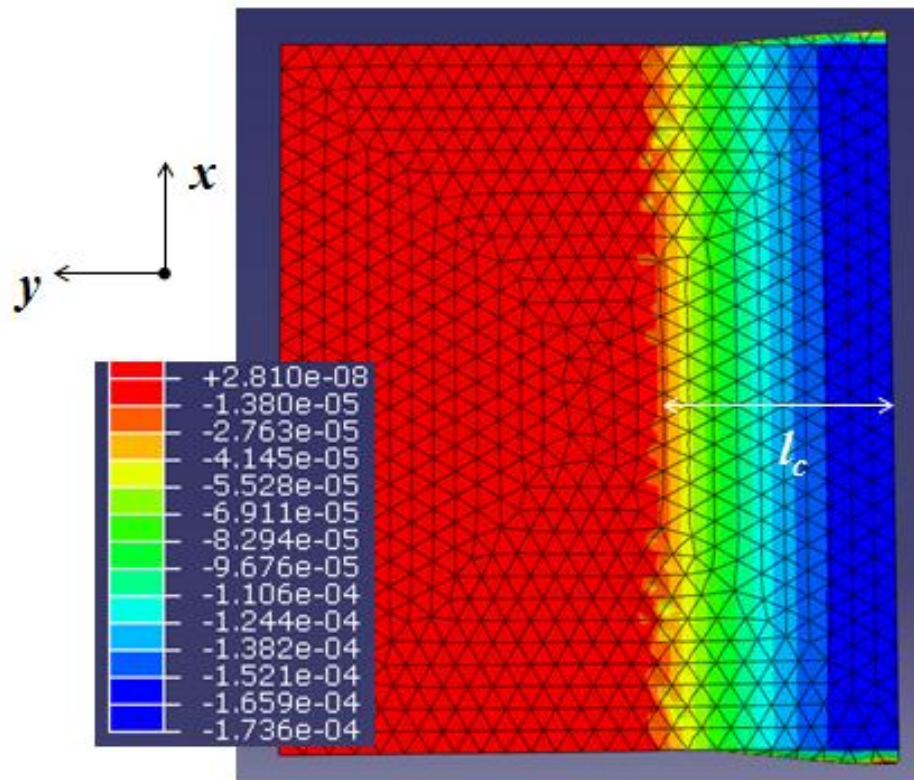


Figure 4.10. A typical contour plot of model displacements in the foil's thickness direction (z -direction). Areas in contact with the sonotrode have displacements in the negative z -direction. l_c is measured in the y -direction. Units are in meters.

The dependence of l_c on each combination of process parameters for the 9.5 x 0.52 mm foil is investigated, including thermal and acoustic softening. The dependence of l_c on the process parameters is shown in Figure 4.11.

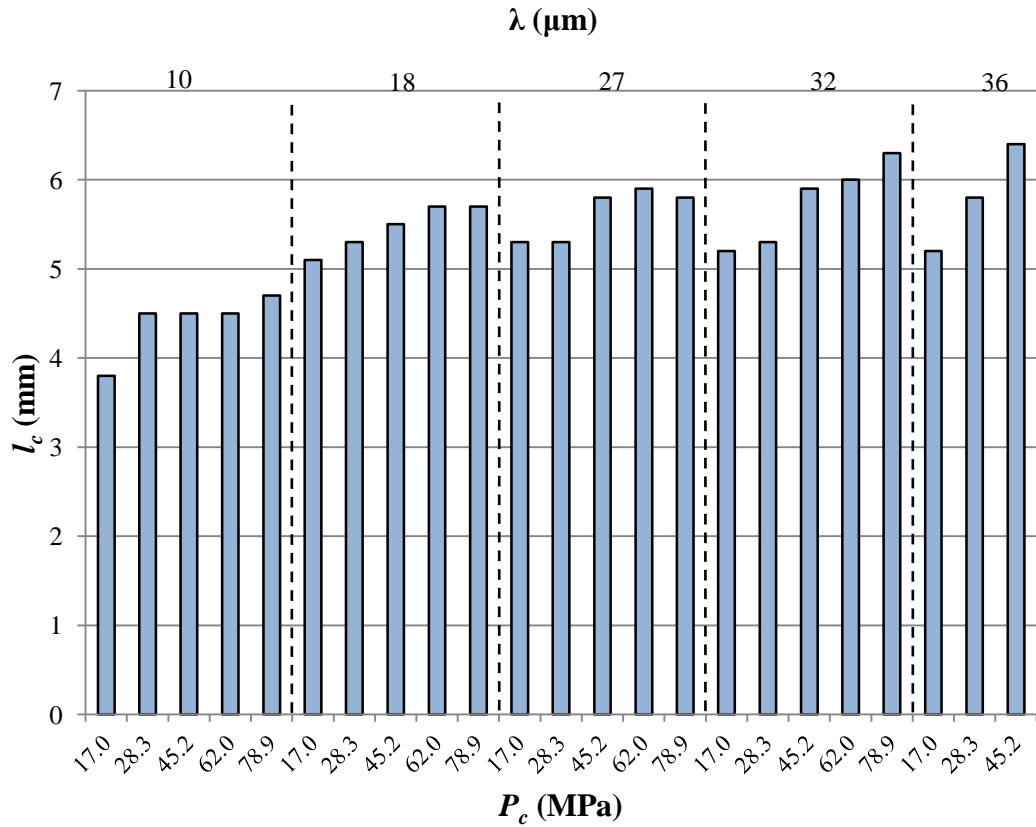


Figure 4.11. Contact length (l_c) as a function of UC process parameters calculated using the mechanical finite element model.

The average l_c across all process parameters is 5.4 mm, as was assumed in Chapter 1. The minimum and maximum modeled l_c are 3.8 mm and 6.4 mm respectively. It is important to note that the assumption of $l_c = 5.4$ mm does not introduce any error into the mechanical modeling process, error is only introduced to the constitutive equation relating ζ to dimensionless amplitude (A) and dimensionless pressure (P) shown in Equation (4.3). This error in the calculation of ζ according to

Equation (4.3) is investigated in Table 4.3. The two greatest differences between modeled and assumed l_c are investigated.

Table 4.3. Influence of l_c on ξ calculation from Equation (4.3).

λ (μm)	F_c (N)	l_c (mm)	P_c (MPa)	ξ
10	874	5.4	17.0	0.264
10	874	3.8	24.2	0.281
36	2317	5.4	45.2	0.178
36	2317	6.4	38.1	0.177

When $\lambda = 10 \mu\text{m}$ and $F_c = 874 \text{ N}$, the assumption of $l_c = 5.4 \text{ mm}$ overestimates the modeled value of l_c and results in a 1.6% difference in the ξ calculation. When $\lambda = 36 \mu\text{m}$ and $F_c = 2317 \text{ N}$, the assumption of $l_c = 5.4 \text{ mm}$ underestimates the modeled value of l_c and results in a 0.1 % difference in the ξ calculation. Therefore, the assumption of $l_c = 5.4 \text{ mm}$ is useful since it greatly simplifies the curve fitting of acoustic softening (ξ) in Figure 4.5 and introduces minimal error to the modeling process.

4.5 Model Validation

In this section, the acoustic softening model presented in section 4.2 is validated using T_{ss} and $\Delta W/W_0$ values from Figure 3.21 and Figure 3.22 for the 13.0 x 0.52 mm and 9.5 x 1.04mm foil geometries. Acoustic softening values from equation (4.3) are used as inputs to the thermo-mechanical model described in Chapter 2 and used to predict $\Delta W/W_0$ for the 13.0 x 0.52mm and 9.5 x 1.04mm foil arrays. Friction coefficients, such as those shown in Figure 4.2 are also input into the thermo-mechanical model. The validation modeling process is summarized in Figure 4.12.

VALIDATION MODEL

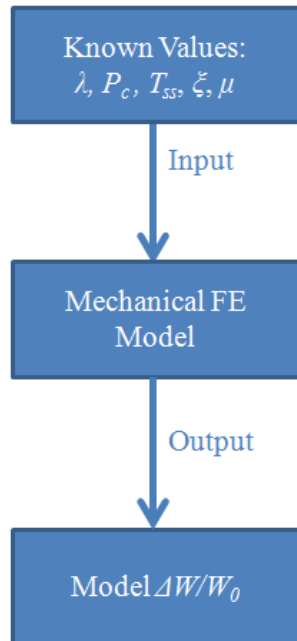


Figure 4.12. Flow chart summarizing the validation model.

Figure 4.13 compares experimental $\Delta W/W_0$ and modeled $\Delta W/W_0$ for the 13.0 x 0.52mm foil array.

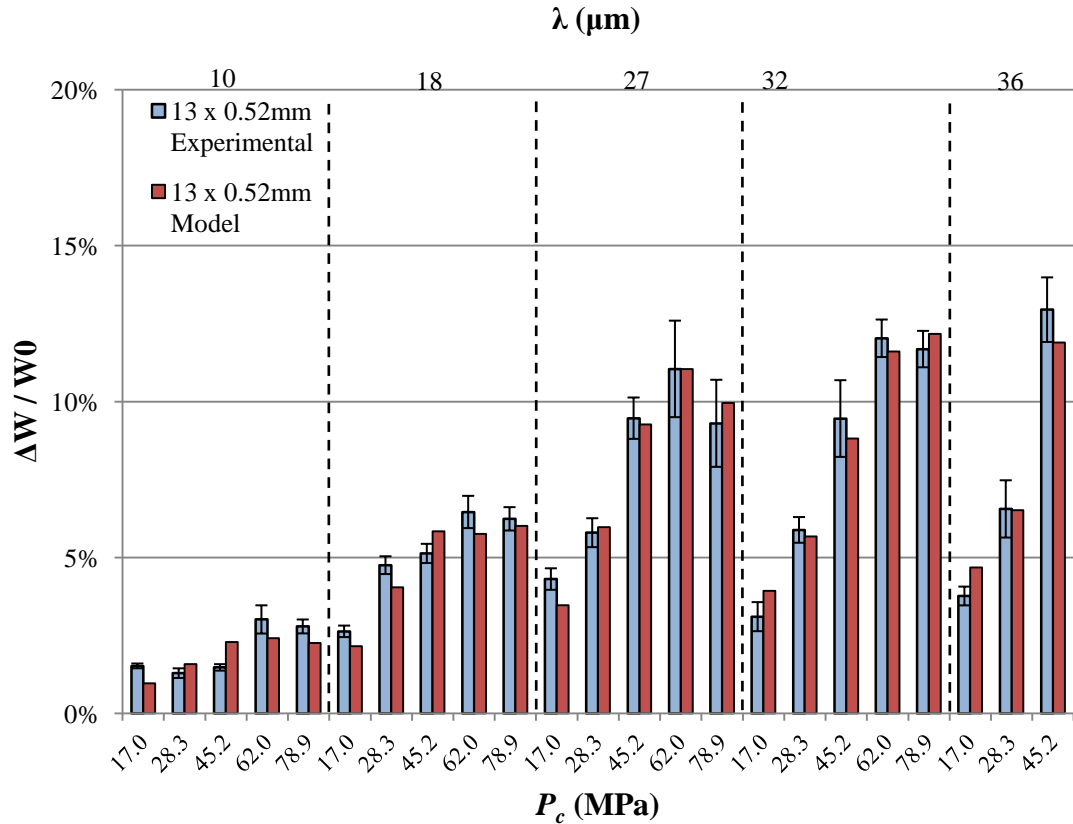


Figure 4.13. Validation test array for the 13.0 x 0.52mm foils. Experimentally measured $\Delta W/W_0$ is compared to model predictions using ζ values from equation (4.3) as an input to the model.

The model predictions in Figure 4.13 show good agreement with experimental measurements. The average difference in $\Delta W/W_0$ between the experimental measurements and the model predictions in Figure 4.13 is 0.5% and the maximum difference is 1.1%. Figure 4.14 shows a similar comparison of experimental measurements and model predictions of $\Delta W/W_0$ for the 9.5 x 1.04mm foil array.

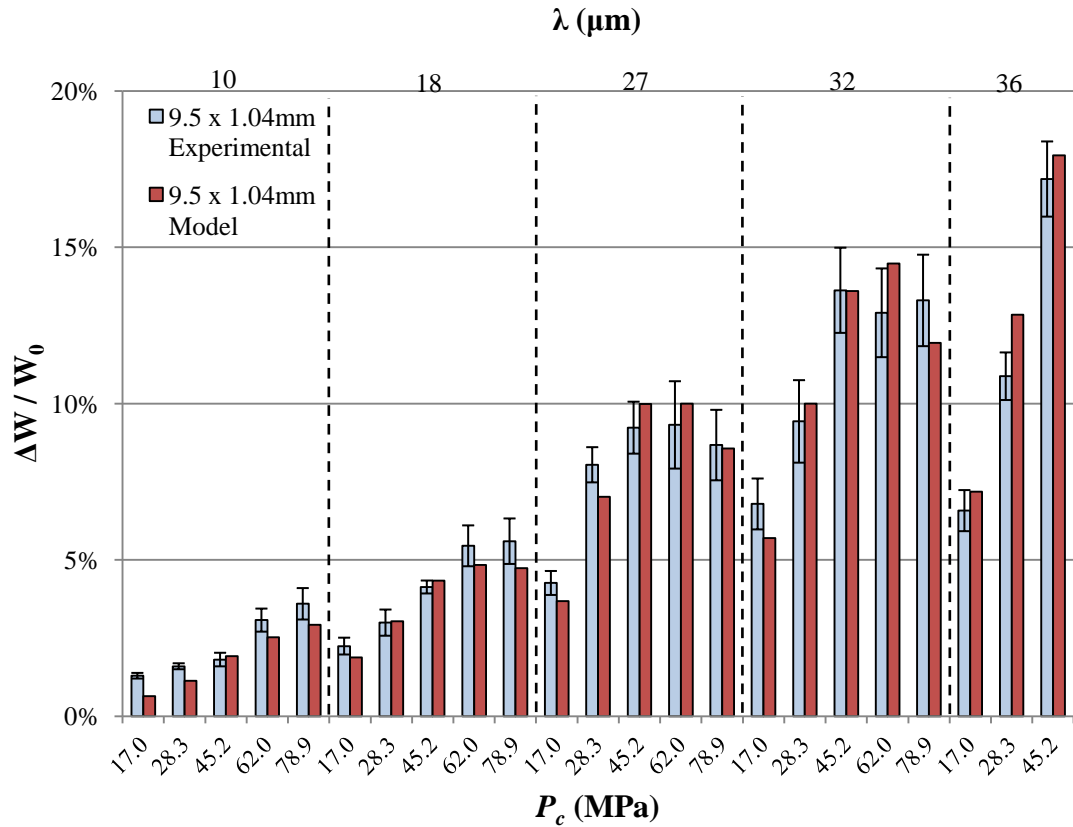


Figure 4.14. Validation test array for the 9.5 x 1.04mm foils. Experimentally measured $\Delta W/W_0$ is compared to model predictions using ζ values from equation (4.3) as an input to the model.

The model predictions in Figure 4.14 also show good agreement with experimental measurements. The average difference in $\Delta W/W_0$ between the experimental measurements and the model predictions in Figure 4.14 is 0.7% and the maximum difference is 2.0%.

4.6 Summary

In this chapter, experimental results from Chapter 3 are supplied to the thermo-mechanical modeling process described in Chapter 2 and the modeling results are presented. Acoustic softening is found to be a function of amplitude and contact pressure. As the amplitude increases, acoustic softening approaches its lowest value of $\xi_0 = 0.177$, indicating that the yield stress has been reduced by acoustic softening to 17.7% of the original value for Al-1100-0. Thermal softening is found to be relatively minor in comparison to acoustic softening. Additionally, volumetric heat generation accounts for less than 5% of the total heat generation where strong bonds are produced. The expression for acoustic softening formulated from one set of experiments over a range of pressures and amplitudes was validated by comparing it two other sets of experiments with different foil width and thickness.

Chapter 5

SUMMARY AND FUTURE WORK

Acoustic softening of Al 1100-0 foils during ultrasonic consolidation is quantified using the experimental and thermo-mechanical modeling technique outlined in this work. A relationship between material thickness, UC process parameters (λ and F_c) and acoustic softening has been identified. A wide range of UC process parameters are covered in this work, ranging from parameters that create very weak bonds that can easily be peeled apart by hand to very strong welds that fail in tension in the base material during peel testing. Once acoustic softening is determined for a given material and geometry using the method described in this work, acoustic softening can be calculated for any other geometry of the same material.

For the UC process parameters investigated in this work, thermal softening alone does not account for the experimentally measured tape deformations. Acoustic softening (ζ) during UC of Al 1100-0 foils is found to be very significant – reducing the yield stress of the material up to 82 %. On the other hand, thermal softening is a small contributor to the total material softening during UC (< 5 %). Friction is the dominant source of heat during UC. Volumetric heat generation accounts for less than 5% of all heat generated under typical UC process parameters that produce strong bonding.

The model and experiments described in this work serve to connect the theoretical literature on acoustic softening with ultrasonic consolidation in a practical method that allows acoustic softening to be quantified during the process. Knowledge

of the yield stress of a material during UC will lead to a better understanding of how materials will come into intimate contact and when bonding will occur. Additionally, the influence of the sonotrode's knurl pattern imprinted on foils during multiple layers of UC bonding can be better understood. Acoustic softening allows a deeper knurl pattern to be filled in than would otherwise be possible under the same process conditions.

5.1 Overview of the Methodology

An overview of the five step method used to quantify acoustic softening for a material during UC can be summarized as follows:

1. Identify the UC process parameters, material type and material geometry to be investigated.
2. Record UC process temperatures with an IR camera.
3. Measure the foil's geometry change during UC processing.
4. Calculate the coefficient of friction and thermal softening for the chosen UC process parameters using IR camera temperature measurements and the thermal model described in Section 2.1.
5. Calculate acoustic softening as a function of process parameters using the calculated friction coefficient and experimentally measured geometry changes according to the mechanical modeling process described in Section 2.2.

A flow chart summarizing all of the steps involved in the process is shown in Figure 5.1:

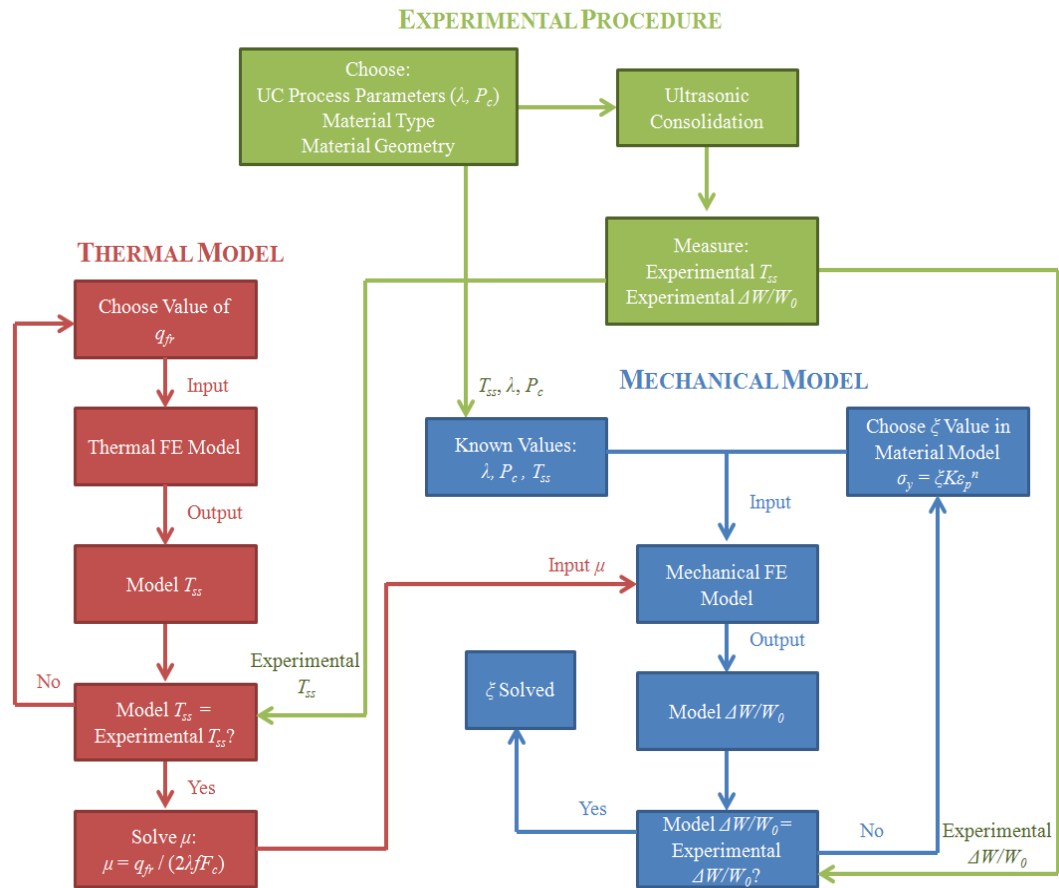


Figure 5.1. Flow chart summarizing the steps required to quantify acoustic softening.

5.2 Future Work

In the future, acoustic softening in additional materials used during UC can be quantified using the method described in this work. Knowledge of how the UC process parameters influence acoustic softening will allow process parameters to be chosen in a systematic method, rather than through trial and error.

The influence of acoustic softening on bond strength and bonded area should be further investigated. Peel testing is a test method with some potential in testing the

strength of UC bonds. Preliminary experiments have been conducted in this area and selected results are shown in Appendix A.

Now that a method has been developed to quantify material softening during UC, a sonotrode design can be optimized. The design must provide a strong grip to the top of the foil while allowing the pattern to be filled in as subsequent layers of material are built up. The optimum sonotrode knurl pattern geometry will likely depend on the material being welded and its thickness. Thin materials require less amplitude to bond and therefore will require a relatively shallow knurl pattern. Thick materials require high amplitudes to bond and will require a relatively deep knurl pattern in order to ensure that the sonotrode properly grips the foil.

REFERENCES

- Bakavos, D., Prangnell, P.B., 2010. Mechanisms of joint and microstructure formation in high power ultrasonic spot welding 6111 aluminum automotive sheet. *Materials Science and Engineering A*. 527, 6320-6334.
- Blaha, F., Langenecker, B., 1955. Dehnung Von Zink_Kristallen Unter Ultraschallein-Wirkung. *Naturwissenschaften* 42, 556.
- Cai, M., 2006. Acousto-plastic deformation of metals by nonlinear stress waves. Dissertation, The Ohio State University.
- Dassault Systems, 2009. Abaqus Analysis User's Manual.
- Daud, Y., Lucas, M., Huang, Z., 2007. Modeling the effects of superimposed ultrasonic vibrations on tension and compression tests of aluminum. *Journal of Materials Processing Technology* 186, 179-190.
- de Vries, E., 2004. Mechanics and Mechanisms of Ultrasonic Metal Welding. Dissertation, The Ohio State University.
- Doumanidis, C., Gao, Y., 2004. Mechanical Modeling of Ultrasonic Welding. *Welding Journal* 83, 140-146.
- Elangovan, S., Semeer, S., Prakasan, K., 2009. Temperature and stress distribution in ultrasonic metal welding – An FEA-based study. *Journal of Materials Processing Technology* 209, 1143-1150.
- Ferreira, T., Rasband, W., 2011. Image J User Guide IJ 1.45m.
- Friel, R.J., Johnson, K.E., Dickens, P.M., Harris, R.A., 2010. The effect of interface topography for Ultrasonic Consolidation of aluminum. *Materials Science and Engineering A* 527, 4474-4483.
- Hockett, J., 1967. On Relating the Flow Stress of Aluminum to Strain, Strain Rate, and Temperature. *Transactions of the Metallurgical Society of AIME* 239, 969-976.

- Hodowany, J., Ravichandran, G., Rosakis, J., Rosakis, P., 1999. Partition of Plastic Work into Heat and Stored Energy in Metals. *Experimental Mechanics* 40(2), 113-123.
- Huang, C., Ghassemieh, E., 2007. 3D Coupled Thermomechanical Finite Element Analysis of Ultrasonic Consolidation. *Materials Science Forum* 539-543, 2651-2656.
- Izumi, I., Oyama, K., Suzuki, Y., 1966a. Effects of Superimposed Ultrasonic Vibration on Compressive Deformation of Metals. *Transactions of the Japan institute of metals* 7, 162-166.
- Izumi, I., Oyama, K., Suzuki, Y., 1966b. On the Superimposing of Ultrasonic Vibration During Compressive Deformation of Metals. *Transactions of the Japan institute of metals* 7, 158-162.
- Janaki Ram, G.D., Yang, Y., Stucker, B.E., 2006. Effect of Process Parameters on Bond Formation During Ultrasonic Consolidation of Aluminum Alloy 3003. *Journal of Manufacturing Systems* 25(3), 221-238.
- Koellhoffer, S., Gillespie, J.W., Advani, S.G., Bogetti, T.A., 2011. Role of friction on the thermal development in ultrasonically consolidated aluminum foils and composites. *Journal of Materials Processing Technology* 211, 1864-1877.
- Kong, C., Soar, R., Dickens, P., 2005. A model for weld strength in ultrasonically consolidated components. *Journal of Mechanical Engineering Science* 219, 83-91.
- Kong, C., Soar, R., Dickens, P., 2004. Optimum process parameters for ultrasonic consolidation of 3003 aluminum. *Journal of Materials Processing Technology* 146, 181-187.
- Kong, C., Soar, R., Dickens, P., 2003. Characterization of aluminum alloy 6061 for the ultrasonic consolidation process. *Materials Science and Engineering A* 363, 99-106.
- Langenecker, B., 1966. Effects of Ultrasound on Deformation Characteristics of Metals. *IEEE Transactions on Sonics and Ultrasonics* 13(1), 1-8.
- Malygin, G.A., 2000. Acoustoplastic Effect and the Stress Superimposition Mechanism. *Physics of the Solid State* 42(1), 69-75.

- Naidu, N., Raman, A., 2005. Effect of contact pressure on fretting fatigue behavior of Al-Mg-Si alloy AA6061. *International Journal of Fatigue* 27, 283-291.
- Obielodan, J.O., Janaki Ram, G.D., Stucker, B.E., Taggart, D.G., 2010. Minimizing Defects Between Adjacent Foils in Ultrasonically Consolidated Parts. *Journal of Engineering materials and Technology* 132, 1-8.
- Obielodan, J.O., Stucker, B.E., Martinez, J.L., Hernandez, D.H., Ramirez, D.A., Murr, L.E., 2011. Optimization of the shear strengths of ultrasonically consolidated Ti/Al 3003 dual-materials structures. *Journal of Materials Processing Technology* 211(6), 988-995.
- Pao, Y., Gilat, A., 1989. Modeling 1100-0 aluminum over a wide range of temperatures and strain rates. *International Journal of Plasticity* 5, 183-196.
- Pitchumani, R., J. W. Gillespie Jr., and M. A. Lamontia, 1997. Design and Optimization of a Thermoplastic Tow-Placement Process with In-situ Consolidation. *Journal of Composite Materials* 31(3), 244-275.
- Puchi, E., Staia, M., Villalobos, C., 1997. On the mechanical behavior of commercial-purity aluminum deformed under axisymmetric compression conditions. *International Journal of Plasticity* 13, 723-742
- Pušćár, A., 1982. *Materials Science Monographs 13, The Use of High-Intensity Ultrasonics*. Elsevier, New York, 105-140.
- Siddiq, A., Ghassemieh, E., 2009. Theoretical and FE Analysis of Ultrasonic Welding of Aluminum Alloy 3003. *Journal of Manufacturing Science and Engineering* 131, 1-11.
- Siddiq, A., Ghassemieh, E., 2008. Thermomechanical analysis of ultrasonic welding process using thermal and acoustic softening effects. *Mechanics of Materials* 40, 982-1000.
- Sriraman, M.R., Gonser, M., Fujii, H.T., Bloss, M., 2011. Thermal transients during processing of materials by very high power ultrasonic additive manufacturing. *Journal of Materials Processing Technology* 211, 1650-1657.
- Tierney, J., J. W. Gillespie, Jr., 2006. Modeling of In-Situ Strength Development for the Thermoplastic Composite Tow Placement Process. *Journal of Composite Materials*, 40(16) 1487-1506.

- Verlinden, B., Driver, J., Samajdar, I., Roger D. Doherty. Thermo-Mechanical Processing of Metallic Materials. Elsevier, 2007, 295.
- Yang, Y., Janaki Ram, G.D., Stucker, B.E., 2009. Bond formation and fiber embedment during ultrasonic consolidation. *Journal of Materials Processing Technology* 209(10), 4915-4924.
- Yao, Z., Kim, G., Faidley, L. Zou, Q., Mei, D., Chen, Z., 2012. Effects of superimposed high-frequency vibration on deformation of aluminum in micro/meso-scale upsetting. *Journal of Materials Processing Technology* 212, 640-646.
- Zhang, C., Li, L., 2010. Effect of substrate dimensions on dynamics of ultrasonic consolidation. *Ultrasonics* 50, 811-823.
- Zhang, C., Li, L., 2009. A Coupled Thermal-Mechanical Analysis of Ultrasonic Bonding Mechanism. *Metallurgical and Materials Transactions B* 40, 196-207.
- Zhang, C., Deceuster, A., Li, L., 2009. A Method for Bond Strength Evaluation for Laminated Structures with Application to Ultrasonic Consolidation. *Journal of Materials Engineering and Performance* 18(8), 1124-1132.
- Zhang, C., Li, L., 2008. A Friction-Based Finite Element Analysis of Ultrasonic Consolidation. *Welding Journal* 87, 187-194.
- Zhang, J., Lewandowski, J., 1997. Delamination study using four-point bending of bilayers. *Journal of Materials Science* 32, 3851-3856.

Appendix A

PRELIMINARY BOND STRENGTH DATA

In this section, preliminary bond strength measurement results are presented. A floating-roller peel test fixture is used to test the strength of UC bonds. Optical microscopy is used to quantify bonded area by investigating bond surfaces after failure in the peel test fixture. Finally, the influence of acoustic softening on the bonding process is briefly examined.

A.1 Experimental Methods

Several experimental methods have been investigated to test the strength of UC bonds. Zhang et al. (2009) used a push-pin type experiment to fail UC bonds in compression. Zhang and Lewandowski (1997) investigated delimitation of specimens using four-point bending. Both methods have significant limitations. Kong et al. (2003) utilized peel testing to investigate the strength of UC bonds made with Al 6061 and were able to identify a window of process parameters that produced the strongest bonds. Kong et al. (2004) noted that peel testing is better for UC bonds than lap shear testing as there is a tendency for the material to fail in tension when strong bonds are present. Peel testing is investigated in this work due to the simplicity of the experiments and its previous success in the literature.

A.1.1 Peel Testing

Figure A.1 shows an image of the floating-roller peel test fixture used in this work.

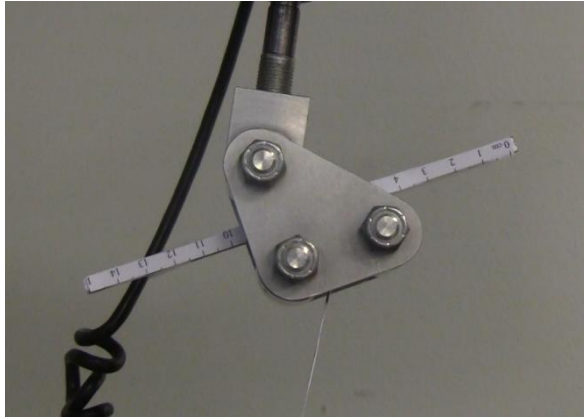


Figure A.1. Image of the floating roller peel test fixture.

Peel strength is recorded along the length of the weld for two sets of UC process parameters that are shown in Figure A.2. Overlaid on the same plot are measure IR camera temperatures at each weld position.

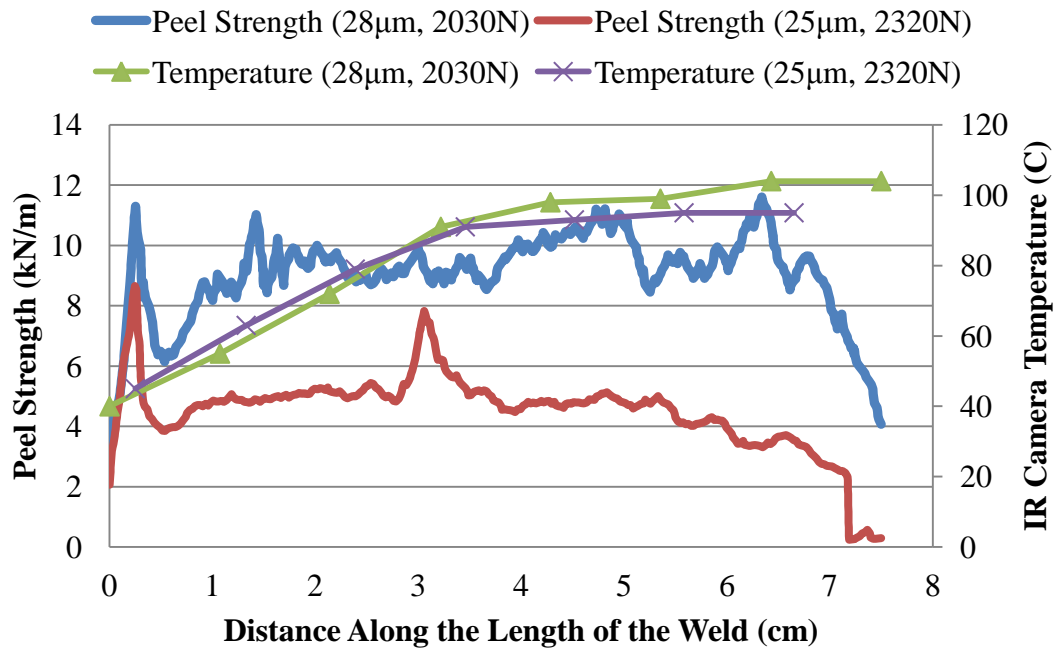


Figure A.2. Plot of peel strength and temperature vs. weld position for UC bonds created with two different sets of process parameters. The Al 1100-0 foils are 9.5 x 0.52mm.

It can be seen that peel strength can vary significantly along the length of a weld. Other bond strength tests will not be able to capture this variation in bond strength since they typically only test a small portion of the weld. The small areas investigated with other bond strength tests will likely lead to inconsistencies, making peel testing a better method.

Sriraman et al. (2011) stated that temperatures during UC are related to the bond strength. Figure A.2 clearly shows that there is no apparent relationship between weld temperature and bond strength. While both welds have the same T_{ss} , the weld with $\lambda = 28 \mu\text{m}$ has approximately twice the peel strength as the weld with $\lambda = 25 \mu\text{m}$.

A.1.2 Optical Microscopy

Friel et al. (2010) investigated failure surfaces of UC bonds using optical microscopy and were able to identify areas of the surface that were processed and bonded during UC. Similarly in this work, optical microscopy is used to determine bonded areas after weld specimens have been failed and the bonded interface during peel testing. Figure A.3 shows an image of a substrate after a foil has been peeled off. In this image, the x -direction is the foil's width direction. Dark regions in the image were bonded during UC. It can be seen that bonded area can vary significantly across the foil's width. The percent bonded area can be calculated for the entire image by measuring the ratio of light / dark areas.

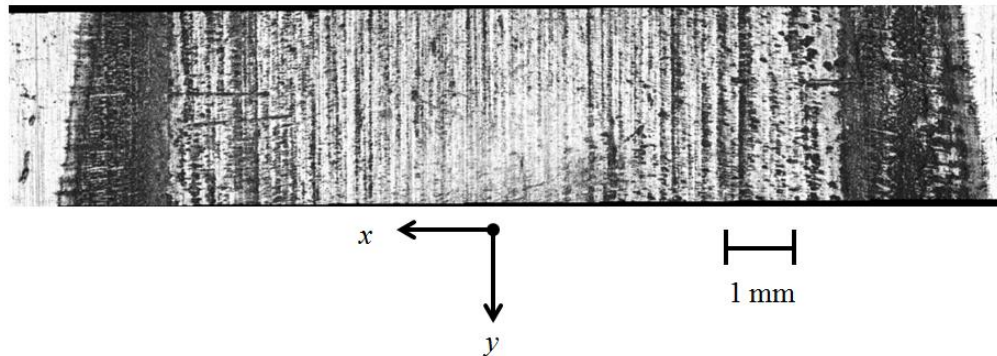


Figure A.3. Optical microscopy image of the surface of the substrate after the peel test. Dark regions in the image were bonded during UC.

A.2 Relationship Between Bond Area and Peel Strength

In this section, the relationship between bonded area as measured in the optical microscope and peel strength will be investigated. Figure A.4 shows peel strength and bonded area measurements for a weld produced at 25 μm and 2320N.

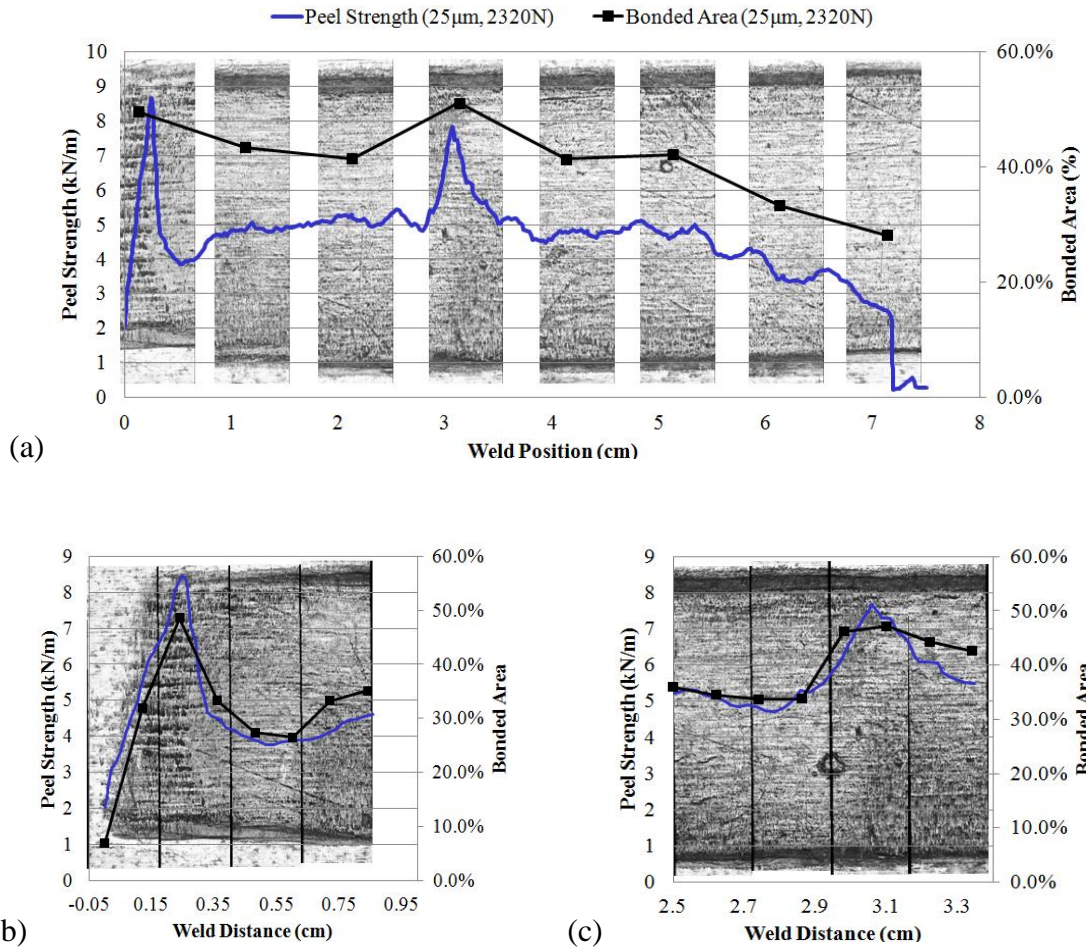


Figure A.4. Comparison of peel strength and bonded area overlaid onto optical microscopy images of the bonded surface. The entire weld length is shown in (a). The two peaks in peel strength in (a) are focused on in more detail in (b) and (c). The Al 1100-0 foils are 9.5 x 0.52mm.

Figure A.4 shows that there is a correlation between bonded area and peel strength. Regions with a relatively high percent of bonded area also have a higher peel strength. This relationship is improved by investigating smaller areas over which to calculate bonded area. This can be seen in Figure A.4 (a), where bonded is averaged over 2.5 mm along the weld length. When the peaks in peel strength in (a) are

investigated in more detail in (b) and (c), it can be seen that bonded area and peel strength are closely related. This result is as expected and serves to validate this test method.

The peel test curves shown in Figure A.2 are again investigated Figure A.5, but this time are compared to bonded area measurements rather than temperature in. It can be seen that the bond with the higher peel strength also has the higher bonded area.

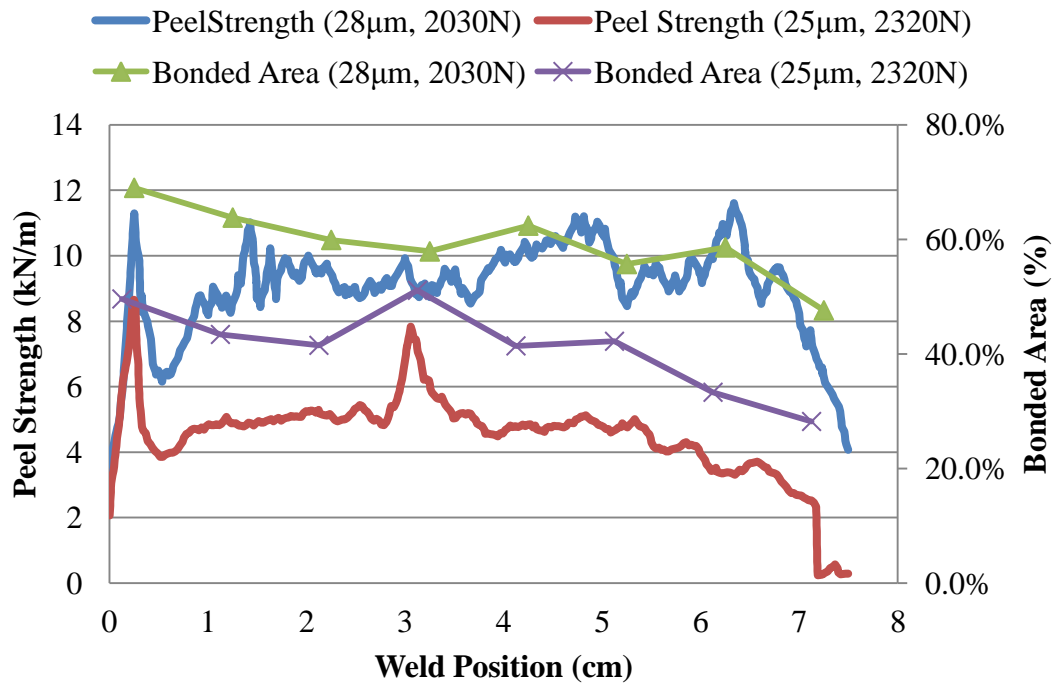
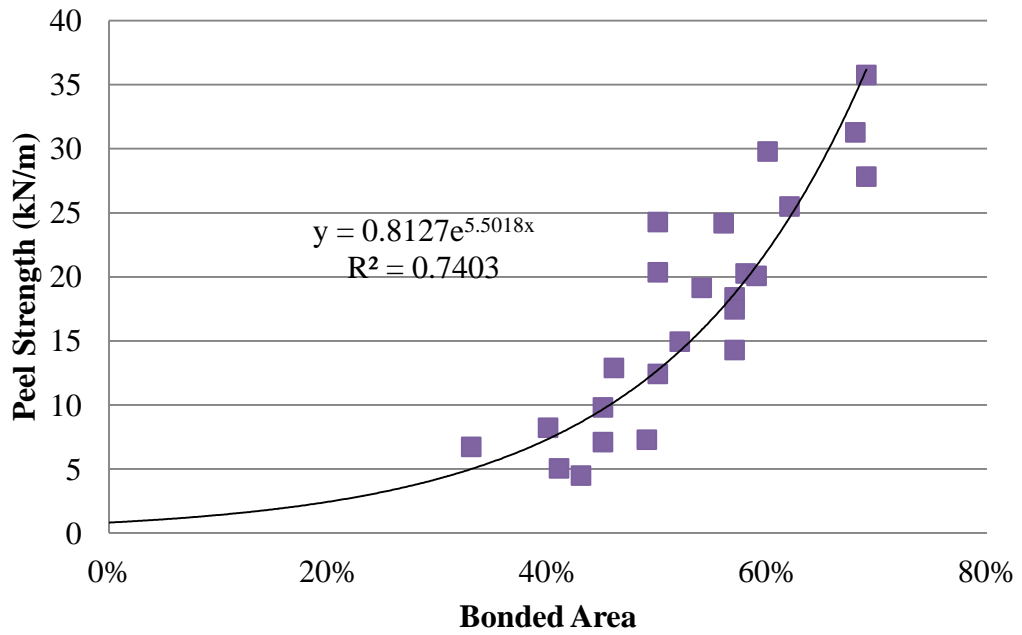
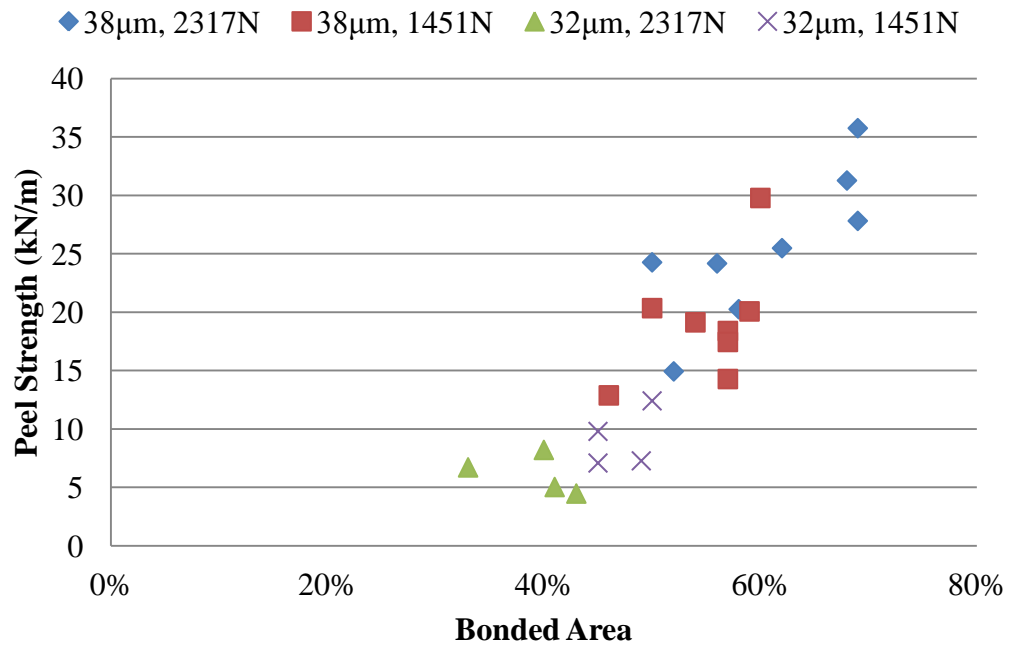


Figure A.5. Plot of peel strength and bonded area vs. weld position for UC bonds created with two different sets of process parameters. The Al 1100-0 foils are 9.5 x 0.52mm.

Figure A.6 shows two plots of bond area vs. bond strength. In (a) it can be seen that there is an exponential relationship between bond area and bond strength. In (b), the specific process parameters are shown at which each bond was made.



(a)



(b)

Figure A.6. Plot of peel strength and bonded area for 9.5 x 1.04 mm Al 1100-0 foils.

It can be seen that bonds made with a higher amplitude are typically stronger. The model described in this work can be used to investigate the influence of acoustic softening on bonded area and bond strength. Acoustic softening is calculated using Equation (4.3) for each set of process parameters shown in Figure A.6 and are shown in Table A.1.

Table A.1. Acoustic softening calculated using Equation (4.3) for the process parameters shown in Figure A.6.

Process Parameters	38 μ m, 2317N	38 μ m, 1451N	32 μ m, 2317N	32 μ m, 1451N
Acoustic Softening (ξ)	0.206	0.190	0.230	0.204

Investigation of Table A.1 and Figure A.6 shows that process parameters that result in the least amount of acoustic softening (32 μ m, 2317N) also result in the weakest bond strength, both in terms of bonded area and peel strength. This could potentially explain why the bonds produced at (32 μ m, 2317N) are weaker than those produced at (32 μ m, 1451N). Additional investigations are required in the future to further investigate this observation.

A.3 Summary

Peel testing to determine bond strength and optical microscopy to determine bonded area are shown to be effective in investigating the properties of UC bonds. A direct relationship is found between bond area and peel strength in the UC bonds tested in this work. Evidence suggests that acoustic softening plays a role in UC bond quality, but further investigation will be required.

Appendix B

FIGURE REPRINT PERMISSIONS

Figure reprint permission for Figure 1.2.

ELSEVIER LICENSE
TERMS AND CONDITIONS
Jun 05, 2012

This is a License Agreement between Gregory S Kelly ("You") and Elsevier ("Elsevier") provided by Copyright Clearance Center ("CCC"). The license consists of your order details, the terms and conditions provided by Elsevier, and the payment terms and conditions.

All payments must be made in full to CCC. For payment instructions, please see information listed at the bottom of this form.

Supplier	Elsevier Limited The Boulevard, Langford Lane Kidlington, Oxford, OX5 1GB, UK
Registered Company Number	1982084
Customer name	Gregory S Kelly
Customer address	202 Composites Manufacturing Science Lab Newark, DE 19716
License number	2922521405783
License date	Jun 05, 2012
Licensed content publisher	Elsevier
Licensed content publication	Journal of Materials Processing Technology
Licensed content title	Role of friction on the thermal development in ultrasonically consolidated aluminum foils and composites
Licensed content author	Steve Koellhoffer, John W. Gillespie, Suresh G. Advani, Travis A. Bogetti

Licensed content date	November 2011
Licensed content volume number	211
Licensed content issue number	11
Number of pages	14
Start Page	1864
End Page	1877
Type of Use	reuse in a thesis/dissertation
Portion	figures/tables/illustrations
Number of figures/tables/illustrations	1
Format	both print and electronic
Are you the author of this Elsevier article?	No
Will you be translating?	No
Order reference number	
Title of your thesis/dissertation	A thermo-mechanical finite element analysis of acoustic softening during ultrasonic consolidation of aluminum foils
Expected completion date	Jun 2012
Estimated size (number of pages)	100
Elsevier VAT number	GB 494 6272 12
Permissions price	0.00 USD
VAT/Local Sales Tax	0.0 USD / 0.0 GBP
Total	0.00 USD
Terms and Conditions	

INTRODUCTION

1. The publisher for this copyrighted material is Elsevier. By clicking "accept" in connection with completing this licensing transaction, you agree that the following terms and conditions apply to this transaction (along with the Billing and Payment terms and conditions established by Copyright Clearance Center, Inc. ("CCC"), at the time that you opened your Rightslink account and that are available at any time at <http://myaccount.copyright.com>).

GENERAL TERMS

2. Elsevier hereby grants you permission to reproduce the aforementioned material

subject to the terms and conditions indicated.

3. Acknowledgement: If any part of the material to be used (for example, figures) has appeared in our publication with credit or acknowledgement to another source, permission must also be sought from that source. If such permission is not obtained then that material may not be included in your publication/copies. Suitable acknowledgement to the source must be made, either as a footnote or in a reference list at the end of your publication, as follows:

“Reprinted from Publication title, Vol /edition number, Author(s), Title of article / title of chapter, Pages No., Copyright (Year), with permission from Elsevier [OR APPLICABLE SOCIETY COPYRIGHT OWNER].” Also Lancet special credit - “Reprinted from The Lancet, Vol. number, Author(s), Title of article, Pages No., Copyright (Year), with permission from Elsevier.”

4. Reproduction of this material is confined to the purpose and/or media for which permission is hereby given.

5. Altering/Modifying Material: Not Permitted. However figures and illustrations may be altered/adapted minimally to serve your work. Any other abbreviations, additions, deletions and/or any other alterations shall be made only with prior written authorization of Elsevier Ltd. (Please contact Elsevier at permissions@elsevier.com)

6. If the permission fee for the requested use of our material is waived in this instance, please be advised that your future requests for Elsevier materials may attract a fee.

7. Reservation of Rights: Publisher reserves all rights not specifically granted in the combination of (i) the license details provided by you and accepted in the course of this licensing transaction, (ii) these terms and conditions and (iii) CCC's Billing and Payment terms and conditions.

8. License Contingent Upon Payment: While you may exercise the rights licensed immediately upon issuance of the license at the end of the licensing process for the transaction, provided that you have disclosed complete and accurate details of your proposed use, no license is finally effective unless and until full payment is received from you (either by publisher or by CCC) as provided in CCC's Billing and Payment terms and conditions. If full payment is not received on a timely basis, then any license preliminarily granted shall be deemed automatically revoked and shall be void as if never granted. Further, in the event that you breach any of these terms and conditions or any of CCC's Billing and Payment terms and conditions, the license is automatically revoked and shall be void as if never granted. Use of materials as described in a revoked license, as well as any use of the materials beyond the scope of an unrevoked license, may constitute copyright infringement and publisher reserves the right to take

any and all action to protect its copyright in the materials.

9. **Warranties:** Publisher makes no representations or warranties with respect to the licensed material.

10. **Indemnity:** You hereby indemnify and agree to hold harmless publisher and CCC, and their respective officers, directors, employees and agents, from and against any and all claims arising out of your use of the licensed material other than as specifically authorized pursuant to this license.

11. **No Transfer of License:** This license is personal to you and may not be sublicensed, assigned, or transferred by you to any other person without publisher's written permission.

12. **No Amendment Except in Writing:** This license may not be amended except in a writing signed by both parties (or, in the case of publisher, by CCC on publisher's behalf).

13. **Objection to Contrary Terms:** Publisher hereby objects to any terms contained in any purchase order, acknowledgment, check endorsement or other writing prepared by you, which terms are inconsistent with these terms and conditions or CCC's Billing and Payment terms and conditions. These terms and conditions, together with CCC's Billing and Payment terms and conditions (which are incorporated herein), comprise the entire agreement between you and publisher (and CCC) concerning this licensing transaction. In the event of any conflict between your obligations established by these terms and conditions and those established by CCC's Billing and Payment terms and conditions, these terms and conditions shall control.

14. **Revocation:** Elsevier or Copyright Clearance Center may deny the permissions described in this License at their sole discretion, for any reason or no reason, with a full refund payable to you. Notice of such denial will be made using the contact information provided by you. Failure to receive such notice will not alter or invalidate the denial. In no event will Elsevier or Copyright Clearance Center be responsible or liable for any costs, expenses or damage incurred by you as a result of a denial of your permission request, other than a refund of the amount(s) paid by you to Elsevier and/or Copyright Clearance Center for denied permissions.

LIMITED LICENSE

The following terms and conditions apply only to specific license types:

15. **Translation:** This permission is granted for non-exclusive world **English** rights only unless your license was granted for translation rights. If you licensed translation

rights you may only translate this content into the languages you requested. A professional translator must perform all translations and reproduce the content word for word preserving the integrity of the article. If this license is to re-use 1 or 2 figures then permission is granted for non-exclusive world rights in all languages.

16. Website: The following terms and conditions apply to electronic reserve and author websites:

Electronic reserve: If licensed material is to be posted to website, the web site is to be password-protected and made available only to bona fide students registered on a relevant course if:

This license was made in connection with a course,

This permission is granted for 1 year only. You may obtain a license for future website posting,

All content posted to the web site must maintain the copyright information line on the bottom of each image,

A hyper-text must be included to the Homepage of the journal from which you are licensing at <http://www.sciencedirect.com/science/journal/xxxxx> or the Elsevier homepage for books at <http://www.elsevier.com> , and

Central Storage: This license does not include permission for a scanned version of the material to be stored in a central repository such as that provided by Heron/XanEdu.

17. Author website for journals with the following additional clauses:

All content posted to the web site must maintain the copyright information line on the bottom of each image, and the permission granted is limited to the personal version of your paper. You are not allowed to download and post the published electronic version of your article (whether PDF or HTML, proof or final version), nor may you scan the printed edition to create an electronic version. A hyper-text must be included to the Homepage of the journal from which you are licensing at <http://www.sciencedirect.com/science/journal/xxxxx> . As part of our normal production process, you will receive an e-mail notice when your article appears on Elsevier's online service ScienceDirect (www.sciencedirect.com). That e-mail will include the article's Digital Object Identifier (DOI). This number provides the electronic link to the published article and should be included in the posting of your personal version. We ask that you wait until you receive this e-mail and have the DOI to do any posting.

Central Storage: This license does not include permission for a scanned version of the material to be stored in a central repository such as that provided by Heron/XanEdu.

18. Author website for books with the following additional clauses:

Authors are permitted to place a brief summary of their work online only.

A hyper-text must be included to the Elsevier homepage at <http://www.elsevier.com> .

All content posted to the web site must maintain the copyright information line on the

bottom of each image. You are not allowed to download and post the published electronic version of your chapter, nor may you scan the printed edition to create an electronic version.

Central Storage: This license does not include permission for a scanned version of the material to be stored in a central repository such as that provided by Heron/XanEdu.

19. **Website** (regular and for author): A hyper-text must be included to the Homepage of the journal from which you are licensing at <http://www.sciencedirect.com/science/journal/xxxxx>. or for books to the Elsevier homepage at <http://www.elsevier.com>

20. **Thesis/Dissertation**: If your license is for use in a thesis/dissertation your thesis may be submitted to your institution in either print or electronic form. Should your thesis be published commercially, please reapply for permission. These requirements include permission for the Library and Archives of Canada to supply single copies, on demand, of the complete thesis and include permission for UMI to supply single copies, on demand, of the complete thesis. Should your thesis be published commercially, please reapply for permission.

21. **Other Conditions**:

v1.6

If you would like to pay for this license now, please remit this license along with your payment made payable to "COPYRIGHT CLEARANCE CENTER" otherwise you will be invoiced within 48 hours of the license date. Payment should be in the form of a check or money order referencing your account number and this invoice number RLNK500792910.

Once you receive your invoice for this order, you may pay your invoice by credit card. Please follow instructions provided at that time.

**Make Payment To:
Copyright Clearance Center
Dept 001
P.O. Box 843006
Boston, MA 02284-3006**

For suggestions or comments regarding this order, contact RightsLink Customer Support: customercare@copyright.com or +1-877-622-5543 (toll free in the US) or +1-978-646-2777.

Gratis licenses (referencing \$0 in the Total field) are free. Please retain this printable license for your reference. No payment is required.

Figure reprint permission for Figure 1.3.

SPRINGER LICENSE TERMS AND CONDITIONS

Jun 05, 2012

This is a License Agreement between Gregory S Kelly ("You") and Springer ("Springer") provided by Copyright Clearance Center ("CCC"). The license consists of your order details, the terms and conditions provided by Springer, and the payment terms and conditions.

All payments must be made in full to CCC. For payment instructions, please see information listed at the bottom of this form.

License Number	2922530588098
License date	Jun 05, 2012
Licensed content publisher	Springer
Licensed content publication	Naturwissenschaften
Licensed content title	Dehnung von Zink-Kristallen unter Ultraschalleinwirkung
Licensed content author	F. Blaha
Licensed content date	Jan 1, 1955
Volume number	42
Issue number	20
Type of Use	Thesis/Dissertation
Portion	Figures
Author of this Springer article	No
Order reference number	
Title of your thesis / dissertation	A thermo-mechanical finite element analysis of acoustic softening during ultrasonic consolidation of aluminum foils
Expected completion date	Jun 2012
Estimated size(pages)	100
Total	0.00 USD
Terms and Conditions	
Introduction	

The publisher for this copyrighted material is Springer Science + Business Media. By clicking "accept" in connection with completing this licensing transaction, you agree that the following terms and conditions apply to this transaction (along with the Billing and Payment terms and conditions established by Copyright Clearance Center, Inc. ("CCC"), at the time that you opened your Rightslink account and that are available at any time at <http://myaccount.copyright.com>).

Limited License

With reference to your request to reprint in your thesis material on which Springer Science and Business Media control the copyright, permission is granted, free of charge, for the use indicated in your enquiry.

Licenses are for one-time use only with a maximum distribution equal to the number that you identified in the licensing process.

This License includes use in an electronic form, provided its password protected or on the university's intranet or repository, including UMI (according to the definition at the Sherpa website: <http://www.sherpa.ac.uk/romeo/>). For any other electronic use, please contact Springer at (permissions.dordrecht@springer.com or permissions.heidelberg@springer.com).

The material can only be used for the purpose of defending your thesis, and with a maximum of 100 extra copies in paper.

Although Springer holds copyright to the material and is entitled to negotiate on rights, this license is only valid, provided permission is also obtained from the (co) author (address is given with the article/chapter) and provided it concerns original material which does not carry references to other sources (if material in question appears with credit to another source, authorization from that source is required as well).

Permission free of charge on this occasion does not prejudice any rights we might have to charge for reproduction of our copyrighted material in the future.

Altering/Modifying Material: Not Permitted

You may not alter or modify the material in any manner. Abbreviations, additions, deletions and/or any other alterations shall be made only with prior written authorization of the author(s) and/or Springer Science + Business Media. (Please contact Springer at (permissions.dordrecht@springer.com or permissions.heidelberg@springer.com))

Reservation of Rights

Springer Science + Business Media reserves all rights not specifically granted in the combination of (i) the license details provided by you and accepted in the course of this licensing transaction, (ii) these terms and conditions and (iii) CCC's Billing and

Payment terms and conditions.

Copyright Notice:Disclaimer

You must include the following copyright and permission notice in connection with any reproduction of the licensed material: "Springer and the original publisher /journal title, volume, year of publication, page, chapter/article title, name(s) of author(s), figure number(s), original copyright notice) is given to the publication in which the material was originally published, by adding; with kind permission from Springer Science and Business Media"

Warranties: None

Example 1: Springer Science + Business Media makes no representations or warranties with respect to the licensed material.

Example 2: Springer Science + Business Media makes no representations or warranties with respect to the licensed material and adopts on its own behalf the limitations and disclaimers established by CCC on its behalf in its Billing and Payment terms and conditions for this licensing transaction.

Indemnity

You hereby indemnify and agree to hold harmless Springer Science + Business Media and CCC, and their respective officers, directors, employees and agents, from and against any and all claims arising out of your use of the licensed material other than as specifically authorized pursuant to this license.

No Transfer of License

This license is personal to you and may not be sublicensed, assigned, or transferred by you to any other person without Springer Science + Business Media's written permission.

No Amendment Except in Writing

This license may not be amended except in a writing signed by both parties (or, in the case of Springer Science + Business Media, by CCC on Springer Science + Business Media's behalf).

Objection to Contrary Terms

Springer Science + Business Media hereby objects to any terms contained in any purchase order, acknowledgment, check endorsement or other writing prepared by you, which terms are inconsistent with these terms and conditions or CCC's Billing and Payment terms and conditions. These terms and conditions, together with CCC's Billing and Payment terms and conditions (which are incorporated herein), comprise the entire agreement between you and Springer Science + Business Media (and CCC) concerning

this licensing transaction. In the event of any conflict between your obligations established by these terms and conditions and those established by CCC's Billing and Payment terms and conditions, these terms and conditions shall control.

Jurisdiction

All disputes that may arise in connection with this present License, or the breach thereof, shall be settled exclusively by arbitration, to be held in The Netherlands, in accordance with Dutch law, and to be conducted under the Rules of the 'Netherlands Arbitrage Instituut' (Netherlands Institute of Arbitration). **OR:**

All disputes that may arise in connection with this present License, or the breach thereof, shall be settled exclusively by arbitration, to be held in the Federal Republic of Germany, in accordance with German law.

Other terms and conditions:

v1.3

If you would like to pay for this license now, please remit this license along with your payment made payable to "COPYRIGHT CLEARANCE CENTER" otherwise you will be invoiced within 48 hours of the license date. Payment should be in the form of a check or money order referencing your account number and this invoice number RLNK500792923.

Once you receive your invoice for this order, you may pay your invoice by credit card. Please follow instructions provided at that time.

Make Payment To:

Copyright Clearance Center
Dept 001
P.O. Box 843006
Boston, MA 02284-3006

For suggestions or comments regarding this order, contact RightsLink Customer Support: customercare@copyright.com or +1-877-622-5543 (toll free in the US) or +1-978-646-2777.

Gratis licenses (referencing \$0 in the Total field) are free. Please retain this printable license for your reference. No payment is required.
